Diverse Genetic and Transcriptional Programs Mediate Dendrite Development of a Nociceptor Neuron

By

Barbara Maledy Jones O'Brien

Dissertation

Submitted to the Faculty of the

Graduate School of Vanderbilt University

in partial fulfillment of the requirements for

the degree of

DOCTOR OF PHILOSOPHY

in

Neuroscience

December 16, 2017

Nashville, Tennessee

Approved:

David M. Miller, III, Ph.D.

Kendal S. Broadie, Ph.D.

Bruce D. Carter, Ph.D.

Matthew J. Tyska, Ph.D.

To my mother and my father, who each taught me the power of perseverance,

and

To my husband, for his unwavering support.

ACKNOWLEDGEMENTS

I would first like to thank my advisor, David Miller. When I first joined the lab, I had a strong systems neuroscience background but very little genetics and cellular/molecular background. David met with me weekly to discuss papers, techniques, and my project to make sure I understood the material and the logic behind the different approaches used to test models and hypotheses. It was through these meetings that I was able to make the transition from the systems world to the cellular and molecular world, and for that I am truly grateful.

In taking me on as a student, David volunteered current lab members to take me on as a mentee as well. Tyne Miller-Fleming and Siwei He were instrumental to my development as a scientist. Even though their research projects focused on an aspect of neuron development far from my own, they were always eager to help me understand the basics behind fundamental techniques or concepts in genetics. I must particularly thank my baymate Tyne who, for better or for worse, was always in earshot of my questions. She could have pretended she could not hear, but instead she would stop what she was doing, remove her headphones, and take a look at what I was working on and needed help with. I would also like to thank those who joined the Miller Lab after I did, Lakshmi Sundararajan, Andrea Cuentas-Condori, and Sierra Palumbos. I have enjoyed working with this collaborative and encouraging group of colleagues. I also thank Rebecca McWhirter for keeping the lab running and for all her help with FACS. I would also like to thank the two undergraduates I worked with, Michaela Novokovic and Xueying Shang for their help with my multiple projects.

I am so thankful for my thesis committee, Kendal Broadie, Matthew Tyska, Bruce Carter, and Donna Webb, for their thoughtful input to my projects and for their encouragement when

negative results led to starting a new thesis project. The participants of Worm Group Meeting, including Brian Nelms and his students at Fisk University and Chelsea Snarrenberg Gibson and Dan Bermingham from Randy Blakely's lab also provided insightful suggestions to my projects.

I would not have been able to do this research without the support of the Neuroscience Program and the Vanderbilt Brain Institute, the program coordinator Roz Johnson, and Beth Sims. I also thank Doug McMahon and Bruce Carter for serving as the director of graduate students for the Neuroscience program, along with Mark Wallace and Ron Emeson for serving as the directors of the Vanderbilt Brain Institute.

Though I was not a student of the Cell and Developmental Biology Program, the CDB faculty, staff, and students welcomed me to their retreats and seminars that contributed to my growth as a scientist. I would also like to thank Chris Wright and the Program in Developmental Biology for providing journal clubs and retreats that explored all aspects of development. I would also like to thank Anthony Tharp and Brian Millis for their help with microscopy and for maintaining core facilities.

I would also like to acknowledge my friends, both the friends I have made while in graduate school, for relating to the ups and downs of science, and the friends I have known since long before I entered a lab, for supporting me even if they did not understand why anyone would want a career in research.

Finally, I truly could not have pursued a doctoral degree without the amazing love and encouragement of my family, the Easons, my Aunt Pat, my Aunt Glenda, and my basically-family, the Abernathys. My sister Robin, my father, and my mother have always been there for me, and it feels wonderful to know I always have their support.

My gratefulness for my husband is two-fold. I am mostly grateful to him for providing a wonderful place to go home to at the end of the day, an attentive ear, fun times, and for being my best friend. But I cannot leave out my appreciation for his knowledge of genetics and cell biology and for our myriad discussions of the nociceptor neuron we both ended up studying.

TABLE OF CONTENTS

LIST OF TABLES

Table Page

LIST OF FIGURES

Figure Page

CHAPTER 1 : INTRODUCTION

Neurons are polarized cells that receive input via dendrites and relay output via axons

The central nervous system is composed of specialized cells that communicate through electrical and chemical signals. The process of receiving and relaying information is polarized in these cell types: a neuron receives input through dendrites and sends information through a single axon (**Figure 1.1a**[1]). Neurons throughout the brain and spinal cord display several distinct morphologies, ranging from a cell body with a single process to a cell body with multiple dendrites and an axon that branches to contact many cells. But despite the variation in anatomical structure among different classes of neurons, the central polarity of input via dendrites and output via an axon is a common property of all neurons within a single animal and across species (**Figure 1.1**[1]). Since this property is observed across species, it suggests conserved signaling pathways and common developmental patterns.

Sensory neurons are a class of neurons that innervate the sensory epithelium to allow the animal to sense the external environment (e.g., feeling through the skin, hearing through the ears, seeing through the eyes, smelling through the nose, and tasting through the tongue) or the internal environment (e.g., muscles and organs). A subset of sensory neurons, termed nociceptors, respond only to intense or extreme sensations to alert the animal of potentially harmful stimuli[2]. For example, thermoreceptors are activated at mild temperatures, while thermal nociceptors are activated at extreme hot or cold temperatures that could be harmful. In addition to temperature, the extremes that activate other types of nociceptors include excess pressure or punctures in the skin through mechanoreceptors and harmful chemicals through chemoreceptors[3].

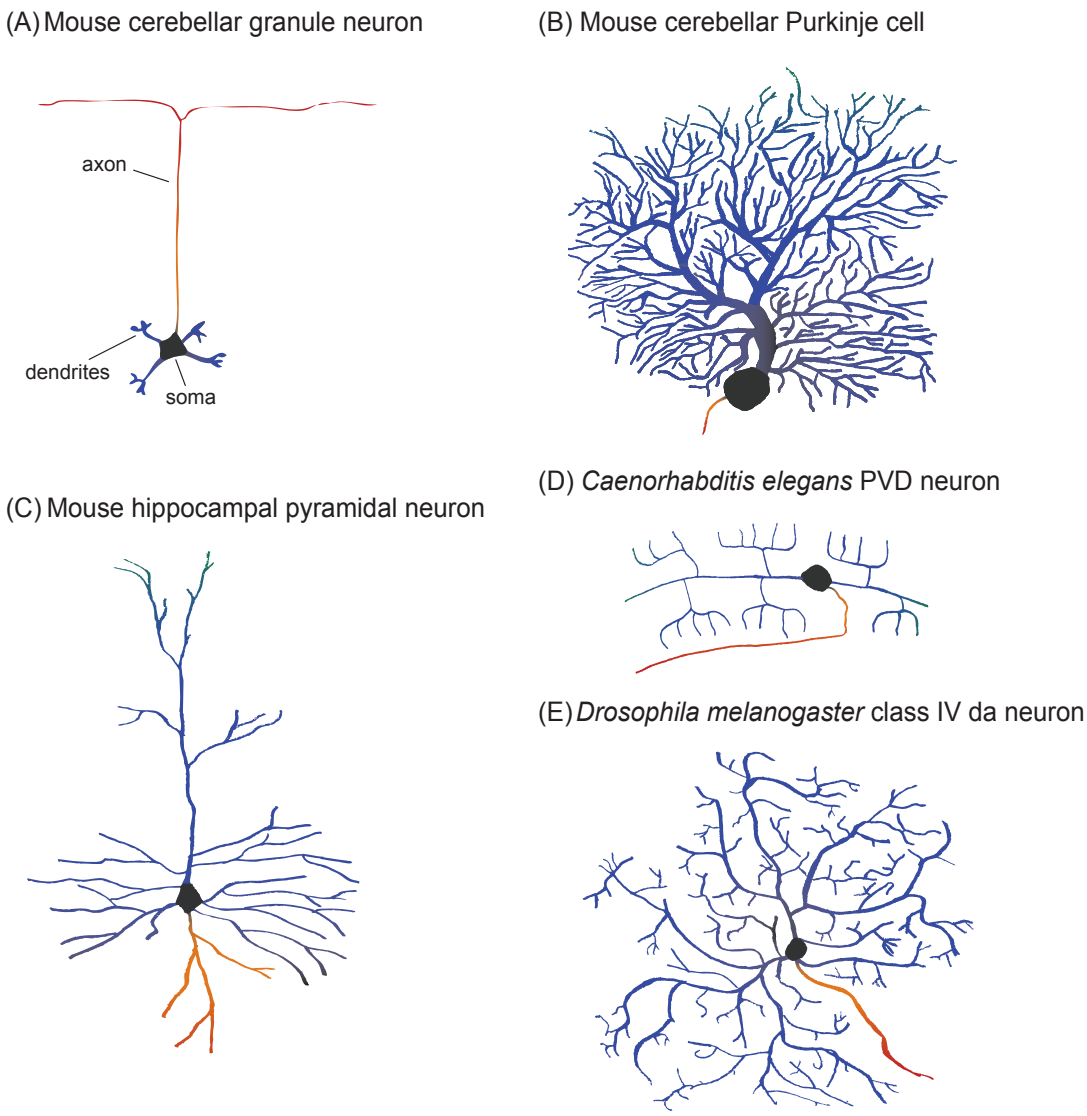

Figure 1.1: Neuronal structure is conserved across cell types and species. Schematics of neurons in mice **(a-c)**, worms **(d)**, and fruit flies **(e)**, each exhibiting dendrites (blue/green), a cell soma (gray), and an axon (orange/red). **Figure is modified from Figure 1, originally published by Pamela Valnegri, Sidharth V. Puram, and Azad Bonni, *Trends in Neurosciences*, 2015.**

Dendrites establish receptive fields

A central property of neurons in the brain and sensory neurons in the periphery is that each neuron contains a receptive field, the area from which a neuron receives input. In the brain, the receptive field is the area from which a neuron receives input from other neurons. In the skin, the receptive field of a sensory neuron is the exact area of the epithelium that activates the neuron. Receptive fields, then, are dictated by the localization of the neuron's dendrites. During development, dendrites must navigate the extracellular space to find their targets, where they will receive input, whether in the sensory epithelium to sense external cues or in the brain to receive signals from the axon of another neuron. To establish the receptive field, dendrites of the same neuron must avoid each other in a process known as self-avoidance (**Figure 1.2a**[4]). In addition to not overlapping with sister dendrites, dendrites of neurons of the same type also avoid overlapping in a process known as tiling (**Figure 1.2b**[4]).

Abnormalities in the development of dendritic size, spine number, and guidance have been implicated in intellectual disabilities (ID)[5], autism spectrum disorders (ASD)[6,7], schizophrenia[6,8,9], major depressive disorder (MDD)[10–14], and bipolar disorder[9]; loss of dendritic spines and dendrite reorganization is a characteristic of Alzheimer's disease[6,15–20]. Therefore, the understanding of dendrite development, stabilization, and maintenance is imperative for understanding the underlying mechanisms of disease, developing therapeutic targets, and eventually finding cures for these diseases.

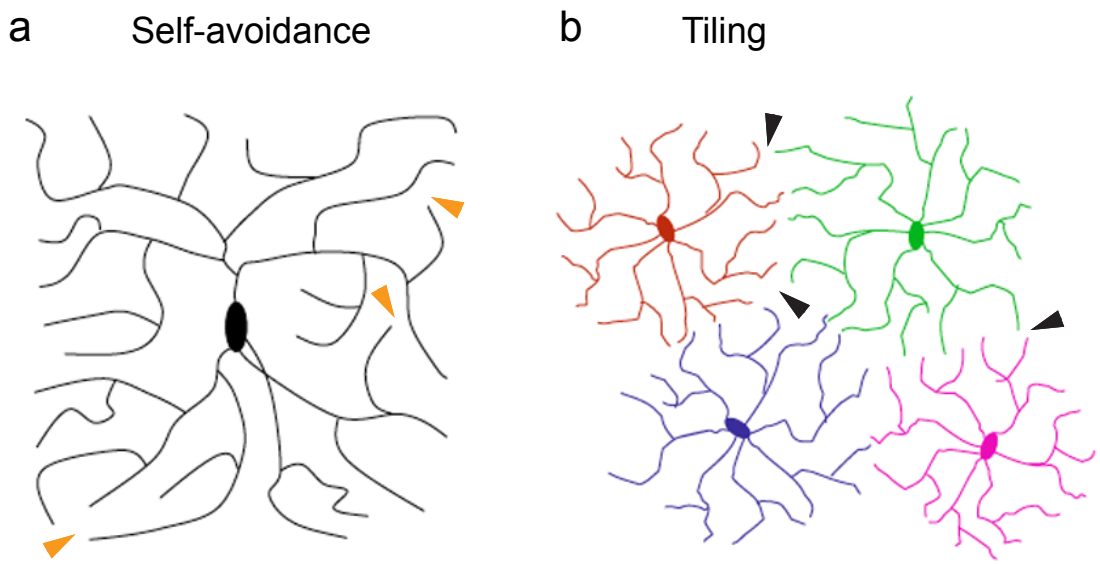

Figure 1.2: Self-avoidance and Tiling. Schematics of the dendrites of *Drosophila* class IV da neurons exemplifying self-avoidance **(a)** and tiling **(b)**. Examples of specific locations of self-avoidance and tiling are marked with orange and black arrowheads, respectively. **Schematics were originally published by Scott Cameron and Yong Rao, *Molecular Brain*, 2010.**

The PVD neurons in *C. elegans* are models for studying dendrite morphogenesis

The nematode *C. elegans* has been used as a model organism for studying the development of neuronal cells[21,22]. The entire cell-lineage of *C. elegans* is known[22–25], and the genome is completely mapped[26], making it a useful tool for studying genetics and cellular mechanisms. There is little redundancy in the *C. elegans* genome, allowing for ease of genetic manipulation and interpretation. For example, *C. elegans* has only one gene for Netrin (*unc-6*)[27], while mammalian genomes contain many different Netrin genes (Netrin-1, Netrin-3, Netrin-4, Netrin-G1, Netrin G2)[28]. Additionally, the nervous system is simple, consisting of only 302 neurons in hermaphrodites and 385 neurons in males, with a completely mapped connectome[22]. Furthermore, the worm is transparent, allowing for easy visualization of cells and cellular development, especially when labeling cells with fluorescent reporters. Cellular development can be traced throughout the life of the worm, from the embryo in the transparent egg, through the four larval stages (L1, L2, L3, and L4), as well as early and late adulthood. These qualities make *C. elegans* an ideal model for studying the genetics of neuron development.

A pair of nociceptor neurons in *C. elegans,* PVDL and PVDR, display an elaborate dendritic arbor[29,30] with a well-ordered developmental pattern in which dendrites adopt orthogonal angles as they branch in a stepwise manner from the cell body to the skin (Figure 1.3[29]). PVD dendrite morphogenesis initiates during the L1 larval stage with the outgrowth of primary (1°) dendrites projecting anteriorly and posteriorly from the cell body along the lateral nerve cord. Next, secondary (2°) branches emerge at right angles to the 1° process to extend along the dorsal/ventral axis. Upon reaching the sublateral nerve cord, 2° dendrites sprout tertiary (3°) branches that extend laterally and in parallel to the 1° branches. Toward the end of

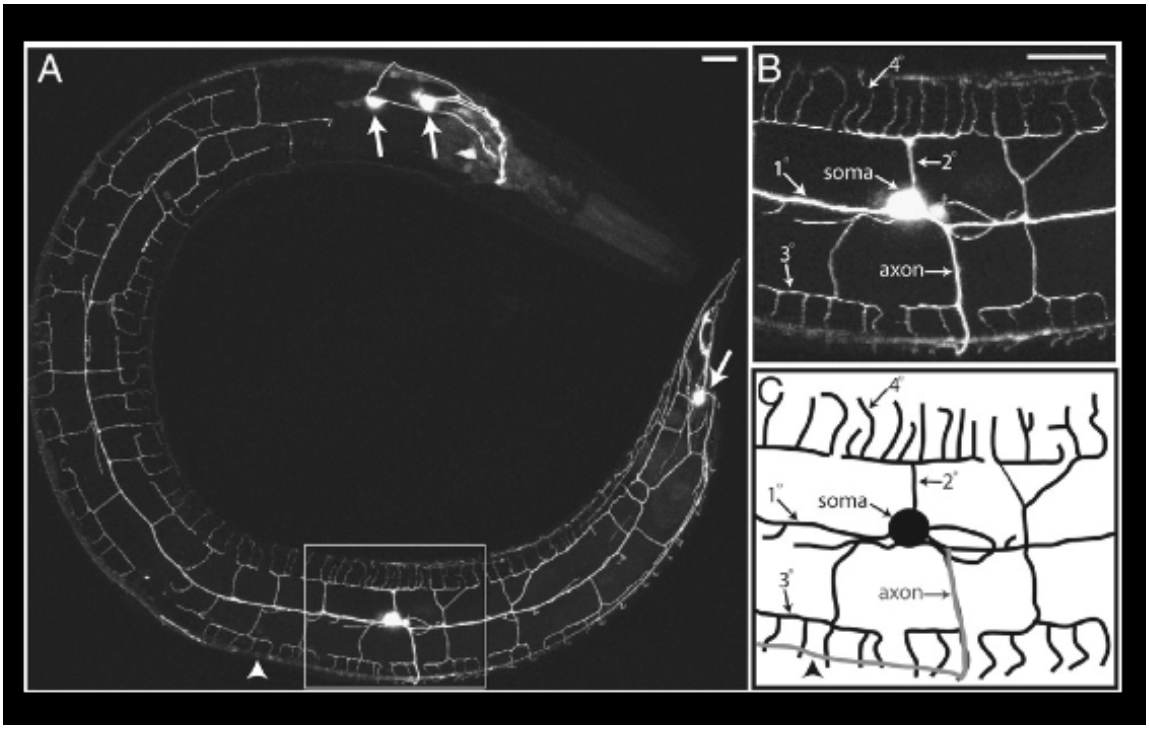

Figure 1.3: The PVD neuron in *C. elegans.* (a-b) Confocal image of an adult worm showing the PVD::GFP marker, with 1°, 2°, 3°, and 4° branches noted in **(b)**, **(c)** schematic highlighting branches. Left is anterior, up is dorsal, scale bar = 15 μm, arrowheads in **a** and **c** denote the axon in the ventral nerve cord, arrows in **a** denote other neurons in the head and tail that express GFP. **This figure was originally published by Cody J. Smith, et al., *Developmental Biology*, 2010.**

PVD development in the L4 larval stage, finger-like 4° branches are generated in the subdermal space between skin and body muscle cells (**Figure 1.4**[31]). Specifically, each 2° branch gives rise to a set of 3° and 4° dendrites that form a distinct candelabra- or menorah-like structure, where the 2° branch is like the base and the 4° branches are like the candles. The gap that separates adjacent menorahs arises from contact-dependent self-avoidance of 3° branches during PVD morphogenesis[29]. Further characterizations of this neuron revealed asymmetry in that PVD-R on the right side of the animal possesses more 2° branches than PVD-L on the left side of the animal; additionally, within each neuron, dorsal 2° branches outnumber ventral 2° branches[29,32].

The *C. elegans* mechanosensory network

The six touch receptor neurons (ALM-L/R, PLM-L/R, AVM, and PVM) were originally identified through ablation studies, whereby ablation of these neurons, either by laser surgery or mutation, resulted in defects in response to light touch[33]. In that study, it was also discovered that these cells could be distinguished from other cells by the size and number of microtubules when reconstructed by electron microscopy (EM)[33]. In fact, the six touch neurons were originally called "microtubule cells" because their dense microtubule staining made them easily identifiable by EM. The function of each touch receptor neuron (TRN) was identified in additional work through a series of ablation and behavioral experiments, where individual cells were ablated with laser microsurgery after hatching and the worms were subsequently touched with an eyebrow-hair pick on either the head, vulva, or tail[34]. It was found that PLM-L/R mediates the response when the tail is touched and ALM-L/R, AVM, and PVM mediate the response when the head is touched. Of note, ablation of all six touch receptor neurons resulted in

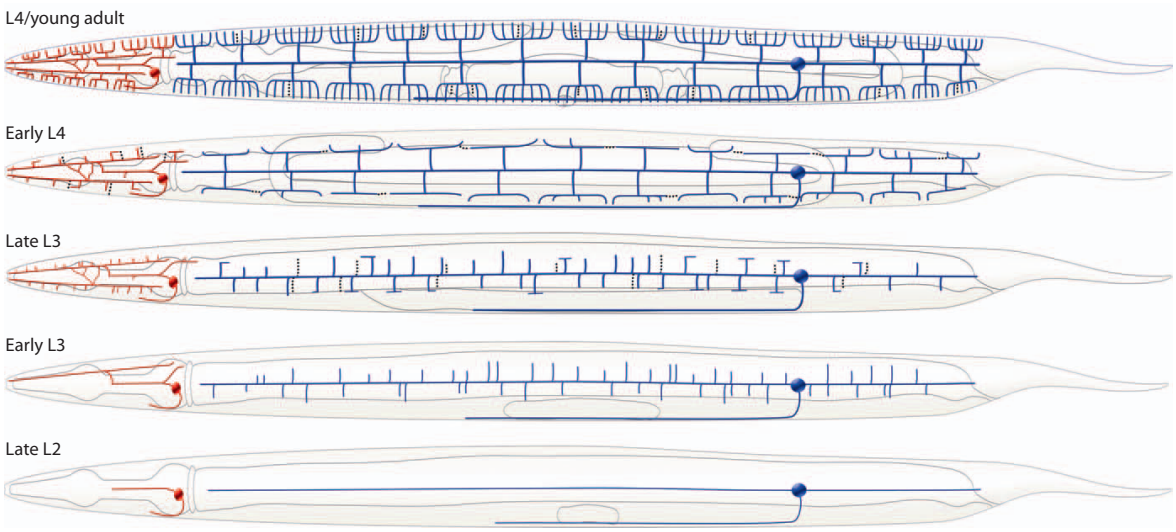

Figure 1.4: *C. elegans* PVD and FLP dendrite development. Schematics of PVD (purple) and FLP (red) throughout the larval stages (L1-L4) of the worm. Note, also, that PVD and FLP exhibit tiling. Left is anterior, up is dorsal. **This figure was originally published by David H. Hall and Millet Treinin, *Trends in Neurosciences*, 2011.**

no response anywhere in the worm, except at the tip of the nose. This suggests a "non-microtubule" cell senses that area[34]. The six touch neurons mediate a response by activating interneurons (AVA, AVB, PVC, and AVD) that then synapse onto muscle cells to mediate movement[35].

Unlike the six light touch neurons described above, the PVD and FLP neurons sense harsh touch[36] and are not "microtubule cells." They are, however, also mechanosensory neurons and were first noted as "mec" cells due to their expression of *mec-3* (see MEC-3 section below)[36]. The PVD neuron is derived post-embryonically, making it an ideal neuron to study, as the full development from the initial generation of the cell can be studied[24], while FLP arises six hours prior to hatching in animals grown at 20°C[25]. Both PVD and FLP have an axon that extends into the ventral nerve cord to synapse onto interneurons and mediate forward and backward movement[22]; specifically, PVD synapses onto AVA and PVC interneurons. PVD is not considered part of the "touch" network because when all the "touch" neurons were ablated, the worms no longer responded to soft touch by the hair-pick; however, these worms still responded to "harsh touch"[37]. Conversely, when PVD neurons were ablated, the animals no longer responded to probing with a platinum wire at the mid-body. This "harsh touch" phenotype was absent in *mec-3* mutants, demonstrating that *mec-3* is required for PVD function (see MEC-3 section below)[36]. The exact mechanisms behind how PVD senses the external environment and mediates a response are not well-known[31], but several components that mediate PVD transduction are discussed below.

PVD sensory transduction molecules

PVD is a polymodal nociceptor that senses harsh touch[36–39], cold shock[39], osmolarity[30], and proprioception[30]. In addition to sensing external cues, this neuron may receive cholinergic input because the nAChR subunits DES-2/DEG-3 are expressed in PVD[40,41]. Since PVD functions as a polymodal nociceptor, the question arises as to how the neuron works. Specifically, one question is whether different sets of receptors dictate responses to specific modalities or if the receptors themselves are "polymodal-sensing"[39]. To answer this question, Chatzigeorgiou et al.,[39] examined the role of two well-known protein superfamilies of nociceptor sensory transduction: transient receptor potential (TRP) channels and degenerin/epithelial sodium channels (DEG/ENaCs).

TRP channels are expressed in a variety of neurons and can sense light, sound, chemicals, temperature, and touch[42]. Therefore, the presence of known TRP channels in PVD, OSM-9 and TRPA-1, is consistent with data that PVD is a sensory neuron and provides a starting point for understanding how PVD senses the environment. OSM-9 is a TRPV channel homologous to capsaicin receptors and has been shown to respond to odors in AWC[43] and AWA olfactory neurons[44], as well as being involved in the animal's ability to adapt to salt[45]. Although OSM-9 is expressed in PVD[44], the mechanism of OSM-9 in PVD is not known[39] and requires further investigation. OSM-9 is not required for sensation of harsh touch or cold shock[39], but the evidence of OSM-9's involvement in salt adaptation suggests it may play a similar role in PVD. Another TRP channel, TRPA-1, functions in mechanosensation in the OLQ polymodal neurons located in the head[46]. In PVD, however, TRPA-1 may function as a thermosensor that responds to cold shock[39]. *trpa-1* mutant worms do not show a response to cold-shock, and expressing the

mammalian mTRPA1 protein in PVD showed partial restoration of calcium transients in response to cold temperatures. Furthermore, expression of TRPA-1 in HEK293T cells was sufficient to evoke depolarizing current in cold temperatures, indicating the TRPA-1 channel is a thermal nociceptor.

The DEG/ENaC superfamily of proteins has been shown in a variety of species to mediate mechanosensation, proprioception, and nociception[47]. The DEG/ENaC protein MEC-10 is required for mechanotransduction in touch neurons and is expressed in PVD[48]. In the ALM touch neuron, MEC-10 interacts with the DEG/ENaC channel MEC-4 to form a complex that mediates soft touch[49]. In PVD, MEC-10 associates with the DEG/ENaC channel DEGT-1 to form a complex so that PVD responds to harsh touch[39]. These results indicate that MEC-10 may function as a soft-touch receptor or a harsh-touch receptor, depending on the expression of other DEG/ENaCs in the cell.

TRPA-1 is specific to noxious cold, and MEC-10 and DEGT-1 are specific to harsh touch[39]. This distinction indicates that rather than receptors being "polymodal-sensing," different sets of receptors expressed in PVD are responsible for the polymodal sensation of this neuron. This is supported by evidence that these receptors are localized in different places throughout the neuron: TRPA-1 localization is restricted to the cell body and the proximal dendrites, while MEC-10 and DEGT-1 are localized throughout the PVD dendrites[39].

Transcription factors that mediate dendritic branching

The LIM homeobox transcription factor MEC-3 is required for dendritic branching in PVD

MEC-3 is a LIM homeobox-containing transcription factor expressed in the six touch neurons and the nociceptor neurons PVD and FLP. The *mec-3* gene was first characterized in PVD and FLP by a *mec-3-LakZ* fusion gene reporter[36]. In that study, it was noted that in addition to *mec-3* requiring its own product for expression, a POU homeobox-containing gene, *unc-86,* was also necessary for *mec-3* expression. "MEC" refers to mechanosensory abnormal and belongs to a set of genes that generate, specify, or produce components of touch cells[34]. In touch neurons, *mec-3* was characterized as the "mec" gene that was responsible for production of cellular components necessary for morphology, as *mec-3* mutants were found to have no processes in the six touch neurons. It was noted that *mec-3* was required for PVD function, as *mec-3* mutants failed to respond to prodding with a platinum wire[36]. When investigators surveyed the EM reconstructions of PVD in *mec-3* mutants, they found no morphological defects, indicating that the altered behavior was not a result of a morphological defect[36]. However, in the earliest studies of PVD, the 2°, 3°, and 4° dendrites had not been discovered[22]. It was not until many years later that research showed that the *mec-3* mutation does alter PVD morphology in that *mec-3* mutants lack higher order dendrites[50], which explains the behavioral defect seen in the original study[36]. This was further confirmed with time-lapse imaging that demonstrated 2° branches never develop in *mec-3* mutants[29]. These findings, that MEC-3 is a

transcription factor and that 2° branches do not develop in *mec-3* mutants, suggest that MEC-3 is required for dendrite branch outgrowth.

The TFIIA-like zinc finger transcription factor EGL-46 is required for 2° branch number in PVD

The presence of the homeobox domain in the *mec-3* gene suggests that its biological role is to regulate transcription of other genes[37]. Additionally, the lack of higher order branches in mutants of *mec-3*[29,50] suggests that MEC-3 regulates genes required for branching. To identify MEC-3 transcriptional targets, an mRNA tagging and microarray experiment of *mec-3* mutants compared to wild type was performed[51]. Specifically, the *ser2prom3* promoter, which is expressed in the two PVD cells, the OLL sensory neurons in the head, and the PDE sensory neurons, was used to express a FLAG-tag attached to polyA binding (PAB) protein. *ser2prom3*::3XFLAG::PAB allowed the FLAG-tag to attach to RNA in PVD through the polyA binding protein, which binds to the polyA tail of RNA, and the specificity of the expression in PVD through the *ser2prom3* promoter. The FLAG-tag was then used to isolate tagged RNA from the worm, and the RNA expression levels were compared between wild-type worms and mutants of *mec-3*. That study showed that the TFIIA-like zinc finger transcription factor EGL-46 is a target of MEC-3. In PVD, mutants of *egl-46* show a decrease in the number of 2° branches[29,51,52], suggesting that EGL-46 is also involved in higher order branching, though to a lesser extent than MEC-3.

EGL-46 has been shown to act with the TEA domain transcription enhancer factor EGL-44 to determine HSN cell-specialization[53], HOB cell-specific traits and male mating behavior[54],

touch cell specific genes[55], and cell cycle exit[56]. In a screen for genes affecting hermaphrodite-specific neurons (HSN), genes were categorized as affecting the generation, identity, sex-specificity, specialization, migration, function, serotonin expression, or axonal outgrowth of these neurons[53]. Mutation of the HSNs often resulted in egg-laying defects, which is why genes discovered that affect this process are referred to as "egl." EGL-44 and EGL-46 were found to be downstream of sex-specific survival. The defects in these mutants showed such variation that these genes were placed in the broad category of "cell specialization"[53]. It is now known that EGL-44 and EGL-46 are transcription factors, which explains why they did not show a specific defect in that original study where they were discovered. Later studies in the male-specific HOB neuron showed that expression levels of the polycystins LOV-1/PKD1 and PKD-2/PKD2, which are required for vulva location behavior in male *C. elegans*, were decreased in mutants of *egl-44* and *egl-46*[54]. The homeodomain protein PROS-1/prospero/Prox1 and the neuropeptide-like protein NLP-8 were also decreased in mutants of *egl-44* and *egl-46*. Finally, one study showed that EGL-44 and EGL-46 physically interact in a yeast two-hybrid system, where it was suggested that the TEA domain of EGL-44 may bind to the three zinc-finger motifs of EGL-46[56]. These studies reveal a role for EGL-44 and EGL-46 in regulating genes required for cell-specificity.

In FLP, EGL-44 regulates EGL-46 to suppress the touch cell-specific genes *mec-4*, *mec-7*, and *mec-18*[55]. That study revealed a complex relationship between EGL-44, EGL-46, and MEC-3 because MEC-3 promotes touch cell-specific genes that are then suppressed by EGL-44 and EGL-46 in FLP. In PVD, both EGL-44 and EGL-46 are upregulated in PVD compared to other cells in the worm[29], but only EGL-46 is regulated by MEC-3, while EGL-44 is not

regulated by MEC-3[51]. Given the evidence that EGL-44 and EGL-46 act together in so many contexts, it is likely that these two transcription factors work together in PVD.

Additional transcription factors involved in dendritic branching

In addition to MEC-3 and EGL-46, other transcription factors have been identified that regulate the elaborate dendritic architecture in other animal models, particularly in the fruit fly *Drosophila melanogaster* dendritic arborization (da) neurons[57]. These neurons are classified from class I to class IV, based on increasing dendritic complexity (**Figure 1.5**[58])[57,59]. The precise classification of da neuron dendritic arborization makes this group of neurons an ideal model for studying how transcription factors and their downstream effectors mediate dendrite development across neuronal types. By studying the effect of a protein that is endogenously expressed in one class of neuron on a different class of neuron where it is not normally expressed, the mechanism of how that protein dictates neuron morphology can be defined. For example, if a protein is required for suppression of excess branches in class I da neurons, then expression of that protein in a class IV da neuron would result in less branches in the class IV da neuron. Such experiments have been performed with the transcription factors Abrupt, Knot, Cut, and Spineless and are discussed briefly below.

Abrupt and Knot/Collier

The BTB-zinc finger transcription factor Abrupt (Ab) is expressed in class I neurons to promote a simplistic dendritic morphology in these cells[60,61]. Loss of Abrupt in class I neurons leads to complex dendrite arborization, whereas overexpression of Abrupt in class II-IV da

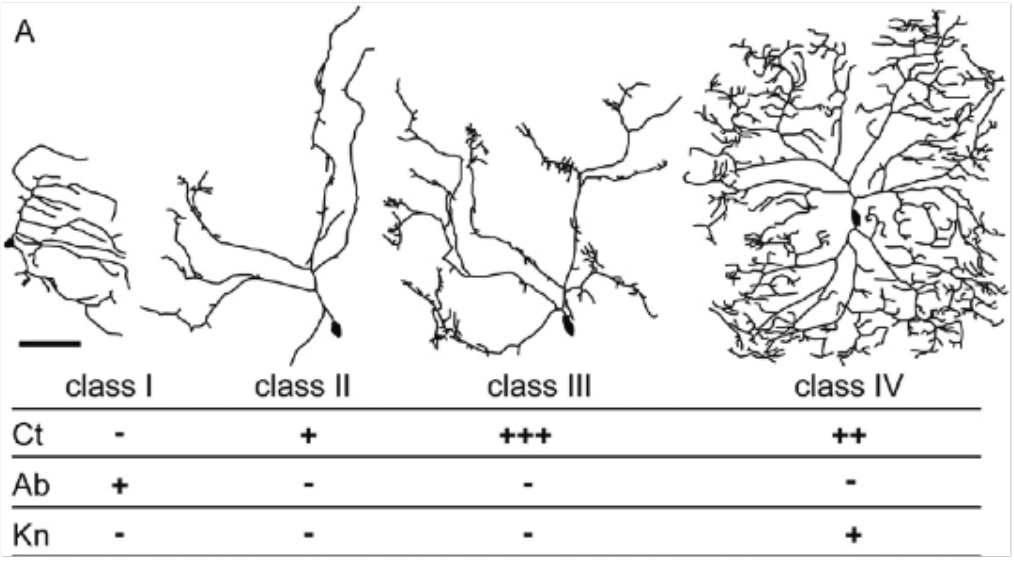

Figure 1.5: Dendritic arborization (da) neurons in *Drosophila melanogaster*. Tracings of simplistic (class I) to complex (class IV) da neurons of the fruit fly, with relative levels of the transcription factors Cut (Ct), Abrupt (Ab), and Knot (Kn). Protein expression level is indicated as none detected (-), low (+), intermediate (++), and high (+++). Scale bar is 75 mm. **This figure was originally published by Shiho Jinushi-Nakao et al., *Neuron*, 2007, adapted from Wesley B. Grueber, Lily Y. Jan, and Yuh Nung Jan, *Development,* 2002.**

neurons results in simplified dendrite morphology. Conversely, Knot (Kn, also called Collier), a member of the COE family of transcription factors, is expressed in class IV neurons to promote complex dendrite arborization[58,62,63]. Expression of Knot/Collier in class I-III da neurons results in complex dendrite morphology. Teneurin-m (ten-m) is a transmembrane cell-adhesion molecule that is a common gene target for both Abrupt and Knot[64]. Ten-m is expressed at high levels in class I neurons and low levels in class IV neurons. That these two transcription factors share a common target gene expressed at different levels in their respective cells suggests that transcriptional regulation plays a major role in the complexity of dendritic arborization.

Cut

Cut is a homeodomain transcription factor expressed in class II-IV da neurons at varying levels, with the highest expression in class III neurons. Overexpression of cut in class II neurons results in a class IV-like dendrite morphology[65]. *Cux1* and *Cux2* are the conserved mammalian homologs of *Cut* and promote dendritic branching in cortical pyramidal neurons[66]. Expression of mammalian *Cux1* and *Cux2* can rescue defects seen in *Cut* mutants in *Drosophila*, suggesting strong conservation of the function of these proteins across species[65]. Additionally, expression of Cut leads to the formation of actin-rich dendrite spikes by promoting the actin-bundling protein fascin[67]. This suggests that Cut promotes dendrite outgrowth by promoting actin-associated proteins that result in dendrite protrusion. This would also suggest that an increase in Cut would lead to an increase in dendritic outgrowth; however, as noted above, the highest expression of Cut is in the class III neurons, not the class IV neurons. The mechanism of how Cut regulates dendrite branching is, therefore, not straightforward, and more research in this area is required

for understanding how levels of a transcription factor may be correlated to levels of dendrite complexity.

AhR/Spineless

The basic helix-loop-helix transcription factor aryl hydrocarbon receptor (AhR/AHR-1/Spineless) is required for the simplistic arborization of class I da neurons and for the complex arborization of class IV da neurons[68]. The exact mechanisms whereby AhR/AHR-1/Spineless regulates dendritic branching appears to be complex because loss of Spineless can cause increased or reduced number of branches: loss of Spineless in class I da neurons leads to increased dendrite complexity, while loss of Spineless in class IV neurons results is decreased dendrite complexity. A similar phenomenon was seen in mutants of *ahr-1* in *C. elegans*. In *C. elegans*, AHR-1 is expressed in the touch neuron AVM to promote *mec-3* while simultaneously inhibiting MEC-3 targets that promote branching[51]. In mutants of *ahr-1*, the AVM touch neuron shows increased dendrite morphology, similar to that of PVD.

One possibility is that Spineless is not so much involved in dendrite branching as it is in cell fate. Indeed, the study described above argues that in *ahr-1* mutants, AVM becomes PVD (termed cAVM for "converted AVM") because there is a loss of touch cell-specific expression of MEC-4[51]. In *Drosophila* da neurons, however, class-specific expression of Abrupt and Cut were normal in *Spineless* mutants, suggesting Spineless does not determine cell fate in that context[68]. These studies suggest that the involvement of AhR/AHR-1/Spineless in dendritic arborizatoin and complexity may depend on the specific cell in which it is expressed and other factors expressed in those cells. For example, as discussed in an earlier section, MEC-10 acts with MEC-4 in the ALM touch neuron to mediate soft touch while acting with DEGT-1 in PVD to

mediate harsh touch. Perhaps the role of transcription factors is similarly dependent on expression of co-effectors in the cell of interest.

Components of dendrite outgrowth and stabilization

During development, dendrite outgrowth is a dynamic process that involves constant protrusion and retraction as dendrites navigate the extracellular space to reach their targets[69–71]. Once neurons have fully developed, morphology of dendrites is, for the most part, stabilized and maintained throughout the life of the animal[72–74]. Any changes that do take place occur at discrete locations. The dynamics of dendrite outgrowth are meditated by both intracellular and extracellular components. This section will briefly cover the major cytoskeletal components, microtubules, motor proteins, actin, and actin-associated proteins, as well as guidance cues, such as UNC-6/Netrin and DMA-1/LRR, that are involved in dendrite outgrowth.

Cytoskeletal components

Microtubules and motor proteins

Unlike axons, where microtubules (MT) are polarized with the plus-end furthest from the cell soma and the minus-end oriented toward the cell soma, dendrites are composed of mixed plus-end and minus-end microtubules[75]. This mixed polarity in dendrites may facilitate bidirectional trafficking of proteins that are involved in development and stabilization[75–77]. Microtubule-associated proteins (MAPs) promote MT polymerization and stabilization[78]. In particular increased MAP1A and MAP2 lead to increased dendrite stabilization of rat neuronal

cells in culture[79,80]. Similarly, decreased MAP1B and MAP2 leads to a decreased number of dendrites in mice[81].

In PVD, microtubules are predominantly found in the 1° branches, while actin is the predominant structural component of 2°, 3°, and 4° branches[82]. Proteins are trafficked to axon-specific and dendrite-specific locations, mediated by UNC-33/CRMP (collapsing response mediator protein) and the adaptor protein UNC-44/ankyrin. UNC-44/ankyrin localizes UNC-33L/CRMP to axons to prevent axonal components from entering dendrites. Together, UNC-44 and UNC-33 assemble the microtubule distribution in PVD to sort dendrite- and axon-specific cellular components to their respective branches.

Kinesin and dynein are MT motor proteins that traffic cellular components along microtubules in the anterograde and retrograde directions, respectively. MT motor proteins are also required for dendrite outgrowth and stabilization[78,83]. Distal (from the vulva to the pharynx) PVD 4° branches may be positively regulated by the dynein regulator BICD-1/BicaudalD, the dynein heavy chain homolog DHC-1, and the kinesin-1 heavy chain ortholog UNC-116[84]. Consistent with mixed MT polarity in dendrites, *bicd-1* and *unc-116* may act in the same genetic pathway, since double mutants of *bicd-1* and *unc-116* do not show a significant difference in the number of 4° branches from either single mutant alone. Intriguingly, *bicd-1* may act in a parallel pathway to *dhc-1* and *unc-116* to block aberrant ectopic branching originating off of 2° branches posterior to the cell soma.

Actin

Filamentous actin (F-actin) is the predominant driver of dendritic growth and stabilization of 2°, 3°, and 4° branches in PVD[82]. While the pathways regulating F-actin in PVD

dendrite outgrowth and stabilization have not been extensively studied, the actin binding protein enabled/VASP homolog UNC-34 has been shown to be required for proper 1°, 2°, and 3° branch development[32]. Intriguingly, UNC-34/enabled/VASP is specifically required for 3° branch retraction downstream of UNC-6-mediated contact-dependent self-avoidance (see UNC-6/Netrin section). This result is counter-intuitive because actin polymerization is typically associated with outgrowth, not retraction. However, mutants of *unc-34* and other actin regulators, *wsp-1*/WASP and subunits of the ARP2/3 complex, *arx-5/*p21 and *arx-3*/p41, all demonstrate self-avoidance defects (Sundararajan, et al., personal communication). Time-lapse imaging of GFP-tagged F-actin supports the hypothesis that actin is required for 3° branch retraction by showing an increase in fluorescent signal upon contact between two sister 3° branches. This retrograde flow of F-actin during retraction may be mediated by NMY-1/non-muscle myosin II and its regulatory light chain MLC-4.

During cell fusion events in embryonic development, WASP-Arp2/3-dependent actin polymerization recruits the fusogen EFF-1 to the plasma membranes of two fusing cells through the actin-binding protein spectraplakin/VAB-10A[85,86]. In PVD, however, EFF-1 acts cell-autonomously to dictate branch pruning, with *eff-1* mutants displaying excess and disorderly branches[87]. In that study, it was proposed that EFF-1 induces retraction to simplify menorahs. How or if EFF-1 fits into the actin-regulated 3° branch retraction model described above remains to be determined.

Lamellipodin/Lpd has been shown to be an enabled/VASP binding partner in cell culture[88]. The Lamellipodin/Lpd *C. elegans* homolog MIG-10 and the enabled/VASP homolog UNC-34 function together in UNC-6 dependent pathways to regulate axonal growth cone guidance[89,90]. Work in the Miller Lab has confirmed that both UNC-34/VASP and MIG-10/Lpd

are required for PVD self-avoidance but that these components function in parallel pathways, with UNC-34 acting downstream of UNC-6[32]. Double mutants of the UNC-6 receptor *unc-5* and *mig-10* show enhanced self-avoidance, whereas no enhancement was observed for double mutants of *unc-5* and *unc-34*. The potential for complementary roles for MIG-10 and UNC-34 is underscored by the finding that *mig-10;unc-34* double mutants are embryonically lethal. These findings suggest there is a more complex relationship between actin and 3° branch self-avoidance that remains to be elucidated.

Extracellular interactions

UNC-6/Netrin

UNC-6/Netrin is a ventrally secreted guidance cue that has been studied extensively in axon guidance[91]. UNC-6 binds to the receptor UNC-40/DCC to mediate an attractive response, whereas the UNC-5 receptor or the UNC-40/UNC-5 heterodimer drive growth cone repulsion in response to UNC-6. A previous study from the Miller Lab demonstrated that self-avoidance of sister 3° PVD dendrites is UNC-6-dependent[52]. Mutations in *unc-6*, *unc-5*, or *unc-40* each result in a self-avoidance defect whereby 3° branches from adjacent menorahs fail to retract upon mutual contact. This work also showed that UNC-6 could function in this pathway as a short range cue where UNC-40/DCC captures YFP-labeled UNC-6 on the surface of PVD dendrites. Thus, a model was proposed in which UNC-40 captures UNC-6 for presentation to UNC-5 in the opposing 3° dendrite, which then drives retraction.

As noted above, actin polymerization is required for self-avoidance and acts downstream of UNC-5[32]. This result is supported by evidence from the Miller Lab showing constitutively

active UNC-5 (MYR::UNC-5) leads to hyper-retraction, where sister dendrites, upon contact, not only avoid each other but increase the space between them (Sundararajan et al., personal communication). This effect is suppressed in mutants of *unc-34* that contain MYR::UNC-5. Furthermore, double mutants of *unc-6* and *wsp-1* show similar 3° branch overlapping defects that are not significantly different than either single mutant, suggesting a role for actin polymerization in the UNC-6 dependent pathway for self-avoidance.

Intriguingly, UNC-5 has also been implicated in promoting distal anterior 4° branch outgrowth and suppressing ectopic branching initiating off of posterior 2° dendrites[84]. Mutants of *unc-5* show decreased distal 4° branches in the anterior portion of the worm. The dynein regulator BICD-1/BicaudalD may act in parallel to UNC-5 to suppress ectopic branching posterior to the PVD cell body, as double mutants of *bicd-1* and *unc-5* show increased ectopic branches compared to either single mutant. The authors concluded, however, that the role of UNC-5 in PVD ectopic and 4° branching is complex and merits further investigation. They suggested that even though the evidence supports a model whereby UNC-5 and BICD-1 act in parallel pathways, BICD-1 may still be involved in transport of the UNC-5 receptor. Furthermore, the role of UNC-5 in this context may be UNC-6-independent, as *unc-6;bicd-1* double mutants do not show increase ectopic branches compared to either single mutant, indicating BICD-1 is downstream of UNC-6 but not UNC-5.

DMA-1/Leucine-rich repeat transmembrane protein

During the L2 larval stage of development, 2° branches begin to emerge from the 1° branches, and this process is regulated by the LIM homeodomain transcription factor MEC-3[29].

DMA-1/LRR[92] and HPO-30/Claudin[51] are two downstream components of MEC-3 that have been implicated in 2° branch stabilization.

The leucine-rich repeat (LRR) transmembrane protein DMA-1/LRR functions cell-autonomously in PVD to regulate 2° branching: *dma-1* mutants show decreased 2° branches, a defect which is rescued by expression of *dma-1* cDNA in PVD[92]. *dma-1* mutants also show loss of harsh touch response, indicating DMA-1 is necessary for PVD function. Also, overexpression of DMA-1/LRR in PVD induces increased branching. Prevention of overexpression of DMA-1/LRR is regulated by the proprotein convertase KPC-1/Furin, which downregulates DMA-1/LRR during 2° branch outgrowth[93]. Similarly, mutants of *kpc-1* show defects in 2° branch outgrowth[94]. A recent study in the Miller Lab showed that KPC-1/Furin and DMA-1/LRR act in a pathway parallel to the UNC-6/Netrin pathway for self-avoidance (Sundararajan et al., personal communication). Double heterozygous mutants of *kpc-1/+;unc-6/+* show increased 3° branch overlap, and this defect is suppressed in *kpc-1/+;unc-6/+;dma-1/+* triple heterozygous mutants. This finding also supports the model where KPC-1/Furin downregulates DMA-1/LRR to prevent excess dendrite growth.

When an accumulation of unfolded or misfolded proteins occurs in the lumen of the endoplasmic reticulum (ER), the transmembrane sensor, inositol requiring enzyme 1 (IRE1), activates the unfolded protein response (UPR) to halt protein production and either discard or correct the misfolded proteins. DMA-1/LRR localization in PVD is dependent on the UPR sensor IRE-1[95,96]. Mutants of *ire-1* show severe dendrite morphology defects, indicating that the UPR pathway is required for normal dendrite development. The GTPase RAB-10 is also required for proper trafficking of DMA-1/LRR[97,98] in the 1° branches of PVD.

The stabilization of 2° branches occurs through a multi-protein complex, whereby the cell adhesion molecule SAX-7/L1CAM and the transmembrane protein MNR-1/FAM151 form a complex in the hypodermis and activate DMA-1/LRR, expressed at the tips of the PVD dendrites, to lead to 2° branch stabilization[99,100]. The affinity of this SAX-7/MNR-1/DMA-1 tripartite complex is increased with the muscle-derived secreted cue LECT-2/LECT2[101,102].

The guidance and stabilization of 4° branches between the muscle and the skin also depends on the DMA-1/SAX-7/MNR-1/LECT-2 complex through guidance by SAX-7 "stripes" that are determined by proteins expressed in the muscle[103,104]. Liang, et al.,[103] published a study providing evidence for a model whereby UNC-112/Integrin in the muscle sarcomere determines the spatial pattern of UNC-52, a proteoglycan in the basement membrane. UNC-52 then dictates the localization of the hemidesmosome MUA-6, an intermediate filament. In turn, MUA-6 excludes SAX-7/L1CAM, forming "stripes." SAX-7 would then interact with DMA-1, as shown in previous work[99,100]. After 4° branches grow along the SAX-7/L1CAM stripes, the receptor tyrosine phosphatase CLR-1 acts in the SAX-7/MNR-1/DMA-1 pathway to stabilize 4° branches after outgrowth[104].

DMA-1/LRR has also been implicated in 1° branch development. Little work has been done to show how 1° branch initiation and stabilization occurs, but Liu et al.,[104] provided evidence that CLR-1 may be involved. Though *clr-1* mutants did not show 1° branch defects alone, mutations of *clr-1* severely enhanced the 1° branch truncation phenotype of *sax-7, dma-1,* or *mnr-1* mutants, suggesting that these components act together in the outgrowth or stabilization of the PVD 1° branches.

Additional components required for dendrite morphogenesis

The components necessary for dendrite morphogenesis outlined in this section have been described as they relate to PVD. Many other components have been shown to be involved in dendrite morphogenesis in other *C. elegans* neurons as well as neurons of other species. For example, Slit-Robo guidance is required for cortical dendrite development in mice[105], *Drosophila*[106,107], and dendrite self-avoidance in cerebellar Purkinje cells[108]. Down Syndrome cell adhesion molecules (DSCAM) genes[109] and the hemophilic cell-adhesion protocadherin genes[110] also regulate dendrite self-avoidance in *Drosophila*, mouse retina, and cell culture. Semaphorin 6a (Sema6a) and its receptor plexin A2 (PlexinA2) regulate dendritic arborization of starburst amacrine cells in the mouse retina[111]. In depth review of these pathways and their mechanisms is beyond the scope of this introduction. However, the mechanisms of the additional components mentioned here, as well as others[1,78,83,112,113], may prove to be involved in PVD branching as future studies reveal the complex genetic and transcriptional relationships that mediate the development of this polymodal nociceptor in *C. elegans*.

Dissertation Overview

Despite the extensive research undertaken in PVD described in the sections above, many questions remain. Among them are: (1) Can neurotransmission of a nearby neuron affect dendrite development? (2) What are the factors that mediate 1° branch development? (3) HPO-30 promotes pioneer branches; what promotes commissural branches? (4) What are the targets of

MEC-3 that mediate 2° and 3° branch development? The work presented in this dissertation will seek to answer those questions.

The role of an EGF-like transmembrane protein, T24F1.4/c-tomoregulin, in dendrite self-avoidance is investigated in **Chapter 2**. I present a proposed topology of this protein and use a genetic approach to investigate its involvement in PVD dendrite development in the UNC-6/Netrin pathway. My experiments show that T24F1.4/c-tomoregulin does not appear to be necessary for proper 1°, 2°, or 3° branch development. However, the involvement of UNC-6/Netrin, and its receptors, UNC-5 and UNC-40/DCC, along with actin-associated proteins, UNC-34/ENA/VASP and MIG-10/Lpd, in 1°, 2°, and 3° branch development were confirmed. In the **Discussion** section of **Chapter 2**, I provide evidence that an unknown mutation, which causes a shrinker behavioral phenotype, may lead to 3° branch self-avoidance defects.

Previous research done in the Miller Lab demonstrated that a claudin-like protein, HPO-30, promotes pioneer 2° branches[51]. In **Chapter 3**, I build upon this research and identify a complementary pathway that promotes commissural 2° branches. This newly discovered pathway is regulated by the TFIIA-like zinc-finger containing transcription factor EGL-46 and its partner, the TEA domain-containing transcription factor EGL-44. I show that EGL-46 is regulated by MEC-3, using single molecule fluorescent in situ hybridization (smFISH) (**Chapter 3**) and RNA sequencing (RNA-Seq) (**Chapter 4**). The complex relationship between MEC-3 and EGL-46, whereby EGL-46 is simultaneously regulated by MEC-3 and yet redundantly promotes MEC-3 targets, is also explored in **Chapter 3**. I also show that MEC-3, but not EGL-46, is required for 1° branch development (**Chapter 3**) using measurements for defining 1° branch characteristics proposed in **Chapter 2**.

To investigate additional components required for 2° branch outgrowth and stabilization, I describe a *C. elegans* strain I built that is optimized for isolating PVD cells by fluoresce-activated cell sorting (FACS) (**Chapter 4**). From these sorted cells, RNA was extracted, and expression levels were compared between wild-type and *mec-3* mutant worms. The resultant RNA-Seq dataset that identifies MEC-3 targets, some of which are discussed in **Chapter 5**, provides a list of candidates that can be explored in future research.

Ultimately, the work described in this thesis provides new avenues for exploring dendrite development. The connection between GABA signaling in axons of motor neurons and dendrite development of a nearby nociceptor neuron observed in **Chapter 2** has not been previously discovered. Future work exploring this connection may provide evidence for how signaling in one type of neuron can affect development of a different type of nearby neuron. A transcription factor that mediates a pathway specific to dendrite branches that use previously-established axons as tracts for guidance and stabilization (**Chapter 3**) has not been observed in previous studies. Further research to identify the components of this pathway may lead to a better understanding of basic dendrite development in more complex environments such as the mammalian brain, where axons and axon bundles abound. Finally, the dataset presented in **Chapter 4** may provide a better understanding of dendrite morphology that may lead to discoveries of therapeutic targets for diseases of abnormal dendrite development.

CHAPTER 2 : EXPLORING THE ROLE OF THE EGF-LIKE TRANSMEMBRANE PROTEIN T24F1.4/C-TOMOREGULIN IN NOCICEPTOR DENDRITE DEVELOPMENT

Introduction

The receptive field for each sensory neuron is defined by its dendritic arbor in which sister dendrites occupy discrete domains and do not overlap. This phenomenon of dendrite self-avoidance is widely observed for neuron types across species, suggesting that a conserved fundamental patterning mechanism during neural development underlies this proces[31,59]. Two neurons in *Caenorhabditis elegans*, PVDL and PVDR, are model nociceptors for studying the development of dendritic self-avoidance because the PVD neurons exhibit an elaborate but well-characterized dendritic arbor that is readily visible in its location directly beneath the skin[29,30]. As shown in **Figure 2.1a**, 1° dendrites extend from the PVD cell soma and give rise to periodic orthogonal 2° branches, each of which produces a pair of 3° dendrites that project outward in opposite directions along the body axis. In turn, 3° dendrites give rise to terminal 4° branches that grow out between body muscles and skin to generate a series of menorah-like structures emanating from the 1° branch. Notably, 3° branches from adjacent menoraahs rarely overlap despite a period of active growth in which each extends outward toward the other. Work from the Miller Lab has shown that the spacing between 3° branches in adjacent menorahs is maintained by the phenomenon of self-avoidance and that this mechanism depends on the diffusible guidance cue UNC-6/Netrin and its receptors, UNC-5 and UNC-40/DCC[32,52].

UNC-6/Netrin is a ventrally secreted cue that has been studied extensively as a signal for steering in axon guidance: available evidence suggests that UNC-6 binding to the receptor UNC-40/DCC mediates an attractive response whereas the UNC-5 receptor or the UNC-40/UNC-5

heterodimer drive growth cone repulsion in response to UNC-6[91]. A previous study from the Miller Lab showed that self-avoidance of sister 3° PVD dendrites is UNC-6-dependent[52]. Mutations in *unc-6*, *unc-5*, or *unc-40* result in a self-avoidance defect in which 3° branches from adjacent menorahs fail to retract upon mutual contact. The results were consistent with the hypothesis that UNC-6 functions in this pathway as a short-range cue. For example, YFP-labeled UNC-6 decorates mCherry-marked UNC-40/DCC on the surface of PVD dendrites. Thus, a model was proposed in which UNC-40 captures UNC-6 for presentation to UNC-5 in the opposing 3° dendrite, which then drives retraction.

Additional studies have shown that the lamellipodin protein MIG-10 and the Enabled/VASP homolog UNC-34 function together in UNC-6-dependent pathways that regulate axonal growth cone guidance[89,90]. Work in the Miller Lab has confirmed that both UNC-34/VASP and MIG-10/Lpd are required for PVD self-avoidance but that these components may function in parallel pathways, with UNC-34 acting downstream of UNC-6[32] (Sundararajan et al., personal communication).

An independent genetic screen to identify targets of the transcription factor MEC-3, which promotes 2° branching in PVD[29,50], identified an additional component of the self-avoidance pathway that we proposed to function as a cell surface signal[51]. A mutant allele of the *T24F1.4* locus showed an elevated fraction of overlapping PVD dendritic branches[51]. *T24F1.4* contains a C-terminal transmembrane domain and a predicted extracellular EGF-like sequence. A related mammalian protein, tomoregulin, is highly expressed in the nervous system, but its function is largely unknown[114]. Due to the similarity in genetic structure, we refer to T24F1.4 as "c-tomoregulin."

In the current study, we examined the role of *T24F1.4/c-tomoregulin* in PVD 3° dendrite self-avoidance. We found that mutants showed increased overlap between branches in a background-specific manner that could be rescued by cell-autonomous expression of T24F1.4 genomic DNA. Our results also indicated that *T24F1.4/c-tomoregulin* acts in a genetic pathway with *unc-40, unc-34,* and *mig-10*. Furthermore, we used a computational tool to predict the structure of the c-tomoregulin protein and its similarity to human tomoregulin (h-tomoregulin). However, as outlined in the **Discussion** section, a surprising but intriguing finding refutes our model of T24F1.4/c-tomoregulin's involvement in self-avoidance: A mutation in an unknown gene, a mutation of which causes a shrinker behavioral phenotype, causes self-avoidance defects in the absence of the *T24F1.4* mutation; conversely, worms with the *T24F1.4* mutant allele that do not show the shrinker behavioral phenotype do not show 3° branch overlapping defects.

Materials and Methods

Genetic strains

All worms were raised on OP50 *Escherichia coli*-seeded nematode growth medium plates at 20°C according to standard protocol[21]. **Table 2.1** lists the strains used in these experiments.

Table 2.1. Genetic strains used in this study

Strain	Genotype
NC1686	*wdIs51 (F49H12.4::GFP + Punc-119::UNC-119) X*
NC2705	*T24F1.4(tm5213) II; shrinker; wdIs51 (F49H12.4::GFP + Punc-119::UNC-119) X*

NC2961	*wdIs51 (F49H12.4::GFP + Punc-119::UNC-119) X; wdEx952[pBMJO1(F49H12.4::T24F1.4 5ng/ul + ceh22::GFP 15 ng/uL + BSII 80 ng/uL]*
NC3950	*T24F1.4(tm5213) II; wdIs51 (F49H12.4::GFP + Punc-119::UNC-119) X; wdEx952[pBMJO1(F49H12.4::T24F1.4) 5ng/ul + ceh22::GFP 15 ng/uL + BSII 80 ng/uL]*
NC2753	*ex(pT24F1.4::GFP; coel::RFP)*
NC2768	*T24F1.4(tm5397) II; wdIs51 (F49H12.4::GFP + Punc-119::UNC-119) X*
NC2888	*T24F1.4(tm6771)II; wdIs51 (F49H12.4::GFP + Punc-119::UNC-119) X*
NC3038	*wdEx957 [pBMJO2(F49H12.4::T24F1.4::GFP) 5ng/uL + ceh22::GFP 15 ng/uL + BSII 80 ng/uL]*
NC3149	*wdIs51 (F49H12.4::GFP + Punc-119::UNC-119) X; wdEx957 [pBMJO2(F49H12.4::T24F1.4::GFP) 5ng/uL + ceh22::GFP 15 ng/uL + BSII 80 ng/uL]*
NC3147	*T24F1.4(tm5213) II; wdIs51 (F49H12.4::GFP + Punc-119::UNC-119) X; wdEx957 [pBMJO2(F49H12.4::T24F1.4::GFP) 5ng/uL + ceh22::GFP 15 ng/uL + BSII 80 ng/uL]*
NC2972	*unc-5(e152) IV; wdIs51 (F49H12.4::GFP + Punc-119::UNC-119) X*
NC2731	*T24F1.4(tm5213) II; unc-5(e152) IV; wdIs51 (F49H12.4::GFP + Punc-119::UNC-119) X*
NC2971	*unc-40(e271) I; wdIs51 (F49H12.4::GFP + Punc-119::UNC-119) X*
NC2772	*T24F1.4(tm5213) II; unc-40(e271) I; wdIs51 (F49H12.4::GFP + Punc-119::UNC-119) X*
NC2580	*unc-34(gm104) V; wdIs51 (F49H12.4::GFP + Punc-119::UNC-119) X*
NC3001	*T24F1.4(tm5213) II; unc-34(gm104) V; wdIs51 (F49H12.4::GFP + Punc-119::UNC-119) X*
NC2978	*mig-10(ct41) III; wdIs51 (F49H12.4::GFP + Punc-119::UNC-119) X*
NC2973	*T24F1.4(tm5213) II; mig-10(ct41) III; wdIs51 (F49H12.4::GFP + Punc-119::UNC-119) X*
TV15918	*wyIs585 (ser2prom3::myr::mCherry::unc-54 3'UTR, podr-1::gfp) IV*
NC2889	*T24F1.4(tm5213) II; wyIs585 (ser2prom3::myr::mCherry::unc-54 3'UTR, podr-1::gfp) IV*
NC2907	*T24F1.4(tm5397) II; wyIs585 (ser2prom3::myr::mCherry::unc-54 3'UTR, podr-1::gfp) IV*
NC2887	*T24F1.4(tm56771) II; wyIs585 (ser2prom3::myr::mCherry::unc-54 3'UTR, podr-1::gfp) IV*
NC2916	*unc-6(ev400) X; wyIs585 (ser2prom3::myr::mCherry::unc-54 3'UTR, podr-1::gfp) IV*
NF2168	*Pmig-24::venus*
NC2930	*unc-5(e152) IV; Pmig-24::venus*
NC3000	*unc-40(e271) I; Pmig-24::venus*
NC2996	*T24F1.4(tm5213) II; Pmig-24::venus*
NC2933	*T24F1.4(tm5397) II; Pmig-24::venus*
NC2929	*T24F1.4(tm56771) II; Pmig-24::venus*

XE1374	*wpIs39 (Punc-47::mCherry) X*
NC2965	*unc-5(e152) IV; wpIs39 (Punc-47::mCherry) X*
NC2969	*unc-40(e271) I; wpIs39 (Punc-47::mCherry) X*
NC2977	*T24F1.4(tm5213) II; wpIs39 (Punc-47::mCherry) X*
NC2963	*T24F1.4(tm5397) II; wpIs39 (Punc-47::mCherry) X*
NC2966	*T24F1.4(tm56771) II; wpIs39 (Punc-47::mCherry) X*
NC3155	*wdEx992 [pBMJO5(pDPY-7::T24F1.4) 5ng/uL + pmyo::mCherry 1ng/uL + BSII 94 ng/uL]*
NC3156	*wdIs51 (F49H12.4::GFP + Punc-119::UNC-119) X; wdEx992 [pBMJO5(pDPY-7::T24F1.4) 5ng/uL + pmyo-2::mCherry 1ng/uL + BSII 94 ng/uL]*
NC3190	*T24F1.4(tm5213) II; wdIs51 (F49H12.4::GFP + Punc-119::UNC-119) X; wdEx992 [pBMJO5(pDPY-7::T24F1.4) 5ng/uL + pmyo-2::mCherry 1ng/uL + BSII 94 ng/uL]*
CX11480	*kyEx3017 (des-2::mry::Gfp + coel::dsred)*
NC3019	*T24F1.4(tm5213) II; kyEx3017 (des-2::mry::Gfp + coel::dsred)*
NC3046	*unc-6(ev400) X; kyEx3017 (des-2::mry::Gfp + coel::dsred)*
TV12498	*wyIs378 (ser2prom3::myr::GFP::unc-54 3'UTR; prab-3::mcherry; podr-1::rfp) X*
NC2920	*T24F1.4(tm5213) II; wyIs378 (ser2prom3::myr::GFP::unc-54 3'UTR; prab-3::mcherry; podr-1::rfp) X*
NC3189	*T24F1.4(tm5213) II; wdIs51 (F49H12.4::GFP + Punc-119::UNC-119) X*
NC3202	*shrinker; wdIs51 (F49H12.4::GFP + Punc-119::UNC-119) X*
NC3203	*shrinker; wyIs378 (ser2prom3::myr::GFP::unc-54 3'UTR; prab-3::mcherry; podr-1::rfp) X*
NC3204	*T24F1.4(tm5213) II; shrinker; wyIs378 (ser2prom3::myr::GFP::unc-54 3'UTR; prab-3::mcherry; podr-1::rfp) X*
NC3205	*unc-25(e152) III; wyIs378 (ser2prom3::myr::GFP::unc-54 3'UTR; prab-3::mcherry; podr-1::rfp) X*

T24F1.4 plasmids

The *pT24F.14*::GFP plasmid was built to visualize T24F1.4 localization. Overlap PCR of the 3kb region upstream of the *T24F1.4* gene was used to drive GFP and injected into wild-type worms with the co-injection marker *Pcoel*::RFP, which expresses RFP in coelomocytes. The presence of the co-injection marker was used as an indicator that the *pT24F1.4::*GFP plasmid was expressed in that worm.

The plasmids pBMJO1 (*F49H12.4*::T24F.14), pBMJO2 (*F49H12.4*::T24F1.4::GFP), and pBMJO5 (*Pdpy-7*::T24F1.4) were separately injected into wild-type worms (*wdIs51*) by microinjection at 5 μg/μL. Each construct was then crossed into mutant strains by keeping track of the co-injection marker (*Pceh-22*::GFP for pBMJO1 and pBMJO2; *Pmyo-2*::mCherry for pBMJO5). Genotypes were confirmed by single-worm PCR of the single parent that had the co-injection marker and multiple progeny that either did or did not have the co-injection marker to determine mutant status.

Sequencing for three T24F1.4 deletion alleles

Two mutant alleles, *T24F1.4(tm5213* and *tm5397)* were used previously[51]. The Mitani lab at Tokyo Women's University identified an additional allele that deleted the first exon and could serve as the "true null." This new allele, *T24F1.4(tm6771)*, was amplified by PCR and sent off for sequencing using the following primers: 5'-ACCTGGCAAGCACGAAATAC-3' with 5'-GAGACAGACAGGTAGGCCTA-3' and 5'- GGCACCAAAAAGTCGCCGTT-3' with 5' AGGCCTACCGTGAAAATCAC-3' (GeneHunter, Vanderbilt University).

Microscopy

Worms were anesthetized with 15 mM levamisole/0.05 tricaine on a 2% agarose pad in M9 buffer, coverslipped and sealed with 1:1 vasoline/paraplast tissue embedding medium, and imaged with either a Leica TCS SP5 or Nikon A1 confocal microscope with the 40X objective at 1μm-steps. Z-stacks spanning the focal depth of the entire PVD neuron were merged into a

single plane for analysis. All worms were imaged during the L4 larval stage. For all analyses, the experimenter was blinded to the genotype.

1° branch morphology

For 1° branch length analysis, the ratio of 1° branch length to body length was calculated. In wild-type worms, the anterior 1° branch extends from the cell body to the base of the pharynx, and the posterior 1° branch extends from the cell body to the anus. ImageJ software was used to trace the 1° branches and the midline of the body (from the cell soma to the base of the pharynx for the anterior body length; from the cell soma to the anus for the posterior body length). Microsoft Excel was used to create a dendrite/body ratio that is the length of the 1° dendrite divided by the length of the body. Dendrite/body ratios were exported to GraphPad Prism software and compared across groups using Tukey's multiple comparisons test to determine statistical significance.

For 1° branch number analysis, anterior and posterior 1° branches were counted. The percent of the worms with defects were calculated. Because wildtype worms never show additional processes out of the cell body except for the single anterior 1° branch and the single posterior 1° branch, any additional outgrowth from the cell body at the midline was considered an extra 1° branch.

We classified worms as having a 1° branch guidance defect if the 1° branch strayed from the midline to the sublateral nerve cord and either returned to the midline or had 2° branches that crossed the midline to the opposite sublateral nerve cord. Contingency tables were made from

the raw numbers, and Fisher's Exact test was used to compare genotypes using GraphPad Prism software.

2° branch number

All branches that were orthogonal to the 1° branch and reached the sublateral nerve cord were counted as 2° branches. Averages per condition were then compared using GraphPad Prism software with Tukey's multiple comparisons test. Worms with 1° branch defects were excluded from further analysis and not scored for number of 2° branches.

3° branch self-avoidance

Overlap was noted if there was no distinguishable gap between adjacent 3° branches. The percent of overlapping branches was then calculated as the number of overlapping occurrences divided by number of possible overlapping occurrences. Averages per condition were compared with GraphPad Prism software using Tukey's multiple comparisons test. Worms with 1° branch defects were excluded from further analysis and not scored for 3° branch self-avoidance.

Distal tip cell migration

Only defects in phase 2 (ventral-to-dorsal migration) were scored. Both the anterior and posterior gonads of each worm were scored. For the *unc-5(e152)*and *T24F1.4(tm6771)* mutants, 2 animals from each genotype were discarded from analysis due to either lack of one of the

gonadal arms, lack of the *Pmig-24*::venus marker in one or more of the gonadal arms, or because the distal tip cell did not complete phase III (ie, it did not return from the distal location). Contingency tables were made from the raw numbers, and Fisher's Exact test was used to compare each mutant phenotype to wildtype using GraphPad Prism software.

GABA motor neuron axon guidance

To visualize the axon commisures, we used an mCherry marker driven by the UNC-47 promoter; UNC-47 is a vesicular GABA transporter expressed in D-type motor neurons[115]. Axons that obviously left the ventral nerve cord were scored in an all-or-nothing fashion; either they reached the dorsal nerve cord or they did not. Percent defect was calculated for each worm by adding up the axons that failed to reach the dorsal nerve cord and dividing them by the total number of axons that obviously left the ventral nerve cord. The percentages were averaged for each condition and compared with one-way ANOVA with Tukey's multiple comparisons test, using GraphPad Prism software.

Assessment of shrinker phenotype

Worms move by alternating excitatory (cholinergic) and inhibitory (GABAergic) input from motor neurons onto dorsal and ventral muscles. Thus, when a worm is tapped on the head, this alternating excitation and relaxation of muscles on the dorsal and ventral sides will cause the worm to move backwards in a sinusoidal motion. In mutants where GABA (inhibitory) signaling is disrupted, instead of moving backwards when tapped on the head, worms appear to "shrink"

inward toward the mid-body by pulling in the head and tail because of the excess excitation, which causes simultaneous contraction to both the dorsal and ventral muscles[116]. The "shrinker" phenotype is characterized by such behavior. In our study, worms freely moving forward on a plate were tapped on the head and scored for either wild-type sinusoidal backward movement or "shrinker" movement. Contingency tables were made from the raw numbers, and Fisher's Exact test was used to compare each mutant phenotype to wildtype using GraphPad Prism software.

Results

The original goal for the project described in this chapter was to characterize the EGF-like transmembrane protein, T24F1.4/c-tomoregulin, and its role in 3° branch self-avoidance as a component in the UNC-6-dependent pathway. We hypothesized that T24F1.4/c-tomoregulin might function downstream of the receptors UNC-5 and UNC-40. However, tests for physical interaction with UNC-5, secretion of the EGF-like domain, topology, and domain-specific roles of the protein were halted when it became apparent that an unknown shrinker-causing background mutation, not a mutation in T24F1.4/c-tomoregulin, was responsible for the mutant PVD morphology observed in earlier experiments. **It is important to note that the single-mutant worms with the *T24F1.4(tm5213)* allele in this section displayed a shrinker behavioral phenotype that was originally thought to be unrelated to the observed PVD defects (see Discussion).**

T24F1.4/c-tomoregulin was hypothesized to act cell-autonomously in PVD to promote 3° branch self-avoidance

We first replicated the results of the previous study[51], which showed *T24F1.4(tm5213)* (**Figure 2.1d**) displayed increased 3° branch overlap ($p<0.0001$, *wt* vs. *T24F1.4(tm5213)*) (**Figure 2.1c-e**). We expressed genomic DNA for the *T24F1.4* gene under the PVD promoter *F49H12.4* to test our hypothesis that T24F1.4/c-tomoregulin acts cell-autonomously in PVD. We found that this construct rescued the 3° branch self-avoidance defect, supporting our hypothesis that T24F1.4 acts in PVD to promote 3° branch self-avoidance ($p<0.0001$ for *T24F1.4(tm5213)* vs. *T24F1.4(tm5213);PVD::*T24F1.4 and $p>0.05$ for *wt* vs. *T24F1.4(tm5213);PVD::*T24F1.4) (**Figure 2.1e**). However, it is important to note that when the rescue construct (*PVD::*T24F1.4) was crossed into *T24F1.4(tm5213)* mutants, the shrinker-causing mutation was not maintained. Therefore, it cannot be concluded that T24F1.4/c-tomoregulin acts cell-autonomously in PVD (see **Discussion**).

Proposed structure of the T24F1.4/c-tomoregulin protein

The *T24F1.4* gene contains four exons with a cysteine-rich EGF-like domain encoded in the second exon, a transmembrane domain in the third exon, and a canonical YXXΦ short signal sequence in the fourth exon (**Figure 2.2a-b**). Although *T24F1.4* does not contain a canonical signal peptide (as predicted by SignalP[117] and PrediSi[118]), we propose the structure shown in **Figure 2.2a (left)** based on the following three criteria: 1) the C-terminal tail contains positively charged residues consistent with the "positive-inside rule"[119]; 2) the YXXΦ short signal

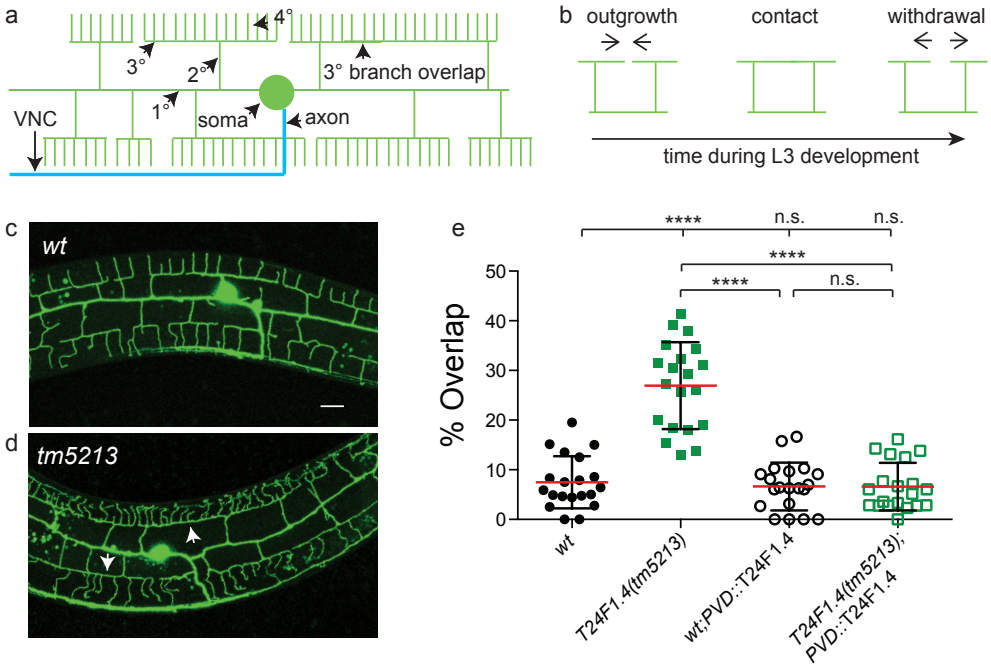

Figure 2.1: *T24F1.4* acts cell-autonomously in PVD to promote 3° branch self-avoidance. **(a)** Schematic of PVD cell and dendrite branch characterization, noting an event of 3° branch overlap, **(b)** schematic of contact-dependent self-avoidance during development, **(c)** confocal image of wild-type worm expressing *PVD*::GFP, **(d)** confocal image of *T24F1.4(tm5213)* mutant worm, white arrowheads denote 3° branch overlap, **(e)** quantification 3° branch overlap. VNC = ventral nerve cord, left is anterior, up is dorsal, scale bar = 10 µm, **** indicates p<0.0001, n.s. = not significant, one-way ANOVA with Tukey's multiple comparisons test, error bars represent SEM, n=20.

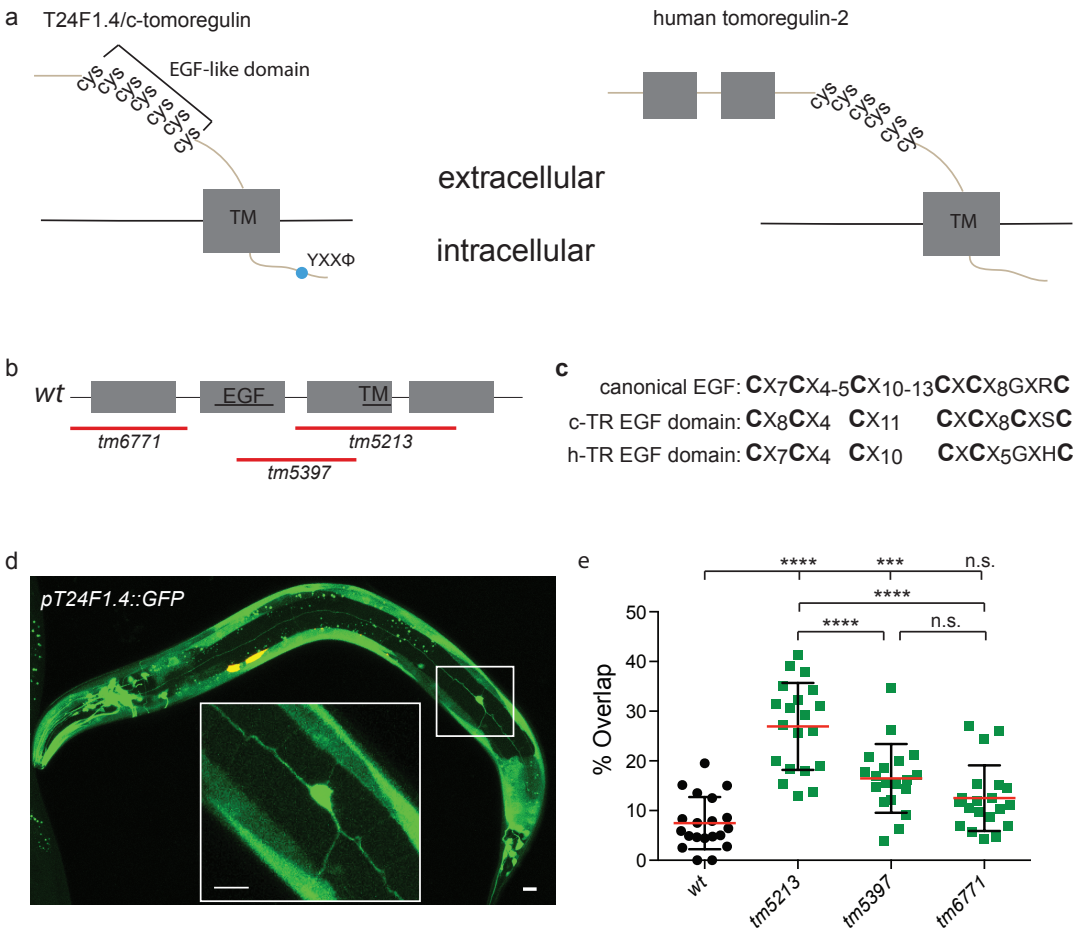

Figure 2.2: T24F1.4/c-tomoregulin is similar to human tomoregulin-2. (a) Proposed structures of T24F1.4/c-tomoregulin (left) and human tomoregulin-2 (right), **(b)** schematic showing locations of the deletions for three available deletion alleles of the *T24F1.4* gene, **(c)** comparison of the EGF-domain sequences, **(d)** confocal image of T24F1.4 expression, as indicated by *pT24F1.4*::GFP, **(e)** quantification of 3° branch overlap across the three alleles show in **(d)**. Data for *wt* and *tm5213* are the same as in **Figure 2.1**. "TM" indicates the transmembrane domain, left is anterior, up is dorsal, scale bar = 10 μm, *** indicates $p<0.001$, **** indicates $p<0.0001$, n.s. = not significant, one-way ANOVA with Tukey's multiple comparisons test, error bars represent SEM, $n\geq19$.

sequence is typically found on cytoplasmic C-termini of proteins located in the cell membrane[120]; and 3) protein modeling software (TOPCONS) predicts that the N-terminus is extracellular and that the C-terminus is located on the cytoplasmic side of the plasma membrane[121].

The BLAST alignment score (1e-06)[122] suggests that *T24F1.4* is most similar to the mammalian protein tomoregulin-2 (**Figure 2.2a, right**). Furthermore, the EGF-like sequence found in *T24F1.4/c-tomoregulin* is similar to the canonical EGF sequence and human tomoregulin-2 (**Figure 2.2c**). Tomoregulin-2 is highly expressed in the brain[114] and has been suggested to function during dendrite outgrowth and as a biomarker for prostate cancer, although the mechanisms for these effects are poorly defined[123–126]. Similarly, the WormVis profile[127] shows that T24F1.4 is highly expressed in neurons during the L2 stage of development. To confirm that T24F1.4/c-tomoregulin is expressed in neurons, a 3kb region upstream of the gene was used to create the *pT24F1.4* promoter and drive green fluorescent protein (GFP). GFP was found throughout the nervous system of the worm (**Figure 2.2d**). Since we propose that T24F1.4 is similar to tomoregulin-2 in both genetic structure and in expression throughout the nervous system, we refer to it as "c-tomoregulin".

Three *T24F1.4/c-tomoregulin* deletion alleles

Two mutant alleles, *T24F1.4(tm5213* and *tm5397)* were described previously[51]. For this study, we obtained an additional *T24F1.4* allele from the Mitani lab at Tokyo Women's University. These three *T24F1.4* alleles are depicted in **Figure 2.2b**; the red lines indicate the deletion in the genetic structure above. We crossed these alleles into the same *PVD::*GFP

cytosolic marker as shown in **Figure 2.1** and quantified the 3° branch overlap. Intriguingly, the three alleles did not show the same phenotype. The 3° branch overlap in the *tm6771* allele showed no defect compared to *wildtype* ($p>0.05$). However, the 3° branch overlap in allele *tm5397* was increased compared to *wildtype* ($p<0.001$) but was decreased compared to *tm5213* ($p<0.0001$) (**Figure 2.2e**). Since *tm5213* showed the most severe phenotype, we selected this allele for subsequent experiments.

c-tomoregulin is expressed throughout the dendrite branches

We next visualized the localization of the protein within PVD by expressing *PVD*::T24F1.4::GFP (**Figure 2.3a**). Although we hypothesized that c-tomoregulin specifically acted at the tips of 3° branches, confocal images showed GFP puncta throughout the branches of both wild-type and mutant worms (**Figure 2.3b**). To determine if this construct was functional, we quantified 3° branch self-avoidance and found that this GFP-tagged c-tomoregulin did not disrupt self-avoidance in wild-type worms ($p>0.05$, *wt* vs. *wt;PVD::*T24F1.4::GFP) and rescued the 3° self-avoidance defect in mutants of *T24F1.4(tm5213)* ($p<0.0001$ for *T24F1.4(tm5213)* vs. *T24F1.4(tm5213);PVD::*T24F1.4::GFP, and $p>0.05$ for *wt;PVD::*T24F1.4::GFP vs. *T24F1.4(tm5213);PVD::*T24F1.4::GFP) (**Figure 2.3c**). However, it is important to note that when the GFP-tagged construct (*PVD::*T24F1.4::GFP) was crossed into *T24F1.4(tm5213)* mutants, the shrinker-causing mutation was not maintained. Therefore, it cannot be concluded that the GFP-tagged T24F1.4/c-tomoregulin is functional (see **Discussion**).

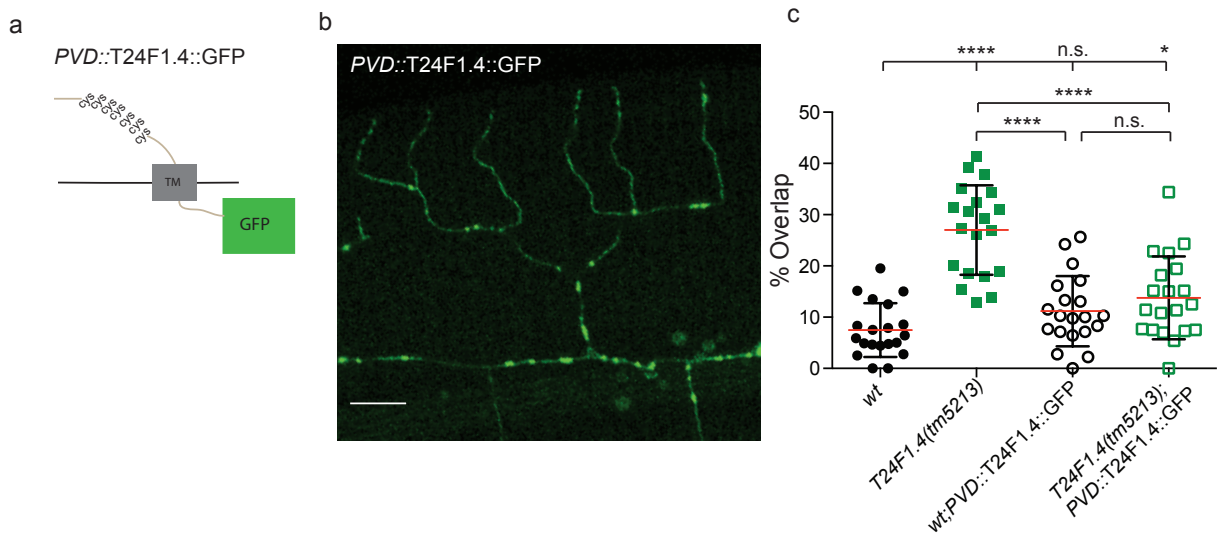

Figure 2.3: c-tomoregulin is expressed throughout PVD dendrites. (a) Schematic of GFP-tagged T24F1.4/c-tomoregulin, **(b)** image of *PVD*::T24F1.4::GFP puncta in PVD, **(c)** quantification of 3° branch overlap. Data for *wt* and *T24F1.4(tm5213)* are the same is in **Figure 2.1**. "TM" indicates the transmembrane domain, left is anterior, up is dorsal, scale bar = 10 μm, * indicates $p<0.05$, **** indicates $p<0.0001$, n.s. = not significant, one-way ANOVA with Tukey's multiple comparisons test, error bars represent SEM, n=20.

c-tomoregulin was hypothesized to act in a genetic pathway with *unc-40/DCC*, *unc-34/Ena/VASP*, and *mig-10/Lpd* to mediate self-avoidance

To test if *c-tomoregulin* acts in the UNC-6 dependent pathway, we generated double mutants of *T24F1.4(tm5213)* with mutations of the UNC-5 and UNC-40 receptors. Surprisingly, our results indicated no difference between *wt* and mutants of *unc-5* ($p>0.05$) (**Figure 2.4a**). Although we detected no significant difference between single mutants of *T24F1.4(tm5213)* and *T24F1.4(tm5213);unc-5* double mutants ($p>0.05$) (**Figure 2.4a**), it is not clear if *c-tomoregulin* and *unc-5* act in the same genetic pathway based on the result that *unc-5* mutants do not show defects. However, our evidence did indicate that *c-tomoregulin* and *unc-40* act in the same genetic pathway, as there is no significant difference between the two single mutants ($p>0.05$, *T24F1.4(tm5213)* vs. *unc-40*) or between single mutants and the double mutant ($p>0.05$ for *T24F1.4(tm5213)* vs. *unc-40;T24F1.4(tm5213)* and $p>0.05$ for *unc-40* vs. *unc-40;T24F1.4(tm5213)*) (**Figure 2.4b**). We also found that 3° branch overlap in double mutants of *unc-34;T24F1.4(tm5213)* and *mig-10;T24F1.4(tm5213)* was not significantly different from the respective single mutants (**Figure 2.4c-d**). These results indicate that *unc-40*, *c-tomoregulin*, *unc-34*, and *mig-10* all act in the same genetic pathway to promote 3° branch self-avoidance (**Figure 2.4e**). However, it is important to note that in double mutants, the shrinker phenotype was not confirmed (see **Discussion**).

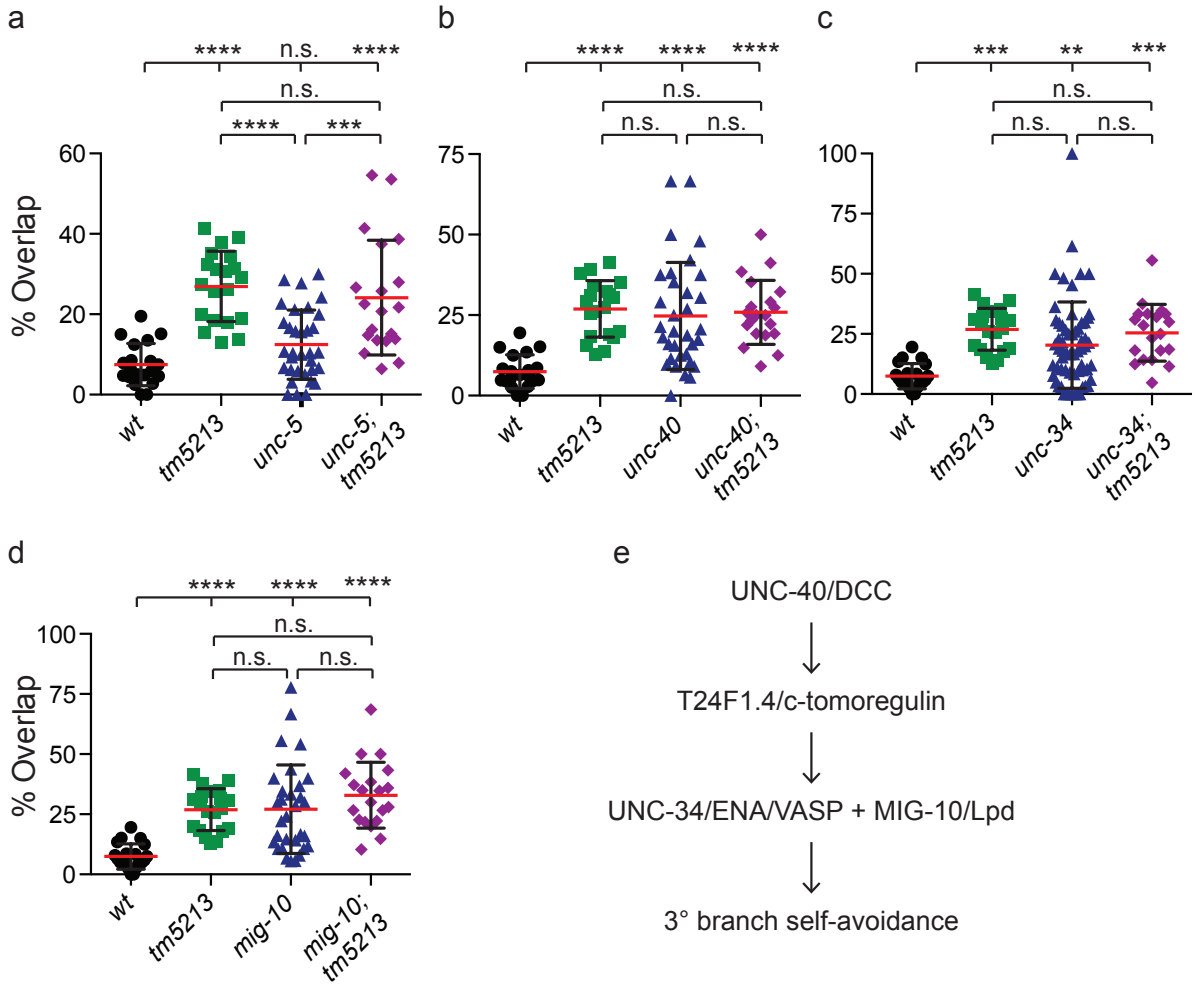

Figure 2.4: c-tomoregulin acts in a genetic pathway with *unc-40*, *unc-34*, and *mig-10*. Quantification of self-avoidance defect, measured as percent overlap of 3° branches for single and double mutants of *T24F1.4(tm5213)* with *unc-5* **(a)**, *unc-40* **(b)**, *unc-34* **(c)**, or *mig-10* **(d)**, **(e)** schematic of genetic pathway, based on results of **a-d**. Data for *wt* and *tm5213* are the same as in **Figure 2.1**. ** indicates p<0.01, *** indicates p<0.001, **** indicates p<0.0001, n.s. = not significant, one-way ANOVA with Tukey's multiple comparisons test, error bars represent SEM, n≥20.

c-tomoregulin is not required for 1° or 2° branch morphology

Having concluded that c-tomoregulin acts with UNC-40, UNC-34, and MIG-10 to promote 3° branch self-avoidance, we next examined the role of c-tomoregulin in 1° and 2° branch development. Localization of GFP-tagged c-tomoregulin throughout the 1° and 2° dendrites (**Figure 2.3b**) indicates that c-tomoregulin could be involved in 1° and 2° branch development. One noticeable difference between wild-type worms versus mutants with PVD dendrite morphology defects is that mutants have short 1° branches (**Figure 2.5a**), show defects in the guidance of 1° branches (**Figure 2.6a**), have extra 1° branches (**Figure 2.8a**), or lack the posterior 1° branch (**Figure 2.10a**).

c-tomoregulin is not required for 1° branch length

The ratio of branch length to body length was no different in mutants of *T24F1.4/c-tomoregulin* compared to *wt* when examined with two cytosolic markers, *F49H12.4::*GFP and *ser2prom3::*mCherry ($p>0.05$ for all *T24F1.4* alleles vs. *wt*) (**Figure 2.5b-e**), indicating that this protein is not necessary for outgrowth and extension of the 1° branch.

Components of the UNC-6 dependent pathway for self-avoidance are required for 1° branch length

Genes in the UNC-6 dependent pathway showed differences in 1° branch length. In *unc-6* mutants, the anterior 1° branch was shorter compared to *wt* ($p<0.0001$) (**Figure 2.5d**), but the

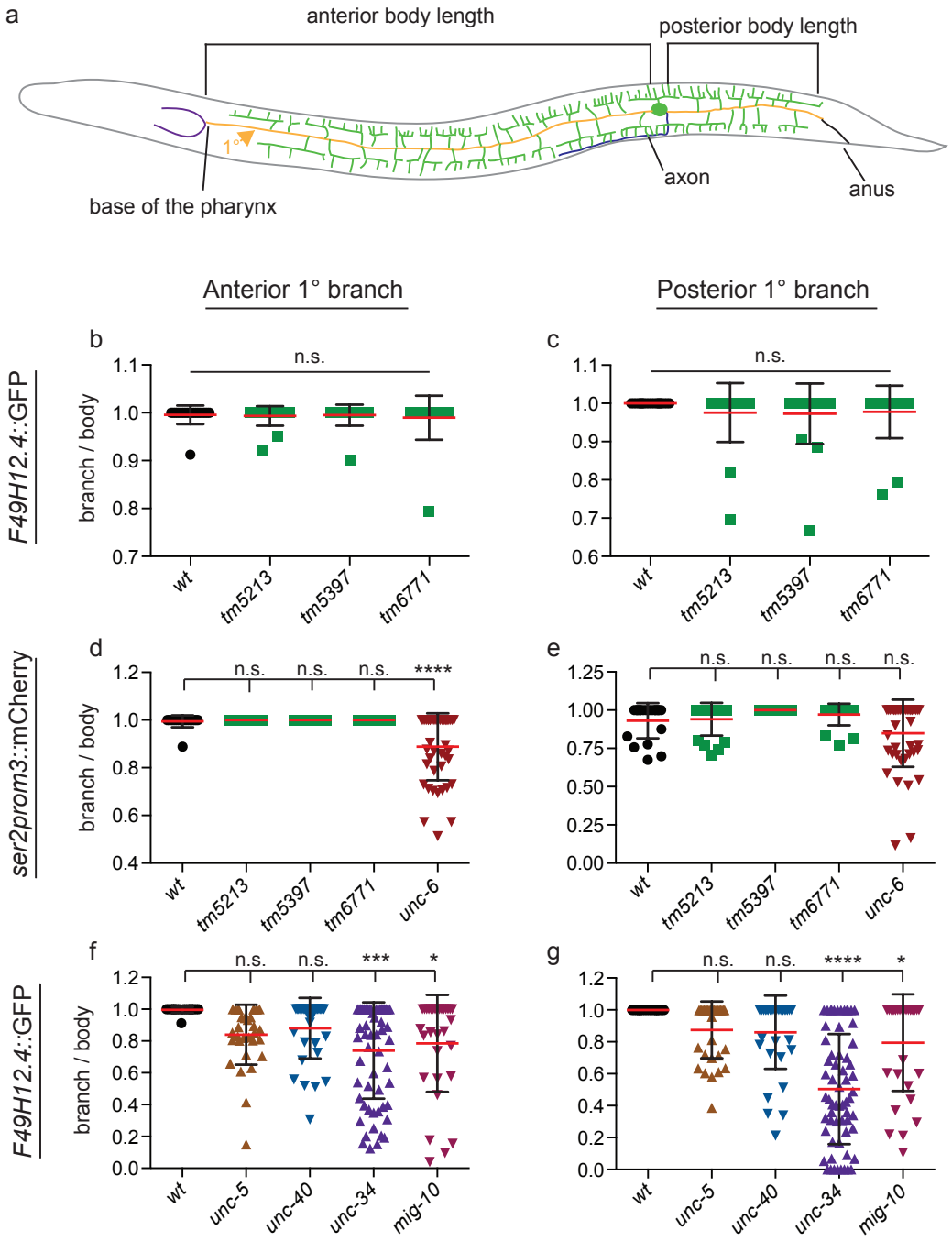

Figure 2.5: T24F1.4/c-tomoregulin is not required for 1° branch length. (a) Schematic of 1° branch-to-body length measurement, 1° branch is denoted as gold, **(b-g)** ratio of 1° branch length to body length as denoted in **a** for the anterior 1° branch **(b, d, f)** and posterior 1° branch **(c, e, g)** as measured with PVD cytosolic marker *F49H12.4::*GFP **(b, c, f, g)** or *ser2prom3::*mCherry **(d and e)**. Data for *wt* in panel **f** is the same as in panel **b**; data for *wt* in panel **g** is the same as in panel **c**. Left is anterior, up is dorsal, * indicates $p<0.05$, *** indicates $p<0.001$, **** indicates $p<0.0001$, n.s. = not significant, one-way ANOVA with Tukey's multiple comparisons test, error bars represent SEM, $n\geq20$.

posterior 1° branch was not significantly different from *wildtype* ($p>0.05$) (**Figure 2.5e**). Mutants of *unc-34* and *mig-10* also had shorter anterior ($p<0.001$ for *wt* vs. *unc-34* and $p<0.05$ for *wt* vs. *mig-10*) and posterior ($p<0.0001$ for *wt* vs. *unc-34* and $p<0.05$ for *wt* vs. *mig-10*) 1° branches compared to wild-type worms (**Figure 2.5f-g**).

c-tomoregulin is not required for 1° branch guidance

Only 5% of worms showed a posterior 1° branch guidance defect in the *tm5213* allele, and all other mutants of *c-tomoregulin* did not show defects in 1° branch guidance, when examined with the *F49H12.4*::GFP cytosolic marker for PVD ($p>0.05$ for all alleles compared to *wt*) (**Figure 2.6b-c**). Similarly, when examined with the *ser2prom3::*mCherry cytosolic marker, 5% of the worms with the *tm5213* allele showed a posterior 1° branch guidance defect, and 5% of worms with the *tm6771* allele showed either an anterior or posterior 1° branch guidance defect, but these results were not significantly different from *wildtype* ($p>0.05$ for all alleles compared to *wt*) (**Figure 2.6d-e**). These results suggest that c-tomoregulin is not required for proper extension of the 1° branches along the midline.

UNC-6/Netrin and the UNC-5 and UNC-40/DCC receptors are required for 1° branch guidance

Mutants of *unc-6*, *unc-5*, and *unc-40* all showed guidance defects in the anterior 1° branch (*unc-6*: 17/46, *unc-5*: 10/33, and *unc-40*: 11/34, $p<0.01$ for each compared to *wt*) (**Figure 2.6f**), whereas *unc-6* and *unc-40*, but not *unc-5*, showed guidance defects in the posterior 1°

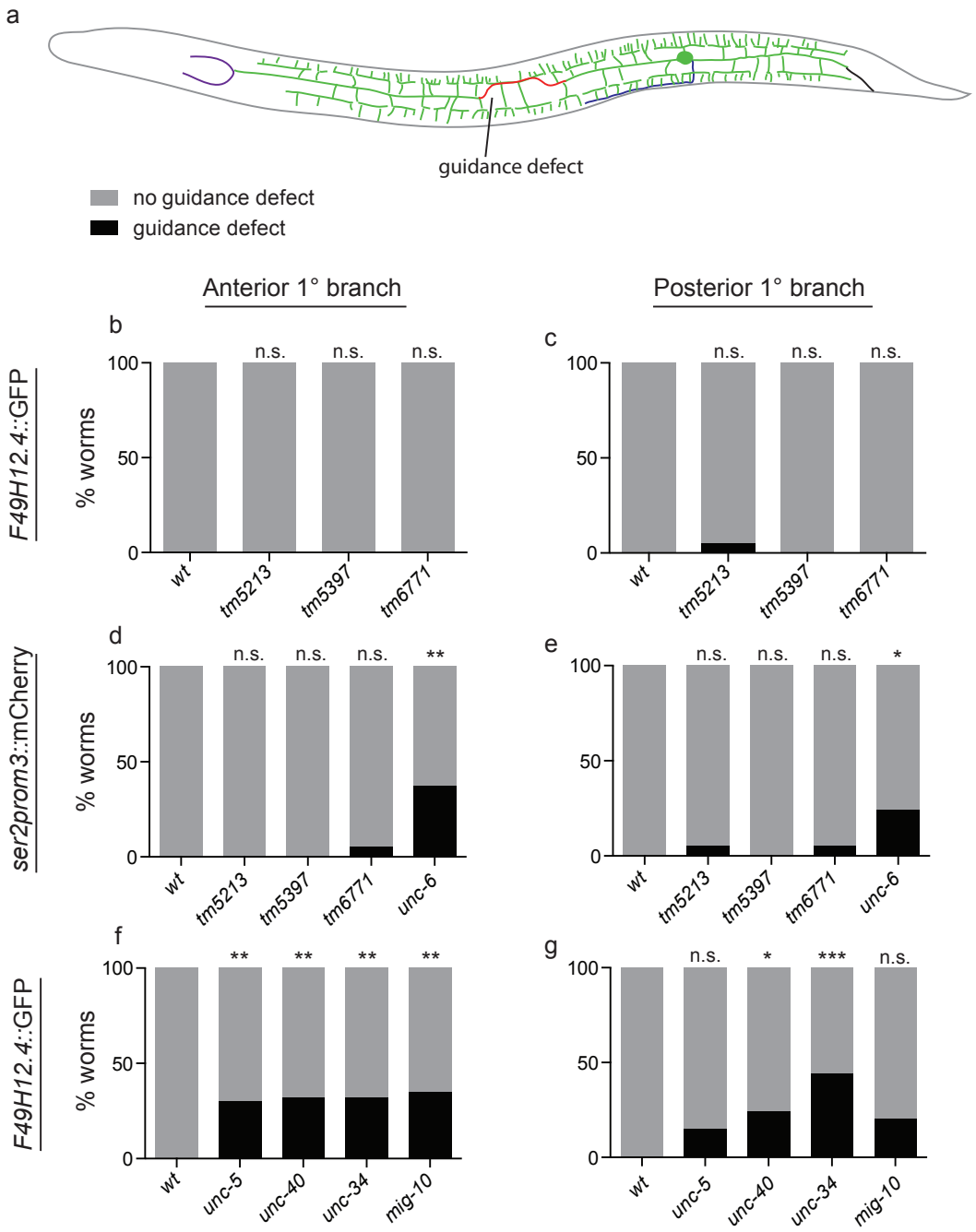

Figure 2.6: T24F1.4/c-tomoregulin is not required for 1° branch guidance. (a) Schematic of PVD (green) with a 1° branch guidance defect (red), **(b-g)** percent worms with (black) or without (gray) a guidance defect in the anterior **(b, d, f)** or posterior **(c, e, g)** 1° dendrite. Data for *wt* in panel **f** is the same as in panel **b**; data for *wt* in panel **g** is the same as in panel **c**. Left is anterior, up is dorsal, * indicates $p<0.05$, ** indicates $p<0.01$, *** indicates $p<0.001$, n.s. = not significant, Fisher's Exact test for each compared to *wt*, $n\geq20$.

branch (*unc-6*: 11/46, $p<0.05$; *unc-5*: 5/33, $p>0.05$; *unc-40*: 8/34, $p<0.05$) (**Figure 2.6g**). The addition of the *c-tomoregulin* mutant allele *T24F1.4(tm5213)* to either *unc-5* or *unc-40* single mutants rescued the anterior 1° branch guidance defect for both *unc-5* and *unc-40* ($p>0.05$ for *unc-5;tm5213* vs. *wt* and for *unc-40;tm5213* vs. *wt*) (**Figure 2.7a**) and for the posterior 1° branch defect for *unc-40* ($p>0.05$, *unc-40;tm5213* vs. *wt*) (**Figure 2.7b**). Similar to *T24F1.4(tm5213)* and *unc-5* single mutants, the posterior 1° branch of *T24F1.4(tm5213);unc-5* double mutants was not different from *wt* ($p>0.05$) (**Figure 2.7b**), indicating the addition of *T24F1.4(tm5213)* to *unc-5* did not cause a defect. However, similar to what was observed for the anterior 1° branch, adding the *T24F1.4(tm5213)* mutation to the *unc-40* mutation rescued the posterior 1° branch defect ($p>0.05$, *unc-40;tm5213* vs. *wt*) (**Figure 2.7b**).

UNC-34/Ena/Vasp and MIG-10/Lpd are required for 1° branch guidance

Mutants of *unc-34* and *mig-10* also showed guidance defects in the anterior 1° dendrite (20/63 and 11/31 for *unc-34* and *mig-10*, respectively, $p<0.01$ for each compared to *wt*) (**Figure 2.6f**). For the posterior 1° dendrite, *unc-34* (24/55, $p<0.001$) but not *mig-10* (6/30, $p>0.05$) showed a guidance defect (**Figure 2.6g**). Combining mutations for *T24F1.4(tm5213)* with *unc-34* did not rescue defects in anterior ($p<0.001$) or posterior ($p<0.01$) 1° branches (**Figure 2.7a-b**). Similarly, *T24F1.4(tm5213)* in combination with *mig-10* did not rescue the defects seen in the anterior 1° branch for *mig-10* single mutants ($p<0.05$, *mig-10;tm5213* vs. *wt*) (**Figure 2.7a**), nor induce defects in the posterior 1° branch ($p>0.05$, *mig-10;tm5213* vs. *wt*) (**Figure 2.7b**). These results suggest that while *unc-34* and *mig-10* are required for proper 1° branch extension along the midline, *c-tomoregulin* does not act in this genetic pathway.

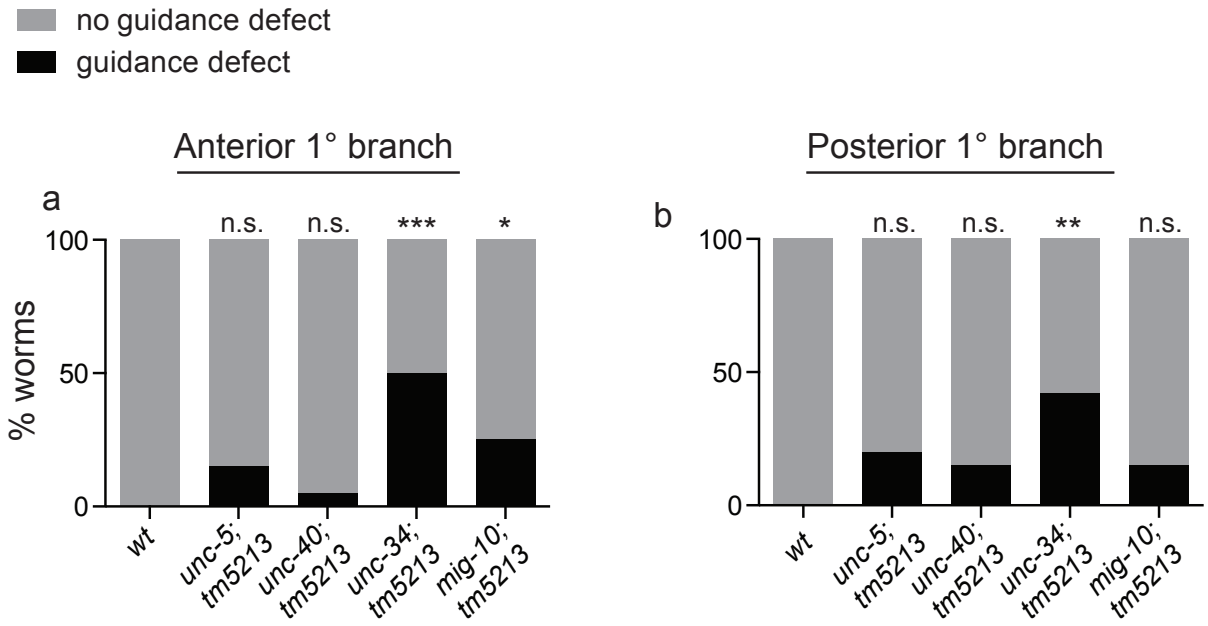

Figure 2.7: Analysis of double mutants in the UNC-6 dependent pathway. Percent worms with (black) or without (gray) a guidance defect in the anterior **(a)** or posterior **(b)** 1° dendrite for double mutants of known components of the UNC-6 dependent pathway for 3° branch self-avoidance and *c-tomoregulin*. Data shown for *wt* in panel **a** is the same as in **Figure 2.6b**; data shown for *wt* in panel **b** is the same as in **Figure 2.6c**. * indicates $p<0.05$, ** indicates $p<0.01$, *** indicates $p<0.001$, n.s. = not significant, Fisher's Exact test for each compared to *wt*, $n\geq20$.

c-tomoregulin is not required for 1° branch number

All wild-type worms and *T24F1.4* mutants had only one anterior 1° dendrite and one posterior 1° dendrite, regardless of allele or cytosolic marker ($p>0.05$ for each allele compared to wild-type) (**Figure 2.8b-e**). From these results, we conclude that T24F1.4/c-tomoregulin is not required for 1° branch number.

Components of the UNC-6/Netrin-dependent pathway for self-avoidance are not required for 1° branch number

At least one animal observed for mutants of *unc-6* (1/46, anterior; 5/46, posterior), *unc-5* (1/33, anterior; 3/33, posterior), *unc-40* (2/34, anterior; 3/34, posterior), *unc-34* (2/63, anterior; 1/55, posterior), and *mig-10* (1/31, anterior; 1/31, posterior) had at least one extra anterior or posterior 1° dendrite, but these values were not significantly different from wild-type levels ($p>0.05$ for each compared to *wt*) (**Figure 2.8d-g**). It is worth noting that no mutants of *unc-6* or *unc-5* had both extra anterior and extra posterior 1° branches, but in mutants of *unc-40*, two worms were found to have both extra anterior and extra posterior 1° branches. Similarly, double mutants of *T24F1.4(tm5213)* and either *unc-5* (0/20, anterior; 1/20, posterior), *unc-40* (2/20, anterior; 1/20, posterior), *unc-34* (1/20, anterior; 0/20, posterior), or *mig-10* (0/20, anterior; 0/20, posterior) did not show significantly different results compared to *wt* ($p>0.05$ for each condition compared to *wt*) (**Figure 2.9a-b**).

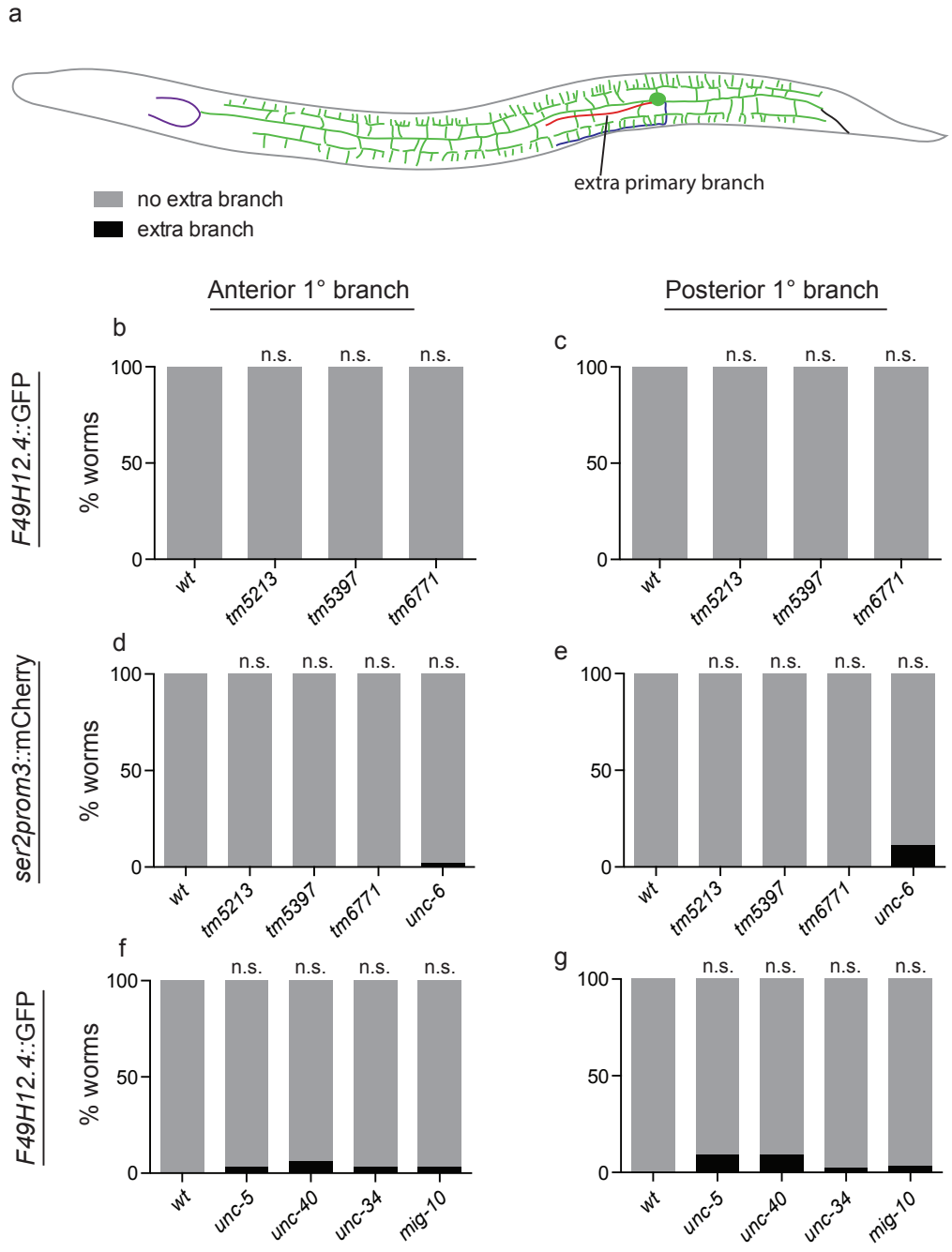

Figure 2.8: T24F1.4/c-tomoregulin is not required for 1° branch number. (a) Schematic of PVD (green) with an extra anterior 1° branch (red), **(b-g)** percent worms with (black) or without (gray) an extra anterior 1° branch **(b, d, f)** or posterior 1° branch **(c, e, g)**. Data for *wt* in panel **f** is the same as in panel **b**; data for *wt* in panel **g** is the same as in panel **c**. Left is anterior, up is dorsal, n.s. = not significant, Fisher's Exact test for each compared to *wt*, n≥20.

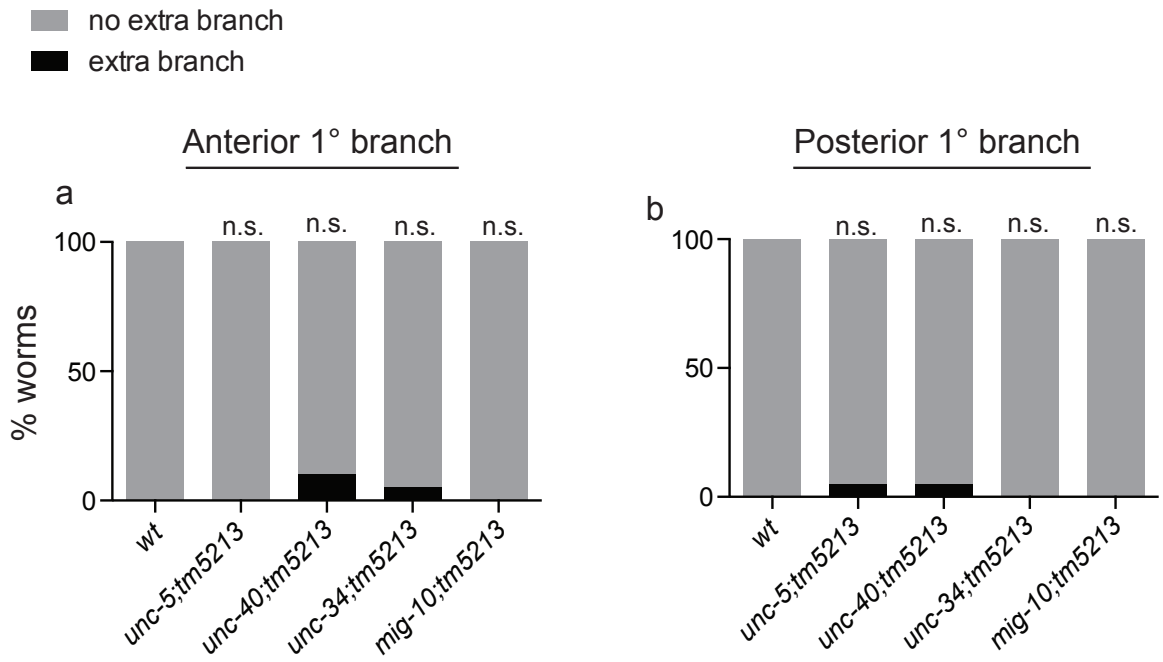

Figure 2.9: Analysis of double mutants in the UNC-6 dependent pathway. Percent worms with (black) or without (gray) an extra anterior **(a)** or posterior **(b)** 1° branch for double mutants of known components of the UNC-6 dependent pathway for 3° branch self-avoidance and *c-tomoregulin*. Data shown for *wt* in panel **a** is the same as in **Figure 2.8b**; data shown for *wt* in panel **b** is the same as in **Figure 2.8c**. n.s. = not significant, Fisher's Exact test for each compared to *wt*, n=20.

c-tomoregulin is not required for posterior 1° branch outgrowth

All wild-type worms and mutants of *T24F1.4* had a posterior 1° dendrite, regardless of allele or cytosolic marker ($p>0.05$ for each allele compared to wild-type) (**Figure 2.10b-c**), suggesting that T24F1.4/c-tomoregulin is not required for posterior 1° branch outgrowth.

Components of the UNC-6/Netrin-dependent pathway for self-avoidance are not required for 1° branch outgrowth

Similarly, we examined mutants of *unc-6, unc-5,* and *unc-40,* and all (100%) worms examined had a posterior 1° dendrite ($p>0.05$ for each allele compared to *wt*) (**Figure 2.10c-d**). From these results, we conclude that the ligand UNC-6/Netrin and its receptors, UNC-5 and UNC-40/DCC, are not required for posterior 1° branch outgrowth. We next interrogated downstream components of the proposed UNC-6-dependent pathway for self-avoidance (**Figure 2.4e**) and discovered that mutants of *unc-34* occasionally had a missing posterior 1° branch, but this was not significantly different from *wildtype* (8/63, $p>0.05$). In contrast, all (100%) of the *mig-10* mutants examined had a posterior 1° dendrite ($p>0.05$ compared to *wt*) (**Figure 2.10d**). No differences in missing posterior 1° branch were detected between double mutants of *T24F1.4(tm5213)* and either *unc-5*, *unc-40*, *unc-34*, or *mig-10* ($p>0.05$ for each compared to *wt*) (**Figure 2.10e**).

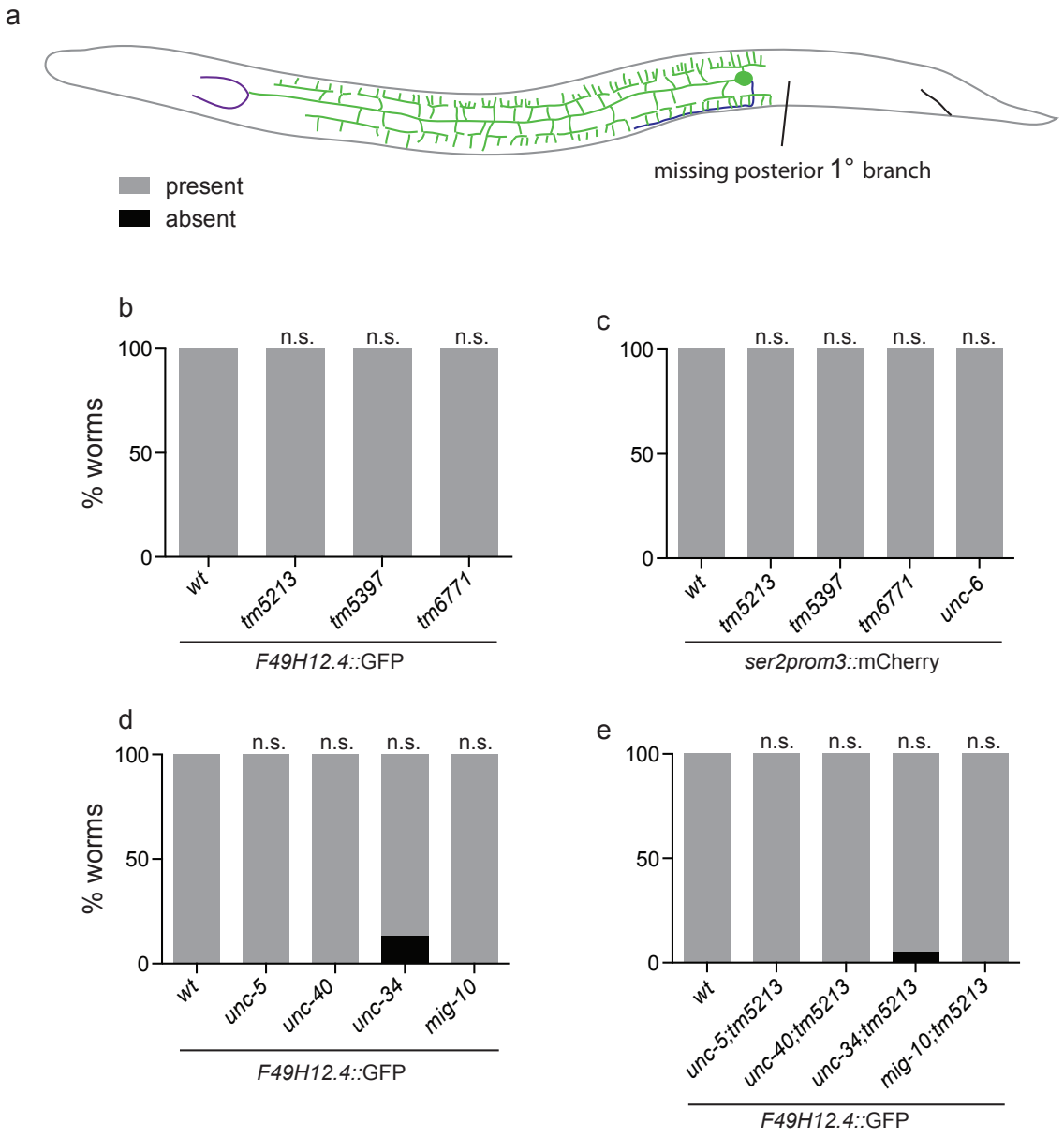

Figure 2.10: T24F1.4/c-tomoregulin is not required for posterior 1° branch outgrowth. (a) Schematic of PVD (green) with a missing posterior 1° branch, **(b-e)** percent worms with (gray) or without (black) a posterior 1° branch. Data for *wt* is the same for panels **b**, **d**, and **e**. Left is anterior, up is dorsal, n.s. = not significant, Fisher's Exact test for each compared to *wt*, n≥20.

c-tomoregulin is not required for 2° branch number

It was previously reported that *T24F1.4(tm5213)* mutants had a decreased number of 2° branches[51], but we were unable to replicate that result (**Figure 2.11a**). For all alleles of *T24F1.4/c-tomoregulin* and for both cytosolic markers of *F49H12.4::*GFP and *ser2prom3::*mCherry, there were no differences between mutant and wild-type numbers of 2° branches ($p>0.05$ for each compared to *wt*) (**Figure 2.11a-b**).

UNC-6/Netrin and the UNC-5 and UNC-40/DCC receptors are required for 2° branch number

Mutants of *unc-6*, *unc-5*, and *unc-40* all had a decreased number of 2° branches compared to *wt* ($p<0.0001$ for each mutant compared to *wt*) (**Figure 2.11b-e**), consistent with previous work that examined the role of UNC-6 and its receptors in PVD development[32]. That combining these mutations with *T24F1.4(tm5213)* neither enhanced nor rescued the defects ($p>0.05$ for *unc-5* vs. *unc-5;tm5213*, $p>0.05$ for *unc-40* vs. *unc-40;tm5213*) (**Figure 2.11d-e**) provides further evidence that *T24F1.4/c-tomoregulin* is not involved in 2° branch development. We conclude that UNC-6/Netrin and its receptors, UNC-5 and UNC-40/DCC, are required for 2° branch outgrowth or stabilization and that c-tomoregulin does not act in this pathway in this context.

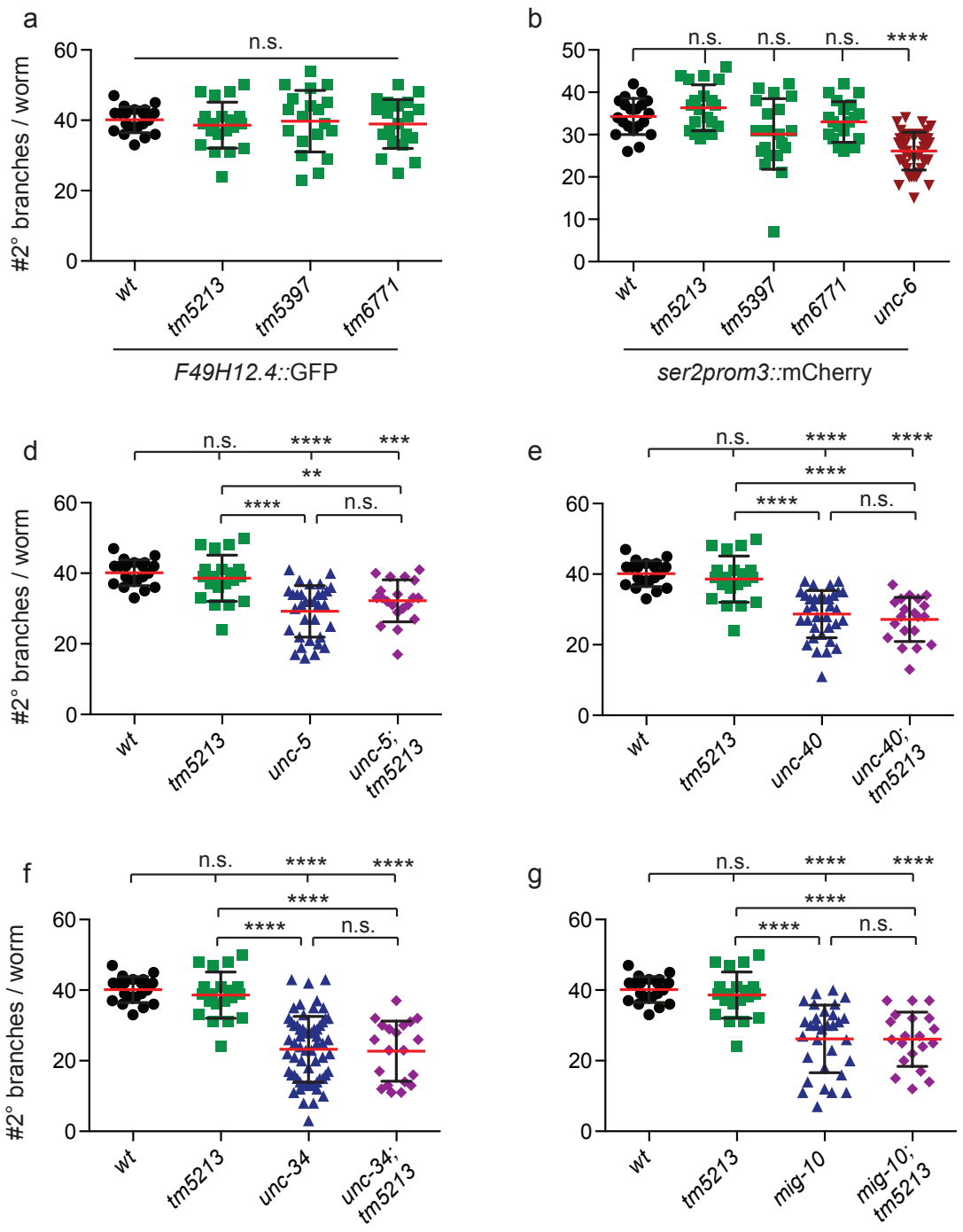

Figure 2.11: c-tomoregulin is not required for 2° branch number. Quantification of the number of 2° branches per worm. Data for *wt* and *tm5213* are the same in panels **a**, **d**, **e**, **f**, and **g**. ** indicates p<0.01, *** indicates p<0.001, **** indicates p<0.0001, n.s. = not significant, one-way ANOVA with Tukey's multiple comparisons test, error bars represent SEM, n≥20.

UNC-34/Ena/Vasp and MIG-10/Lpd are required for 2° branch number

Consistent with previous work[32], mutants of *unc-34* and *mig-10* also showed a decreased number of 2° branches compared to *wt* ($p<0.0001$ for each compared to *wt*) (**Figure 2.11f-g**). Combining these mutations with *T24F1.4(tm5213)* did not enhance or rescue the defect ($p>0.05$ for *unc-34* vs. *unc-34;tm5213*, $p>0.05$ for *mig-10* vs. *mig-10;tm5213*) (**Figure 2.11f-g**), providing further evidence that *T24F1.4/c-tomoregulin* is not involved in 2° branch development. We conclude that UNC-34/Ena/VASP and MIG-10/Lpd are required for 2° outgrowth or stabilization and that c-tomoregulin does not act in this pathway in this context.

c-tomoregulin is not required for other known UNC-6 mediated guidance mechanisms

Since c-tomoregulin specifically acted in the UNC-6 pathway to mediate self-avoidance and not 1° or 2° branch development, we next tested if c-tomoregulin acted in other UNC-6-dependent pathways. UNC-6 is proposed to regulate axon outgrowth and cell migration. Motor neurons extend commissures toward to the dorsal nerve cord in response to an UNC-6 cue secreted from ventral cells[128]. Similarly, distal tip cells induce a dorsalward turn in the developing hermaphrodite gonad in an *unc-5*-dependent response to ventrally derived UNC-6[129]. Since double mutants containing both *T24F1.4* mutations and mutations in the *unc-6* pathway do not show enhanced self-avoidance defect in PVD 3° dendrites, it is suggested that T24F1.4 acts in conjunction with UNC-6 or its receptors, UNC-5 and/or UNC-40. To ascertain if T24F1.4 acts in other UNC-6 dependent pathways, we examined two long-range UNC-6-dependent guidance mechanisms: distal tip cell migration and GABA motor neuron axon commissure guidance.

Based on our results that *PVD::*T24F1.4 rescues the 3° branch self-avoidance defect and that c-tomoregulin appears to act specifically in 3° branch development, we hypothesized that c-tomoregulin would not be involved in non-PVD-self-avoidance pathways that are also UNC-6-dependent.

c-tomoregulin is not required for distal tip cell migration

The gonads of hermaphrodite worms exhibit a U shape formed by leader cells known as distal tip cells (DTCs) that complete a three-phase migration (phase I: migration away from the vulva, phase II: migration from ventral to dorsal, phase III: migration back to vulva) (**Figure 2.12a**). Phase II guides the DTC from ventral to dorsal and is dependent on UNC-6/netrin and its receptors, UNC-5 and UNC-40/DCC[129–132]. Previous studies[129,131,132] demonstrate that *unc-5* and *unc-40* mutants exhibit posterior arm defects more frequently than anterior arm defects. To investigate if c-tomoregulin acts in this long-range UNC-6-dependent pathway, we used the *Pmig-24::*venus marker[133] to quantify defect of the phase II ventral-to-dorsal migration of DTCs in mutants of *unc-5* (**Figure 2.12c**), *unc-40* (**Figure 2.12d**), and the three alleles of *c-tomoregulin* (*T24F1.4(tm5213, tm5397,* and *tm6771)*) (**Figure 2.12e-g**) compared to *wildtype* (**Figure 2.12b**). We found that wild-type animals, along with all three *c-tomoregulin* mutant animals, displayed no defects in DTC migration ($p>0.05$ for each allele compared to *wt*) (**Figure 2.12h**). Consistent with results of previous studies[129,131,132], we found that the percent defect for *unc-5(e152)* mutant worms was more severe than *unc-40(e271)* mutants (*unc-5*, 50%; *unc-40*, 20%). Within *unc-5* mutants, the defects of the anterior arm DTC migration was less severe than that of the posterior arm (anterior, 25%; posterior, 75%).

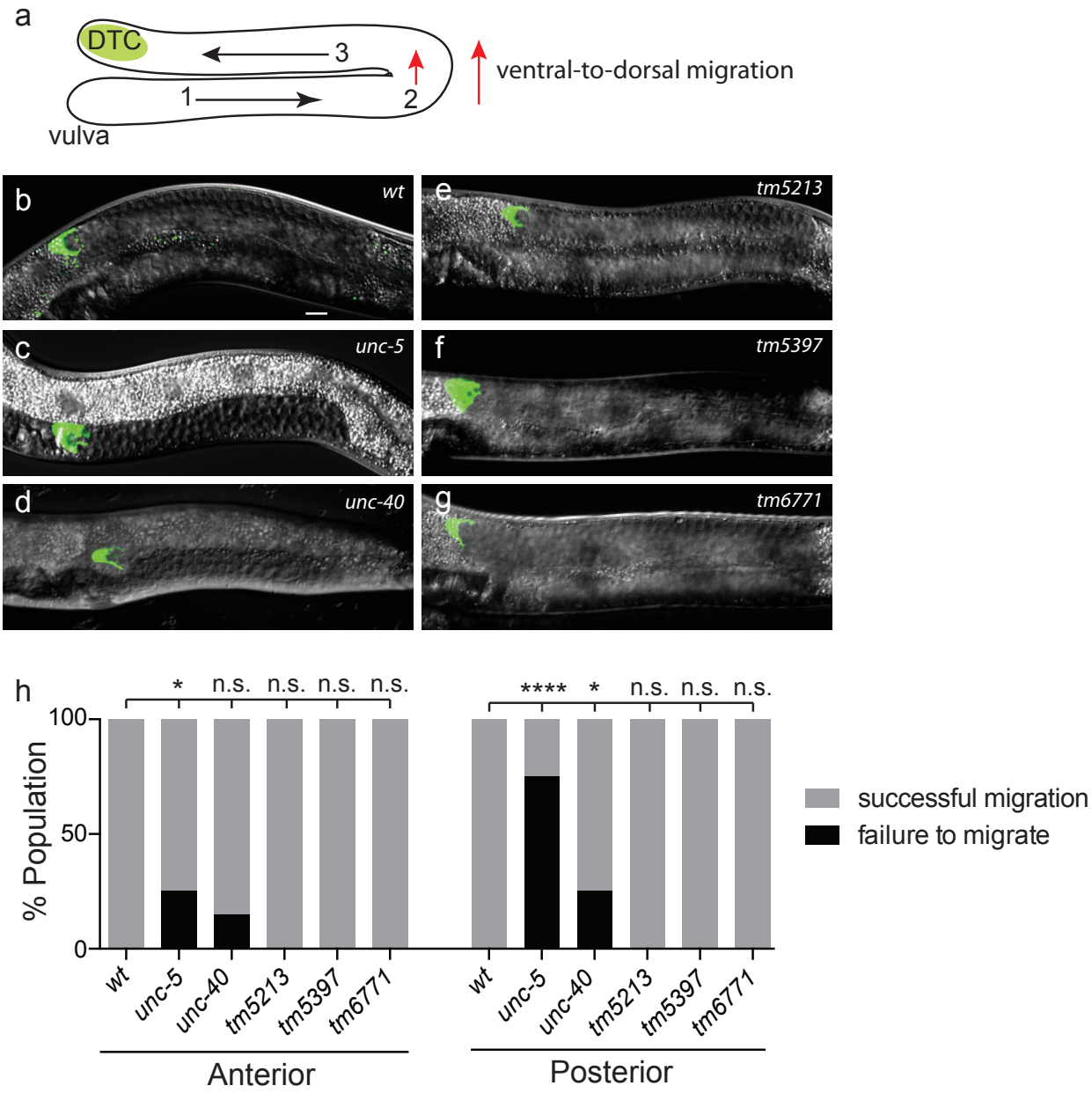

Figure 2.12: c-tomoregulin is not required for distal tip cell ventral-to-dorsal migration. (a) Schematic of distal tip cell (DTC, green) leading gonad development by migrating along the anterior-posterior axis away from the vulva (phase 1), turning to migrate from the ventral side to the dorsal side of the worm (phase 2), and then migrating back toward the vulva on the dorsal side (phase 3), **(b-g)** images of DTCs, labeled with *Pmig-24*::Venus, in various genetic backgrounds, **(h)** percentage of anterior and posterior DTCs that successfully (gray) or unsuccessfully (black) migrated from the ventral side of the worm to the dorsal side of the worm (phase 2 in panel **a**). Left is anterior, up is dorsal, scale bar = 10 μm, * indicates $p<0.05$, **** indicates $p<0.0001$, n.s. = not significant, Fisher's Exact test for each compared to *wt*, n=20.

c-tomoregulin is not required for GABA motor neuron axon guidance

Similar to distal tip cell migration, the ventral-to-dorsal axon guidance of D-type motor neurons (**Figure 2.13a**) utilizes the UNC-6 gradient as a long-range cue. In wild-type development (**Figure 2.13b**), axons grow out of the ventrally located cell body and extend along the body wall to the dorsal nerve cord to form commissures. Mutants of *unc-5* (**Figure 2.13c**) and *unc-40* (**Figure 2.13d**) show defects with axons failing to reach the dorsal nerve cord[131,132]. As another measure for possible interaction of c-tomoregulin with UNC-5 and UNC-40 in a pathway that uses UNC-6 as a long-range cue, we looked at axon commissures in *c-tomoregulin* mutants (**Figure 2.13e-g**) and compared them with mutants of *unc-5* and *unc-40.* Wild-type worms and all three *T24F1.4* mutant alleles showed no defects ($p>0.05$ for each compared to *wt*) (**Figure 2.13h**). As a control, we analyzed worms with mutations in UNC-5 and UNC-40 and found defects similar to results from previous studies[131,132] ($p<0.0001$ for *unc-5* and *unc-40* each compared to *wildtype*) (**Figure 2.13h**).

Discussion: A shrinker-causing mutation, not mutations in *T24F1.4/c-tomoregulin*, causes 3° branch overlap in PVD

The *T24F1.4(tm5213)* strain had an additional "shrinker" behavioral phenotype, where the animal shrinks its body by pulling in the head and the tail to make the body shorter in response to being tapped on the head. The "shrinker" phenotype has been attributed to GABA motor neuron dysfunction[116]. Normally, worms move in a sinusoidal motion by simultaneous excitation (via cholinergic input) of muscles on one side and relaxation (via GABA input) of muscles on the opposite side. In mutations that disrupt GABA signaling, body muscles on both

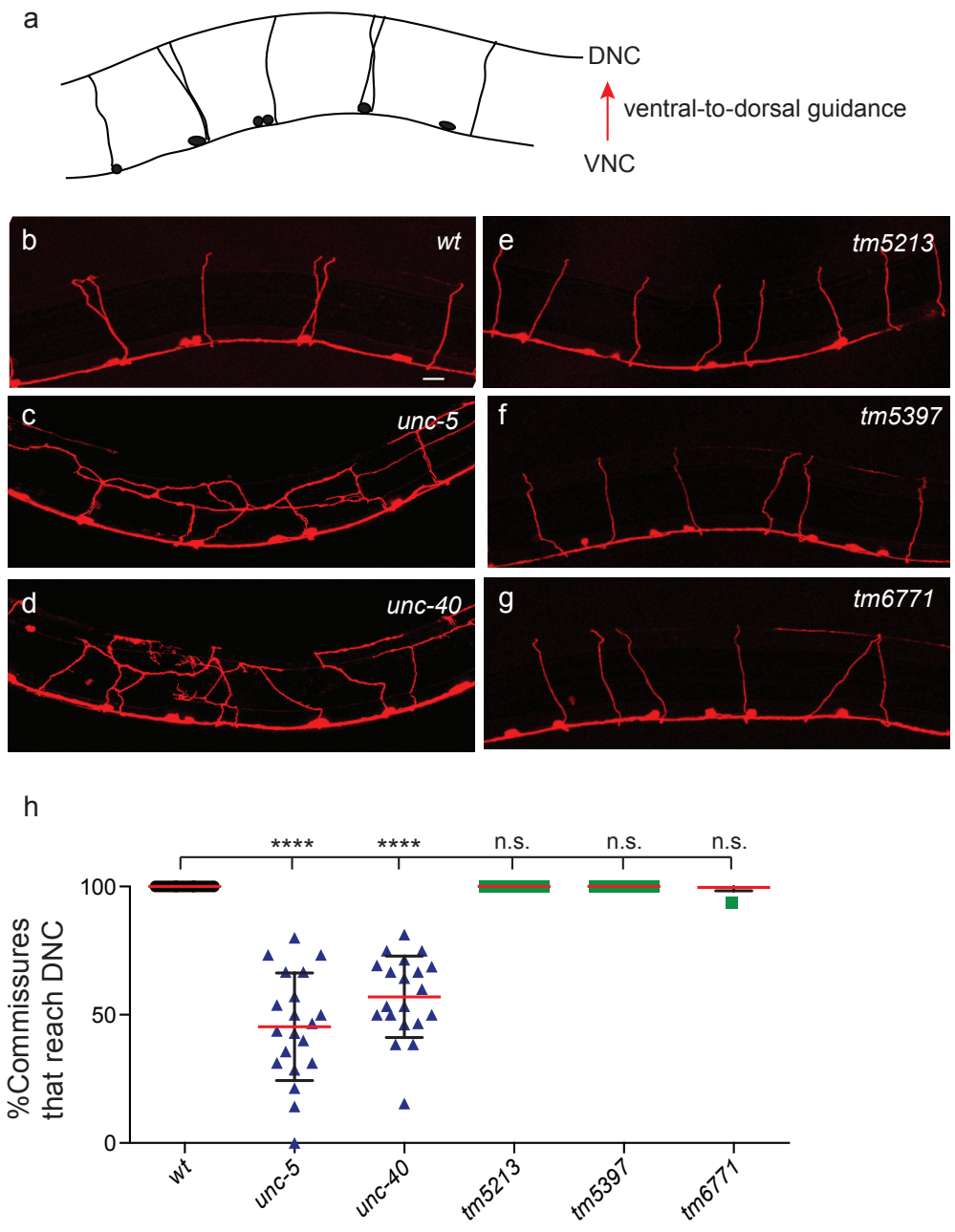

Figure 2.13: c-tomoregulin is not required for D-type GABA motor neuron axon ventral-to-dorsal guidance. (a) Schematic of cell bodies (black circles) located ventrally along the ventral nerve cord (VNC) of the body of the worm and motor neuron commissures that extend from the ventral side of the worm to the dorsal nerve cord (red arrow), **(b-g)** images of motor neurons, labeled with *Punc-47*::mCherry, in various genetic backgrounds, **(h)** percentage of axons per worm that successfully reached to the dorsal nerve cord (DNC). VNC = ventral nerve cord, DNC = dorsal nerve cord, left is anterior, up is dorsal, scale bar = 10 μm, **** indicates $p<0.0001$, n.s. = not significant, one-way ANOVA with Tukey's multiple comparisons test, error bars represent SEM, n=20.

sides are induced to contract by the cholinergic signal. This results in the worm pulling the head and tail in toward the middle, in effect, shrinking. Because the other *T24F1.4* alleles, *tm5397* and *tm6771,* do not display the shrinker phenotype, we hypothesized this was a transgene effect caused by random mutagenesis[134]. To test this hypothesis, we quantified the shrinker phenotype in wildtype, *T24F1.4(tm5213)*, and *c-tomoregulin* expressing *PVD::*T24F1.4 worms by tapping the worms on the head and noting if they "shrank" or if they exhibited wild-type sinusoidal backward motion. If c-tomoregulin is not related to the shrinker phenotype, then the extrachromosomal *PVD::*T24F1.4 should rescue 3° branch self-avoidance but not the shrinker phenotype. These results, however, showed that only *T24F1.4(tm5213)* displayed the shrinker phenotype ($p<0.0001$ for *T24F1.4(tm5213)* vs. *wt*, $p>0.05$ for *T24F1.4(tm5213);PVD::*T24F1.4 vs. *wt*) (**Figure 2.14a**). While PVD does synapse onto interneurons that then lead to movement, the PVD neuron could not specifically activate GABA neurons to rescue the shrinker phenotype, which is what would have to happen since our construct expressed c-tomoregulin only in PVD.

One explanation for this result would be that c-tomoregulin is secreted. There is no signal peptide at the N-terminus, but there is the possibility that a non-canonical signal sequence is present. This hypothesis is supported by evidence that expressing c-tomregulin in the skin rescues the self-avoidance defect ($p<0.0001$ for *T24F.14(tm5213)* vs. *T24F1.4(tm5213);DPY-7*::T24F1.4, $p>0.05$ for *T24F1.4(tm5213);DPY-7*::T24F1.4 vs. *wt*) (**Figure 2.14b**). However, for the *T24F1.4(tm5213)* strains containing either the *PVD::*T24F1.4 or the *Skin*::T24F1.4 extrachromosomal arrays, all the worms exhibited wild-type behavior, whether or not they carried the construct expressing c-tomoregulin (personal observation, data not shown). This led to the hypothesis that the shrinker-causing mutation was not a transgene with *tm5213* as a result of mutagenesis but rather was a separate mutation that had been present in the original strain

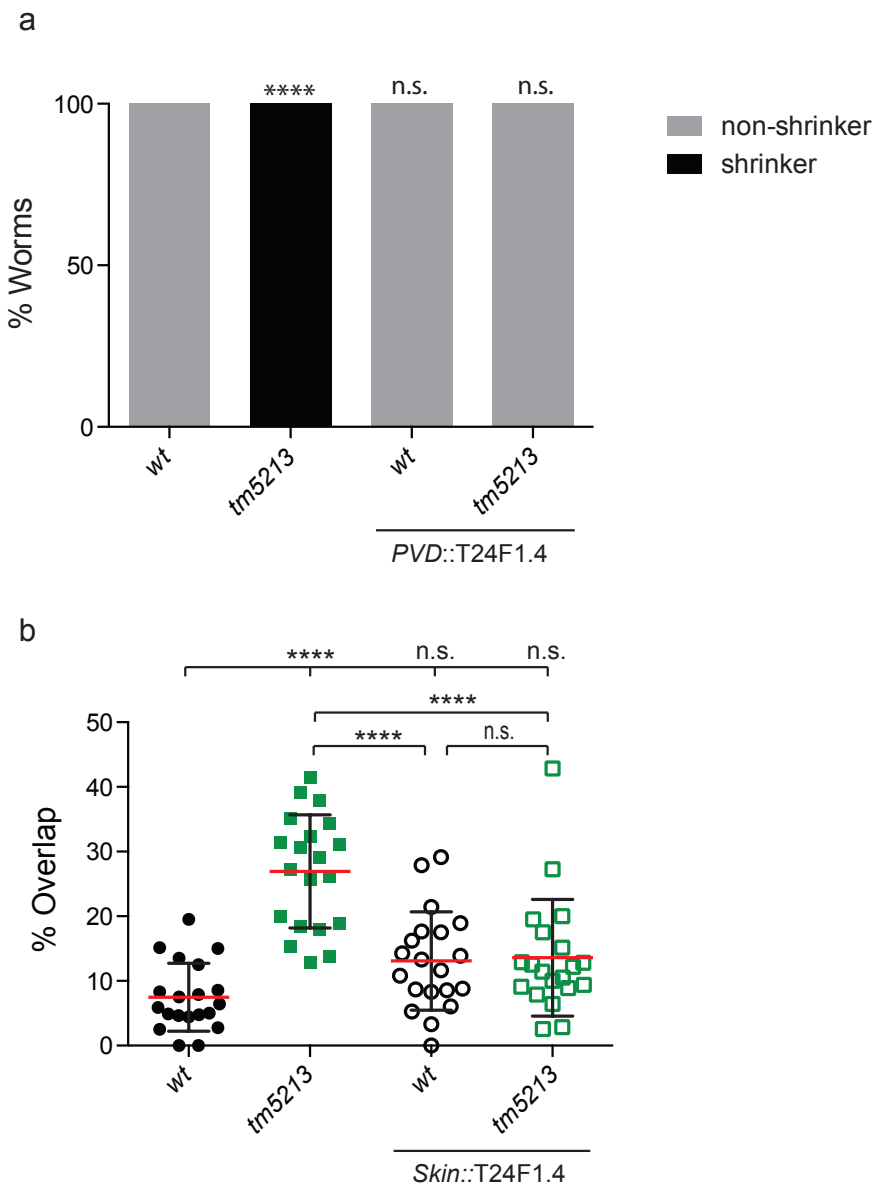

Figure 2.14: Exploring the shrinker phenotype and the question of c-tomoregulin being secreted. (a) Percent worms with (black) or without (gray) the shrinker phenotype in various genetic backgrounds, **(b)** percent 3° branch overlap. Data for *wt* and *tm5213* in panel **b** are the same as in **Figure 2.1e**. **** indicates p<0.0001, n.s. = not significant, Fisher's Exact test for each compared to *wt* (panel **a**), one-way ANOVA with Tukey's multiple comparisons test (panel **b**), error bars represent SEM, n=20.

described[51] (**Figure 2.1e**) and had been crossed out. Furthermore, it was also possible that the shrinker-causing mutation, not a mutation in *c-tomoregulin*, was causing the self-avoidance defect described in the **Results** section.

To test this hypothesis, the *c-tomoregulin* mutations, but not the shrinker phenotype, were crossed into multiple backgrounds and scored for the self-avoidance defect. With the cytosolic marker *ser2prom3::*mCherry, all three alleles of *c-tomoregulin* were not significantly different than *wildtype* ($p>0.05$ for each compared to *wt*) (Figure 2.15). Similarly, with the cytosolic marker *Pdes-2*::GFP, there was no difference in 3° branch overlap for mutants of *c-tomoregulin* compared to *wildtype* ($p>0.05$). To rule out the possibility that there was a background mutation or transgene effect associated with the cytosolic markers, the percentage of overlapping branches in mutants of *unc-6* was also quantified in these two backgrounds. The 3° branch self-avoidance defect for *unc-6* mutants was maintained with these cytosolic markers ($p<0.0001$, *unc-6* compared to the respective *wt*). There was a noticeable difference in the amount of overlap for both wild-type and mutants of *c-tomoregulin* between the *ser2prom3::*mCherry and *Pdes-2::*GFP cytosolic markers (wild-type levels were 8.7% and 3.6%, respectively, and *T24F1.4(tm5213)* levels were 7.7% and 3.4%, respectively). Thus, another cytosolic marker, *ser2prom3*::GFP, was used, and again no difference was observed between *wt* and *c-tomoregulin* mutants ($p>0.05$). These results are summarized in **Figure 2.15** and indicate that c-tomoregulin is not required for 3° branch self-avoidance.

These results suggest that the shrinker-causing background mutation in the original mutant characterized[51] in **Figure 2.1e** causes self-avoidance defects in PVD. To test this hypothesis, the shrinker-causing mutation was separated from *T24F1.4(tm5213)* by tracking the shrinker behavioral phenotype and confirming *T24F1.4(tm5213)* by sequencing. Mutants with

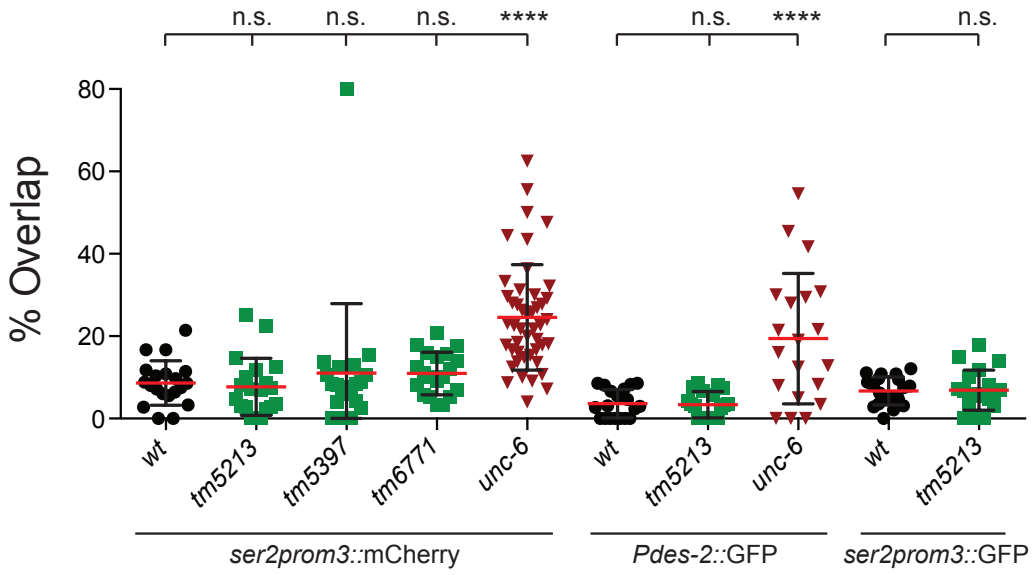

Figure 2.15: Self-avoidance defects of *c-tomoregulin* mutants using different PVD cytosolic markers. Quantification of 3° branch self-avoidance defect, measured as percent overlap, for mutants of *c-tomoregulin* mutant alleles *T24F1.4(tm5213*, *tm5397*, and *tm6771*) measured with the cytosolic PVD marker *ser2prom3::*mCherry, and the *c-tomoregulin* mutant allele *T24F1.4(tm5213)* measured with the PVD cytosolic markers *Pdes-2::*GFP and *ser2prom3::*GFP. As a control, mutants of *unc-6* were also scored with PVD markers *ser2prom3::*mCherry and *Pdes-2::*GFP. **** indicates $p<0.0001$, n.s. = not significant, one-way ANOVA with Tukey's multiple comparisons test (for *ser2prom3::*mCherry and *Pdes-2::*GFP), unpaired t-test (*ser2prom3::*GFP), error bars represent SEM, $n\geq20$.

and without the shrinker phenotype and with and without the *T24F1.4(tm5213)* allele were then compared with two cytosolic markers. Without the unknown shrinker-causing mutation ("*shrinker*"), mutants of *c-tomoregulin* with the allele *T24F1.4(tm5213)* showed no defect in 3° branch self-avoidance compared to *wt* ($p>0.05$ for both cytosolic markers), while the *shrinker* mutation did show defects ($p<0.001$ in *F49H12.4::*GFP and $p<0.0001$ in *ser2prom3*::GFP) (Figure 2.16). Intriguingly, in the *F49H12.4::*GFP background, combining the *T24F1.4(tm5213)* allele and the *shrinker* mutation caused an additive effect for an enhanced overlapping phenotype that is significantly higher than either single mutant ($p<0.0001$ for *tm5213;shrinker* vs. either *tm5213* or *shrinker*). In the *ser2prom3*::GFP background, however, combining the two mutations does not cause an enhanced effect ($p>0.05$, *tm5213;shrinker* vs. *shrinker*) (**Figure 2.16a)**. These results support the hypothesis that the unknown shrinker-causing mutation that was in the original strain characterized[51] (**Figure 2.1e**) and not *T24F1.4(tm5213)* causes an overlapping defect in PVD 3° branches.

Finally, to confirm that defects in GABA signaling could result in 3° branch self-avoidance defects, 3° branch overlap was examined in mutants of *unc-25*. UNC-25 is the ortholog of glutamic acid decarboxylase (GAD), the enzyme required for GABA synthesis; in the absence of UNC-25, the 26 GABAergic neurons in the worm are defective[135]. In theory, this should not affect PVD dendrite morphogenesis because PVD is a somatosensory neuron, part of a separate system than that of the motor circuit, and contains no known GABA receptors. However, mutants of *unc-25* showed increased 3° branch overlap ($p<0.001$) (**Figure 2.16b**).

Our discovery that an unknown shrinker-causing mutation, which is likely in a gene involved in GABA signaling, and a known mutation in GABA signaling disrupts PVD 3° branch self-avoidance is surprising, given that PVD and GABAergic motor neurons have not been

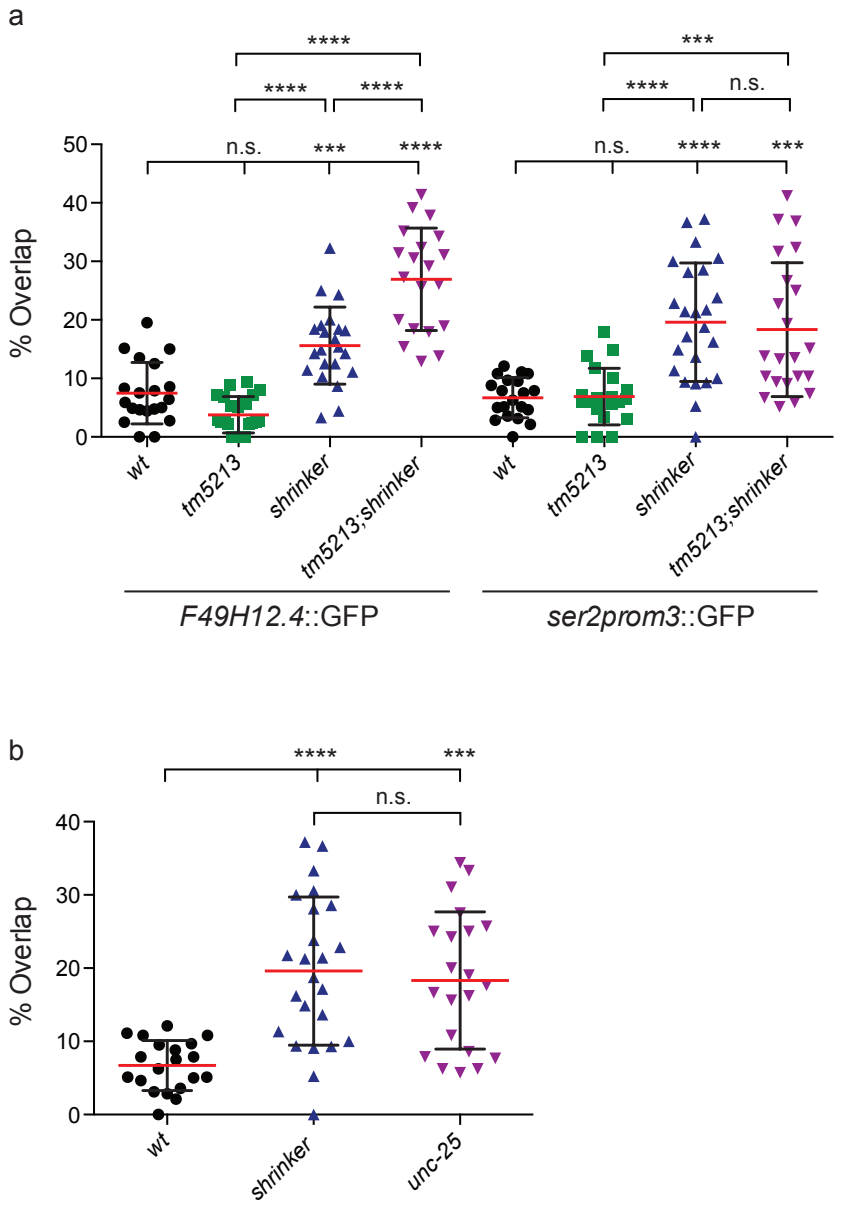

Figure 2.16: A shrinker-causing mutation, not a mutation in *c-tomoregulin*, causes 3° branch self-avoidance defects. (a) Percent 3° branch overlap for single mutants of *c-tomoregulin* (*T24F1.4(tm5213)*, the unknown shrinker-causing mutation ("*shrinker"*), and double mutants of both *T24F1.4(tm5213)* and the unknown shrinker-causing mutation ("*tm5213;shrinker"*). Data for *wt* and *tm5213;shrinker* in the *F49H12.4::*GFP condition are the same as in **Figure 2.1e**; data for *wt* and *tm5213* in the *ser2prom3::*GFP condition are the same as in **Figure 2.15**, **(b)** percent 3° branch overlap for single mutants of the unknown shrinker-causing mutation ("*shrinker"*) and the known shrinker-causing mutation *unc-25*. Data for *wt* and *shrinker* are the same as in the *ser2prom3::*GFP condition in panel **a**. *** indicates <0.001, **** indicates p<0.0001, n.s. = not significant, one-way ANOVA with Tukey's multiple comparisons test, error bars represent SEM, n≥20.

linked in development. One hypothesis for this process is that PVD dendrites contain unknown GABA receptors, the activation of which shapes dendrite development. One study found that reduced GABA signaling led to reduced dendrite length in hippocampal neurons in culture[136].

Another hypothesis for this finding might be that during development, GABA signaling on muscles could affect secretion of guidance cues that then affect signaling cascades that would disrupt self-avoidance. One example of a muscle-derived cue is LECT-2/Chondromodulin II[101,102]. The diffusible molecule LECT-2 is secreted from muscles and interacts with skin-derived MNR-1/FAM151 and SAX-7/L1CAM to increase the binding efficiency of this complex with the receptor DMA-1/LRR localized on PVD, which then orchestrates dendritic patterning along the skin[101,102]. Mutants of *lect-2* show decreased 3° branches[101], but expression of LECT-2 in seam cells causes dendrites to grow toward seam cells instead of the skin and muscle. If secretion of muscle-derived guidance cues such as LECT-2 is dependent on relative levels of excitation and inhibition, then the absence of GABA would disrupt this process. This disruption would result in an imbalance of inhibition/excitation in muscles, potentially leading to excess guidance cues from the muscles, which could cause 3° branch overlap. Such a mechanism would also result in increased 2° and 4° branch outgrowth. However, LECT-2 has been shown to be required for patterning 4°, but not 2° or 3°, dendrites[101]. Thus, one hypothesis is that a muscle-derived cue is required for 3° but not 2° or 4° dendrite patterning. This hypothetical muscle-derived cue might be disrupted in the absence of GABA signaling, resulting in 3° branch overlap.

Acknowledgements

We thank Cori Bargmaan of Rockefeller University for the CX11480 strain, Kang Shen of Stanford University for the *wyIs585* and *wyIs378* strains, and Shohei Mitani of Tokyo Women's University for the *tm5213*, *tm5397*, and *tm6771* mutant strains.

Author Contributions

David M. Miller, III, conceived the study and supervised the experiments. Timothy D. O'Brien built the original *tm5213;wdIs51* strain, the *tm5213;unc-40;wdIs51* strain, and the *pT24F1.4*::GFP plasmid and strain. Michaela Novakovic quantified 1° branch presence/absence and quantified 3° branch results for single mutants. Barbara M. J. O'Brien performed all the remaining experiments and analyses and wrote the manuscript.

CHAPTER 3 : SEPARATE MEC-3 REGULATED PATHWAYS SPECIFY DISTINCT CLASSES OF SISTER DENDRITES

Introduction

Sensory neurons extend dendrites into the skin to detect external signals. To achieve this complex process, dendrites must navigate the sub-epithelium during development to reach their targets in the sensory epithelium and establish their receptive fields. Despite the importance of dendrite outgrowth and stabilization to this function, the transcriptional pathways that specify this process are not well characterized. One transcription factor (TF) known to be involved in dendrite outgrowth is the conserved LIM homeodomain transcription factor MEC-3. *mec-3* mutants show a striking morphological phenotype where each PVD neuron extends 1° dendrites along the body of the worm but then fails to produce the lateral or 2° branches that give rise to the elaborate network of PVD dendrites that normally envelops the animal[29,50,51] (**Figure 3.1a-c**). To identify potential genes that mediate dendritic branching and are regulated by MEC-3, a gene expression profiling strategy was used, with a follow-up RNAi screen that identified MEC-3-regulated transcripts that were involved in dendritic branching in PVD. This approach determined that MEC-3 promotes expression of the TFIIA-like zinc finger transcription factor EGL-46 and the claudin-like membrane protein HPO-30; furthermore, it was found that HPO-30 is required for stabilizing lateral PVD dendritic branches[51]. This chapter reports that EGL-46 functions in parallel to HPO-30 to promote PVD lateral branching.

EGL-46 and its binding partner, the TEA domain transcription enhancer factor EGL-44, function together in *C. elegans* to regulate cell cycle exit in neural progenitors[55,56] and to define cell-specific traits in postmitotic neurons[53–55,137]. Our work previously revealed an additional role

for EGL-46 in dendritic branching: *egl-46* mutant PVD neurons show significantly fewer lateral branches than wild type[29,51,52]. That the PVD lateral branching phenotype of *egl-46* is less severe than that of *mec-3* is consistent with our microarray results showing that *egl-46* is regulated by MEC-3 and supports our conclusion that MEC-3 likely controls more than one downstream effector of dendritic branching[51]. In this chapter, we substantiate this prediction by showing that HPO-30 and EGL-46 act in separate pathways to drive lateral branching and that these roles correlate with two distinct classes of PVD dendrites: "commissural" and "pioneer."

Approximately half of PVD lateral branches fasciculate with pre-existing circumferential motor neuron commissures that bridge the gap between dorsal and ventral nerve cords. In contrast to these "commissural" PVD branches, "pioneer" 2° branches grow out in contact with the epidermis but are not bundled with motor neuron commissures. We have previously shown that HPO-30 is preferentially required for stabilizing pioneer branches[51]. Here we report that the EGL-46/EGL-44 complex performs the complementary role of supporting commissural branch outgrowth. These findings suggest the existence of a distinct class of downstream effectors of EGL-44/EGL-46 for either commissural branch formation or maintenance. Moreover, our discovery that the 2° branching defect of double mutants of *egl-44* and *hpo-30* is less severe than that of *mec-3* argues for at least one additional lateral branch promoting pathway that is also regulated by MEC-3. Finally, our observation that *mec-3* also defines the overall lengths of the PVD axon and 1° dendrites, traits that are not regulated by *egl-44*/*egl-46*, points to the existence of a separate class of *mec-3*-regulated targets that contribute to PVD 1° branch and axon morphogenesis.

Materials and Methods

Genetic strains

All *C. elegans* strains were grown on OP50 *Escherichia coli*-seeded nematode growth medium plates at 20°C as described[21]. Strains used in this study are listed in **Table 3.1**.

Table 3.1. Genetic strains used in this study

Strain	Genotype
NC1686	*wdIs51 (F49H12.4::GFP + unc119) X*
NC3160	*mec-3(e1338) IV; wdIs51(F49H12.4::GFP + unc119) X*
NC3044	*egl-44(n1080) II; wdIs51(F49H12.4::GFP + unc119) X*
NC2230	*egl-46(gk692) V; wdIs51(F49H12.4::GFP + unc119) X*
NC3075	*egl-44(n1080) II;egl-46(gk692) V; wdIs51 (F49H12.4::GFP + unc119) X*
NC3239	*wdIs51 [F49H12.4::GFP+UNC-119] X; wdEx1006 [pBMJO12 (F49H12.4::egl-46 genomic DNA, 15ng/uL); pCJS04 (F49H12.4::mCherry, 30ng/uL)]*
NC3266	*mec-3(e1338) IV; wdIs51 [F49H12.4::GFP+UNC-119] X; wdEx1006 [pBMJO12 (F49H12.4::egl-46 genomic DNA, 15ng/uL); pCJS04 (F49H12.4::mCherry, 30ng/uL)]*
NC3267	*egl-44(n1080) II; wdIs51 [F49H12.4::GFP+UNC-119] X; wdEx1006 [pBMJO12 (F49H12.4::egl-46 genomic DNA, 15ng/uL); pCJS04 (F49H12.4::mCherry, 30ng/uL)]*
NC3268	*egl-46(gk692) V; wdIs51 [F49H12.4::GFP+UNC-119] X; wdEx1006 [pBMJO12 (F49H12.4::egl-46 genomic DNA, 15ng/uL); pCJS04 (F49H12.4::mCherry, 30ng/uL)]*
TV12498	*wyIs378 [ser-2prom3::myrGFP::unc-54 3'UTR; prab-3::mCherry; podr-1::rfp] X*
NC3163	*mec-3(e1338) IV; wyIs378 [ser-2prom3::myrGFP::unc-54 3'UTR; prab 3::mCherry; podr-1::rfp] X*
NC3045	*egl-44(n1080) II; wyIs378 ([ser-2prom3::myrGFP::unc-54 3'UTR; prab-3::mCherry; podr-1::rfp] X*
NC3159	*egl-46(gk692) V; wyIs378 [ser-2prom3::myrGFP::unc-54 3'UTR; prab-3::mCherry; podr-1::rfp] X*
NC3154	*mec-3(e1338) IV; wdIs51(F49H12.4::GFP + unc119) X; wdEx991 (F49H12.4::egl-46cdna + pmyo-2::mCherry)*
NC3151	*egl-46(gk692) V; wdIs51 (F49H12.4::GFP + unc119) X; wdEx991 (F49H12.4::egl-46cdna + pmyo-2::mCherry)*

NC3280	*hpo-30(ok2047) V; wyIs378 [ser-2prom3::myrGFP::unc-54 3'UTR; prab-3::mCherry; podr-1::rfp] X*
NC3281	*egl-44(n1080) II; hpo-30(ok2047) V; wyIs378 [ser-2prom3::myrGFP::unc-54 3'UTR; prab-3::mCherry; podr-1::rfp] X*
NC3235	*hpo-30(ok2047) V; wdIs51 (F49H12.4::GFP + unc119) X*
NC3264	*egl-44(n1080) II; hpo-30(ok2047) V; wdIs51 (F49H12.4::GFP + unc119) X*
NC1891	*wdIs52 (F49H12.4::GFP + unc-119(+)); otIs181 (Pdat-1::mCherry)*
NC3165	*mec-3(e1338) IV; wdIs52 (F49H12.4::GFP + unc-119(+)); otIs181 (Pdat-1::mCherry)*
NC3164	*egl-46 (gk692) V; wdIs52 (F49H12.4::GFP + unc-119(+)); otIs181 (Pdat-1::mCherry)*
NC3236	*wdEx1005 [F49H12.4::rab-3::mCherry, Pmyo-2::mCh]*
NC3265	*mec-3(e1338) IV; wdIs51(F49H12.4::GFP + unc119) X; wdEx1005 [F49H12.4::rab-3::mCherry, Pmyo-2::mCh]*
NC3166	*egl-44(n1080) II; mec-3(e1338) IV; wdIs51 (F49H12.4::GFP + unc119) X*
NC3233	*egl-46(gk692) V; mec-3(e1338) IV; wdIs51 (F49H12.4::GFP + unc119) X*
NC3095	*egl-44(n1080) II; mec-3(e1338) IV; wyIs378 [ser-2prom3::myrGFP::unc-54 3'UTR; prab-3::mCherry; podr-1::rfp] X*
NC3096	*mec-3(e1338) IV; egl-46(gk692) V; wyIs378 [ser-2prom3::myrGFP::unc-54 3'UTR; prab-3::mCherry; podr-1::rfp] X*
NC2831	*uIs22 (Pmec-3::GFP + dpy-20(+))*
NC3228	*egl-44(n1080) II; uIs22 (Pmec-3::GFP + dpy-20(+))*
NC3229	*egl-46(gk692) V; uIs22 (Pmec-3::GFP + dpy-20(+))*
NC3273	*wyIs585 (ser2prom3::myr-mCherry::unc-54 3'UTR, podr1::GFP)IV; casEx1116[Pegl-44::gfp; Pegl-17::Myri-mCherry, Pegl-17::mCherry-TEV-S::his-24; unc-76(+)]*
NC3274	*mec-3(e1338) IV; wyIs585 (ser2prom3::myr-mCherry::unc-54 3'UTR, podr1::GFP)IV; casEx1116[Pegl-44::gfp; Pegl-17::Myri-mCherry, Pegl-17::mCherry-TEV-S::his-24; unc-76(+)]*
NC3275	*egl-46(gk692) V; wyIs585 (ser2prom3::myr-mCherry::unc-54 3'UTR, podr1::GFP)IV; casEx1116[Pegl-44::gfp; Pegl-17::Myri-mCherry, Pegl-17::mCherry-TEV-S::his-24; unc-76(+)]*
NC3148	*wdEx1015 (TU625 ex(pegl-44::gfp::egl-44); coel::RFP)*
NC3254	*egl-44 (n1080) II; wdEx1015 (TU625 ex(pegl-44::gfp::egl-44); coel::RFP)*
NC3269	*wyIs585 (ser2prom3::myr-mCherry::unc-54 3'UTR, podr1::GFP)IV; casEX1115[Pegl-46::gfp; Pegl-17::Myri-mCherry; Pegl-17::mCherry-TEV-S::his-24; unc-76(+)]*
NC3270	*mec-3(e1338) IV; wyIs585 (ser2prom3::myr-mCherry::unc-54 3'UTR, podr1::GFP)IV; casEX1115[Pegl-46::gfp; Pegl-17::Myri-mCherry; Pegl-17::mCherry-TEV-S::his-24; unc-76(+)]*

NC3271	*egl-44(n1080) II; wyIs585 (ser2prom3::myr-mCherry::unc-54 3'UTR, podr1::GFP)IV; casEX1115[Pegl-46::gfp; Pegl-17::Myri-mCherry; Pegl-17::mCherry-TEV-S::his-24; unc-76(+)]*
NC3272	*egl-46(gk692) V; wyIs585 (ser2prom3::myr-mCherry::unc-54 3'UTR, podr1::GFP)IV; casEX1115[Pegl-46::gfp; Pegl-17::Myri-mCherry; Pegl-17::mCherry-TEV-S::his-24; unc-76(+)]*
NC2647	*wdEx893 (Phpo-30::GFP + Pmec-4::mCherry + F49H12.4::mCherry)*
NC3241	*mec-3(e1338) IV; wdEx893 (Phpo-30::GFP + Pmec-4::mCherry + F49H12.4::mCherry)*
NC3240	*egl-44(n1080) II; wdEX893 (Phpo-30:GFP + F49H12.4::mCherry + Pmec-4::mCherry)*
NC2619	*wdEx890 [F49H12.4::HPO-30::GFP;ceh-22::GFP;PCJS04(PVD::mcherry)]*
NC3242	*mec-3(e1338) IV; wdEx890 [F49H12.4::HPO-30::GFP;ceh-22::GFP;PCJS04(PVD::mcherry)]*
NC3243	*egl-44(n1080) II; wdEx890 [F49H12.4::HPO-30::GFP;ceh-22::GFP;PCJS04(PVD::mcherry)]*
NC3244	*egl-46(gk692) V; wdEx890 [F49H12.4::HPO-30::GFP;ceh-22::GFP;PCJS04(PVD::mcherry)]*
RJP1748	*rpIs32[Pegl-13::GFP]; rpEx743(Pegl-46::dsRed2::NLS; Pelt-2::GFP)*
NC3313	*wdIs51 (F49H12.4::GFP); rpIs32[Pegl-13::GFP]; rpEx743(Pegl-46::dsRed2::NLS; Pelt-2::GFP)*
NC3314	*mec-3; wdIs51; rpIs32[Pegl-13::GFP]; rpEx743(Pegl-46::dsRed2::NLS; Pelt-2::GFP)*

Molecular cloning and generation of transgenic animals

To generate the *PVD::EGL-46* plasmid pBMJO12, the *egl-46* coding region was amplified from N2 genomic DNA using polymerase chain reaction (PCR) with 5' and 3' primers containing adaptors for Asc1 (tttttGGCGCGCCATGGTGCCTATGAATGACTT) and SacII (acacaCCGCGGctagattcactttcagcaaa), respectively. The resultant amplified fragment was digested with Asc1 and SacII and cloned into an expression plasmid (pBMJO1) containing the *F49H12.4* promoter. pBMJO12 (15 ng/µl) was co-injected with a plasmid that marked PVD with mCherry, pCJS04 (*F49H12.4::*mCherry) (30 ng/µl), into the strain *NC1686*, which contains an integrated marker for PVD labeled with GFP[32]. The resultant extrachromosomal array

(*wdEx1006*) was then crossed into different genetic backgrounds by monitoring the *F49H12.4*::mCherry co-injection marker.

The PVD::EGL-46(cDNA) plasmid was injected into N2 worms at 5 ng/µl along with the co-injection marker *Pmyo2*::mCherry (1 ng/µl). The strain with the resultant extrachromosomal array (*wdEx911*) was then crossed with *egl-46* and *mec-3* mutant worms by monitoring *Pmyo2*::mCherry.

The plasmid pCJS06 (*F49H12.4*::mCherry::RAB-3) was injected into N2 worms at 10 ng/µl with the co-injection marker *Pmyo2*::mCherry (2 ng/µl). The strain containing this extrachromosomal array (*wdEx1005*) was then crossed with *mec-3* mutant worms by monitoring *Pmyo2*::mCherry.

Pegl-44::GFP::EGL-44 (#TU625[55]) was injected into N2 worms at 15 ng/µl with the co-injection marker *Pcoel*::RFP (15 ng/µl). The strain containing this extrachromosomal array (*wdEx1015*) was then crossed with *egl-44* mutant worms by monitoring the *Pcoel*::RFP co-injection marker.

Single molecule mRNA FISH

smFISH was performed with custom Stellaris FISH probes purchased from Biosearch Technologies. The EGL-46 probe was hybridized to CAL Fluor® Red 590 dye. Synchronized late L2 animals were collected by washing plates with M9 and fixed in 4% paraformaldehyde in 1X PBS for 45 minutes. Fixed animals were permeabilized in 70% ethanol for 48 hours. Hybridization was performed following the suggested Stellaris protocol adapted from Raj et al., 2008[138]. Images were taken in z-stacks using a Nikon spinning disk confocal microscope and

appropriate optical filters for DAPI, CAL Fluor® Red 590, and Alexa 488. Experiments were performed using wild-type or *mec-3* mutant animals expressing *PVD*::GFP. Nuclei were stained with DAPI. Z-stacks were collected at 60X in 0.05 μm steps spanning the cell body and merged to quantify puncta. The *PVD*::GFP expression was used to limit smFISH puncta quantification to the PVD cell body. A specific CAL Fluor® Red 590 signal level was used as a threshold to minimize background. Discrete puncta were then counted manually using NIS elements. In all animals, distinct smFISH expression was also confirmed in head neurons to confirm successful smFISH expression.

Confocal microscopy

Worms were immobilized as previously described using 15 mM levamisole/0.05 tricaine on a 2% agarose pad in M9[29]. All images and quantitative data were obtained from L4 stage hermaphrodites. PVD neurons were visualized with cytosolic GFP driven by the *F49H12.4* or *ser2prom3* promoters; motor neuron commissures were visualized with mCherry driven by the pan-neural marker *Prab-3*. Confocal images were obtained on either a Leica TCS SP5 or Nikon A1R laser-scanning confocal microscope. Z-stacks were collected in 1 μm steps at 40X (oil objective, NA=1.3) to capture the cell body and all dendritic branches of one PVD neuron. Individual Z-stacks were merged into a single z-plane projection to visualize 1° and 2° branches. All images shown throughout the figures are adjusted for brightness and contrast (ImageJ) for clarity and to decrease background autofluorescence but are otherwise unaltered.

Quantification of neuronal features

A 2° branch was defined as a lateral branch that grew orthogonally from the 1° branch and reached the sublateral nerve cord. 2° branches that fasciculated with motor neuron commissures were counted as "commissural" branches, whereas 2° branches that did not fasciculate with motor neuron commissures were counted as "pioneer" branches.

1° branch length, axon length, and body length were measured using ImageJ. Branch or axon lengths were then divided by body lengths to obtain the branch/body or axon/body length ratios.

To score for the presence or absence of the PVD posterior 1° branch, worms were examined with a Zeiss Axiovert microscope (40X oil objective, NA=1.3) and results pooled from three separate experiments.

For the number of 2° branches in mutants of *egl-44* and mutants of *egl-44* containing the *Pegl-44*::GFP::EGL-44 construct[55], the number of 2° branches was counted by examining mutants immobilized on a slide using a Zeiss Axiovert microscope (40X oil objective, NA=1.3). Experimenter was not blinded to condition because the co-injection marker of *Pcoel*::RFP was visible for worms containing the construct. For all other experiments, the experimenter was blinded to condition when scoring.

Fluorescence intensity measurements

Immobilized worms were imaged on a Nikon A1R laser-scanning confocal microscope at 100X (oil objective, NA=1.49, 0.5 μm steps), spanning the depth of the cell body. ImageJ was

used to measure the fluorescence intensity of max-projection z-stacks. The segmented line tool was used to draw an outline of the cell soma, and the mean fluorescent intensity was divided by the area for each soma. The averages for each condition were then compared using one-way ANOVA with Kruskal-Wallis test for multiple comparisons using Graphpad Prism 6. Data were collected from worms in the L2 and L3 larval stages and pooled together.

Statistics

A Mann-Whitney test was used to determine significance between the two groups for the smFISH experiment. For all other comparisons between only two conditions, an unpaired t-test was used. One-way ANOVA with Tukey's test for multiple comparisons was used for comparisons of multiple conditions. For posterior 1° branch presence/absence analysis, Fisher's Exact test was used to determine statistical significance. All statistics were performed using Graphpad Prism 6.

Results

MEC-3 and EGL-46 promote 2° branches

We used the fluorescent marker *F49H12.4::GFP* to visualize PVD morphology. In wild-type worms, each PVD neuron adopts a striking orthogonal array of dendritic branches: lateral 2° dendrites arise from a central 1° dendritic process to constitute the "trunk" of menorah-like structures[29,30,87] (**Figure 3.1a-b**). Prior to our analyses performed below, we confirmed previous

findings that both *mec-3* and *egl-46* are required for the full complement of PVD menorahs[29,50,51]. We found that in *mec-3* mutants, all lateral branches (2°, 3°, and 4°) are absent with only anterior and posterior 1° dendrites projecting along the body axis and a single axon extending from the PVD cell body into the ventral nerve cord (**Figure 3.1c**). We observed a less severe branching defect for *egl-46* mutants consistent with previous studies[29,51]; *egl-46* mutants display about 25% fewer 2° branches than wild type (**Figure 3.1e**). Importantly, 3° and 4° branches are normal in *egl-46* mutants[52]. The PVD 2° branch defects for *mec-3* and *egl-46* are highly significant ($p<0.0001$, each compared to *wt*) (**Figure 3.1e**). Similar results were obtained when PVD was visualized with *ser2prom3::GFP* (**Figure 3.2e**). Having replicated these previously published results, we further explored the role of EGL-46 in 2° branching.

egl-44 and *egl-46* act in a common genetic pathway to regulate PVD 2° branching

Previous studies involving EGL-46 have illustrated that the TEA domain transcription factor EGL-44 typically functions in concert with EGL-46 to specify cell-specific traits in *C. elegans*[54,55,137]. Therefore, we hypothesized that EGL-44 may play a similar role in PVD dendritic development. We found that in *egl-44* mutants, the 2° branch defect is virtually identical to that of *egl-46* ($p>0.05$) and this mutation also results in a significant reduction (~25%) in PVD 2° branches ($p<0.001$ vs *wt*) (**Figure 3.1e** and **Figure 3.2e**).

Since our results indicated that *egl-44* and *egl-46* mutants show similar deficits in the number of 2° branches per worm, we generated an *egl-44;egl-46* double mutant to determine if *egl-44* and *egl-46* act in the same genetic pathway to affect 2° dendrite development. Our results showed that *egl-44;egl-46* animals had fewer 2° branches than wild type ($p<0.001$), but these

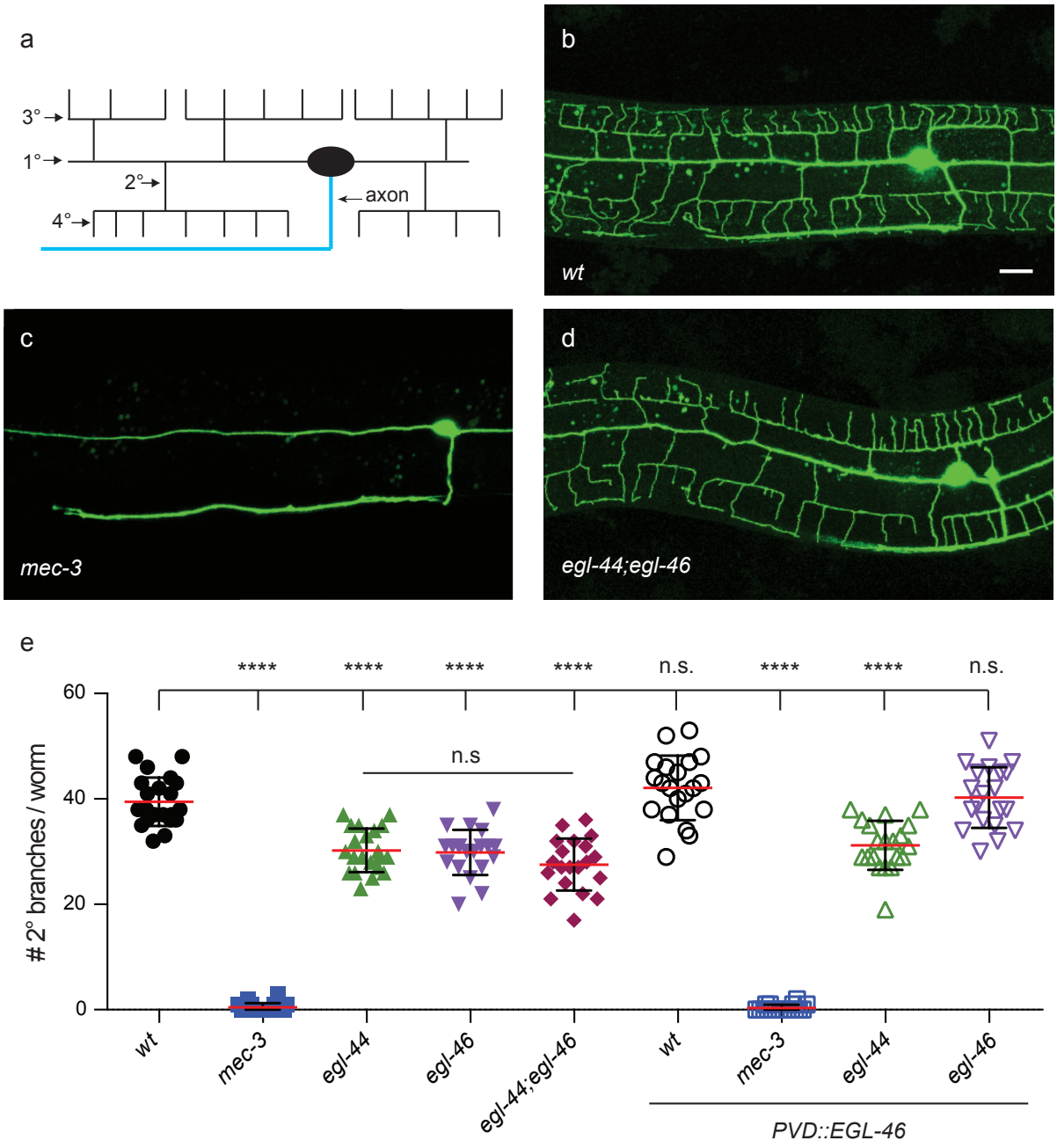

Figure 3.1: EGL-46 acts cell-autonomously with EGL-44 to promote 2° branches in PVD neurons. (a) Schematic of PVD morphology, highlighting 1°, 2°, 3°, and 4° dendritic branches and single axon, **(b-d)** confocal images of PVD in wild-type (*wt*) **(b)** and mutants of *mec-3* **(c)** and *egl-44;egl-46* **(d)**, visualized with cytosolic GFP driven by the *F49H12.4* promoter, **(e)** quantification of 2° branches in different genetic backgrounds. Left is anterior, up is dorsal, scale bar = 10 µm, **** indicates $p<0.0001$, n.s. = not significant, one-way ANOVA with Tukey's test for multiple comparisons, error bars represent SEM, $n\geq18$.

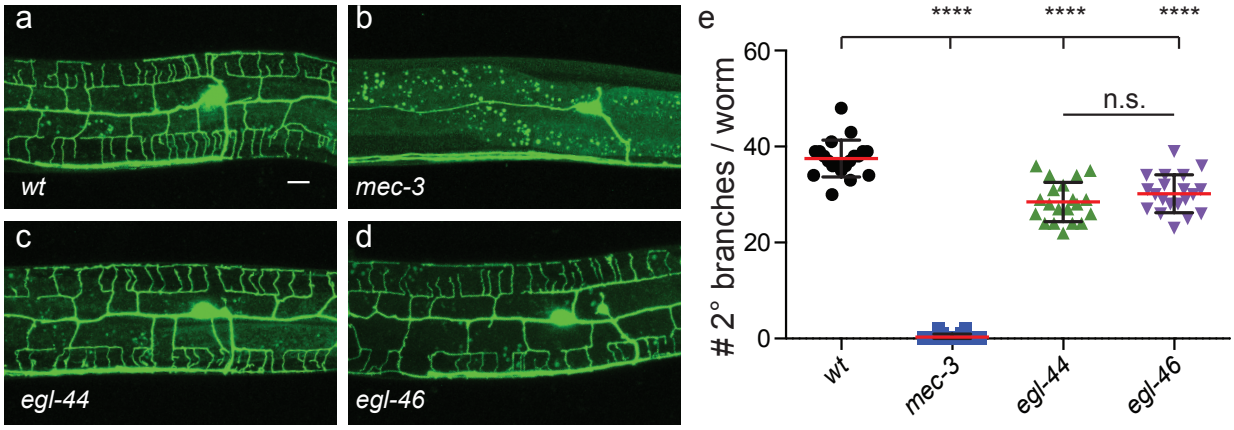

Figure 3.2: MEC-3, EGL-44, and EGL-46 promote 2° branches. (a-d) Confocal images of PVD in *wt* **(a)** and mutants of *mec-3* **(b)**, *egl-44* **(c)**, and *egl-46* **(d)**, visualized with cytosolic GFP expressed with the *ser2prom3* promoter, **(e)** quantification of 2° branches in different genetic backgrounds. A second GFP-labeled ventral process visible in panel **b** corresponds to the PDE axon. Left is anterior, up is dorsal, scale bar = 10 μm, **** indicates $p<0.0001$, n.s. = not significant, one-way ANOVA with Tukey's test for multiple comparisons, error bars represent SEM, n=20.

values did not differ significantly from either *egl-44* or *egl-46* single mutants alone ($p>0.05$) (**Figure 3.1e**). This result suggests that *egl-44* and *egl-46* act in the same genetic pathway to facilitate PVD 2° branching.

Expression of EGL-46 in PVD is sufficient to restore wild-type 2° branch number in *egl-46* mutants

Our previous study demonstrated that *egl-46* expression in PVD depends on *mec-3*[51]. Since *mec-3* is required for all higher order branching, this result suggests that *egl-46* likely functions in PVD to promote 2° branch outgrowth. To determine if *egl-46* acts in PVD to promote 2° branch outgrowth, we fused the EGL-46 coding region to the PVD-specific *F49H12.4* promoter to test cell-autonomy. We determined that expression of the resultant *PVD*::EGL-46 transgene sufficiently rescued the 2° branch defect of *egl-46* mutants ($p<0.0001$ for *egl-46* compared to *egl-46;PVD::*EGL-46 and $p>0.05$ for *wt* compared to *egl-46;PVD::*EGL-46). Interestingly, the cell-specific expression of *egl-46* in PVD did not rescue the *egl-44* defect ($p>0.05$ for *egl-44* compared to *egl-44;PVD::*EGL-46) (**Figure 3.1e**). These results suggest that EGL-46 acts cell autonomously in PVD and that this function depends on *egl-44*. Our discovery that the *PVD*::EGL-46 construct did not restore 2° branches to a *mec-3* mutant suggests that EGL-46-dependent branching may also require other components that are independently regulated by *mec-3* ($p>0.05$ for *mec-3* compared to *mec-3;PVD::*EGL-46). Finally, our observation that overexpression of *PVD*::EGL-46 does not induce additional 2° branches in the wild type ($p>0.05$ for *wt* compared to *wt;PVD::*EGL-46) suggests that EGL-46-dependent branching may also be limited by additional pathways that prevent the creation of ectopic 2° branches.

Interestingly, cell-specific expression of EGL-46 cDNA in PVD failed to rescue the 2° branch phenotype in *egl-46* mutants. Also, no branches were induced in *mec-3* mutants carrying this construct ($p>0.05$ for mutants with the construct compared to mutants without construct; $p<0.0001$ for all mutants with and without construct compared to wildtype) (**Figure 3.3**).

EGL-44/EGL-46 selectively promote the formation of commissural 2° branches

Once we established that mutations in *egl-44* and *egl-46* only eliminated a fraction (~25%) of PVD lateral branches, we next sought to identify if the *egl-44/egl-46* regulated pathway is required for a specific subset of 2° dendrites. We reanalyzed our results from **Figure 3.1e** and determined that *egl-44/egl-46* mutants do not selectively eliminate either dorsally or ventrally projecting 2° branches, nor do *egl-44/egl-46* mutants selectively eliminate 2° branches that arise either anterior or posterior to the PVD cell soma (**Figure 3.4**). Finally, we investigated the 2° branches that arise from PVDR on the right side of the animal vs PVDL on the left. Our results agreed with our previous finding[29,51] that PVDR contains more 2° branches than PVDL in the wild type ($p<0.001$) (**Figure 3.5a**, **Figure 3.6**). Strikingly, this right-left bias was largely reduced or absent in *egl-44* and *egl-46* mutants (**Figure 3.5a**, **Figure 3.6**), despite a significant loss of 2° branches for both PVDR and PVDL. This finding is suggestive of a specific role for *egl-44*/*egl-46* in PVDR branching and provides important insights into the subtype of 2° branch that depends on the *egl-44/egl-46* pathway.

We previously reported that a subset of PVD 2° branches fasciculate with commissures from ventral cord motor neurons and suggested that this interaction may stabilize the circumferential outgrowth of these "commissural" 2° branches[29]. This hypothesis is consistent

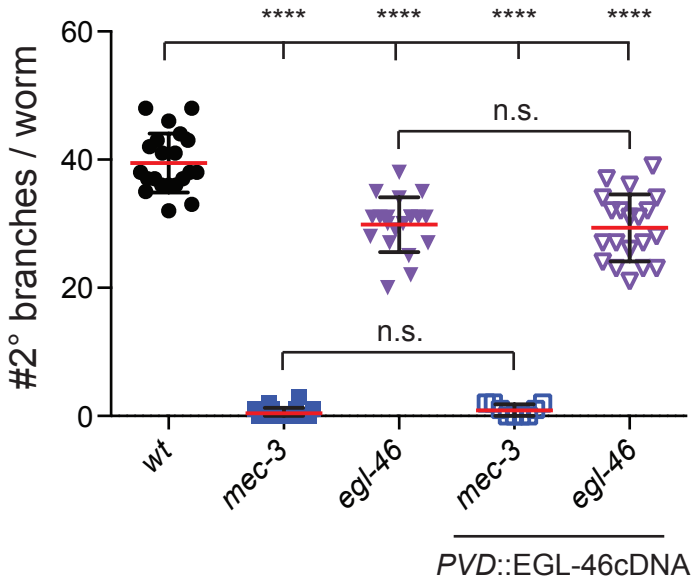

Figure 3.3: Expression of EGL-46(cDNA) in PVD is not sufficient for 2° branch number. Quantification of 2° branches in different genetic backgrounds. Data for *wt*, *mec-3*, and *egl-46* are the same as those presented in **Figure 3.1**. **** indicates $p<0.0001$, n.s. = not significant, one-way ANOVA with Tukey's multiple comparison test, $n\geq 9$.

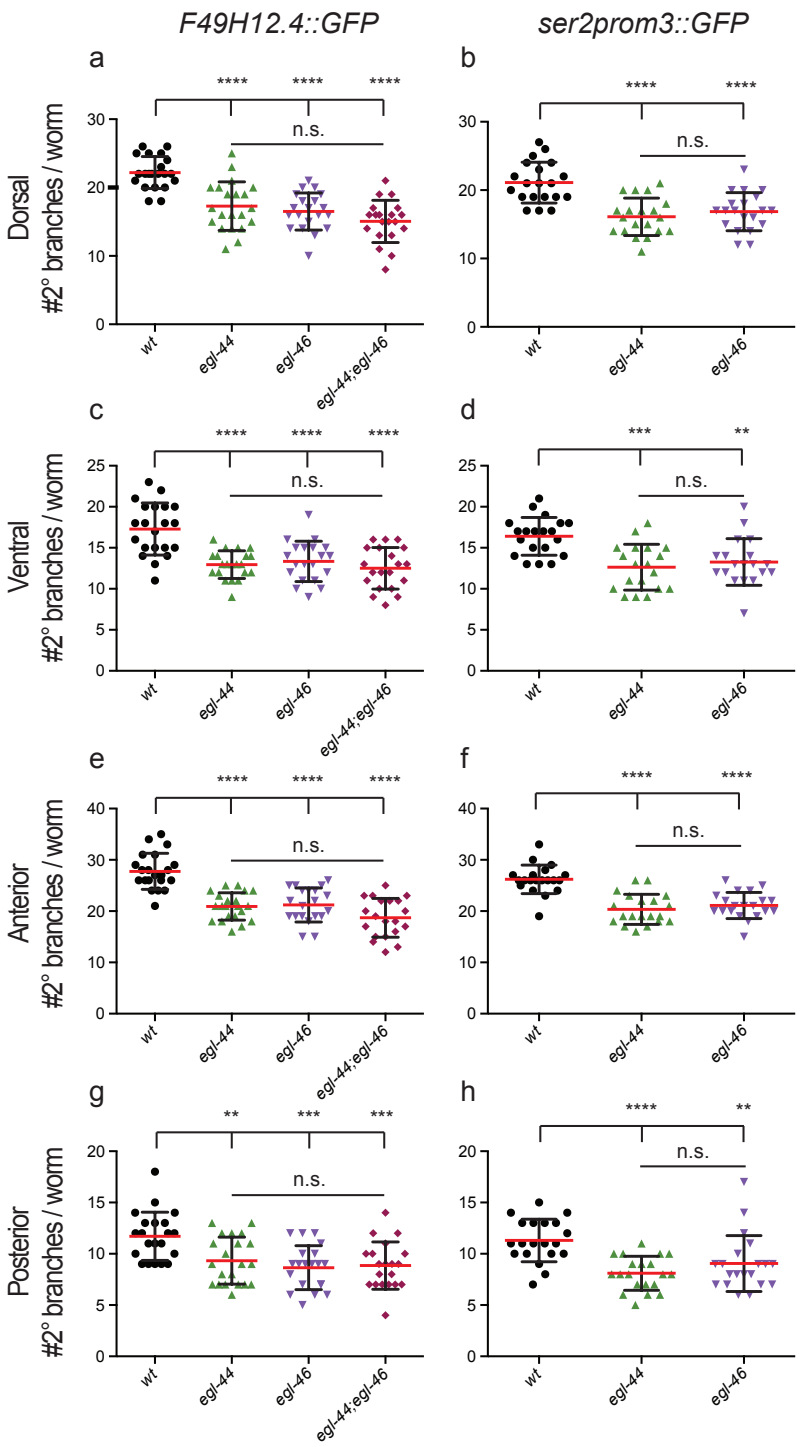

Figure 3.4: 2° branch decrease is similar across dorsal, ventral, anterior, and posterior regions. 2° branch number data from **Figure 3.1 (a, c, e, and g)** and **Figure 3.2 (b, d, f, and h)** re-analyzed to depict results for dorsal **(a,b)** and ventral **(c,d)** 2° branches and for 2° branches anterior **(e,f)** and posterior **(g,h)** to the PVD cell body. ** indicates $p<0.01$, *** indicates $p<0.001$, **** indicates $p<0.0001$, n.s. = not significant, one-way ANOVA with Tukey's test for multiple comparisons, error bars represent SEM, $n\geq18$.

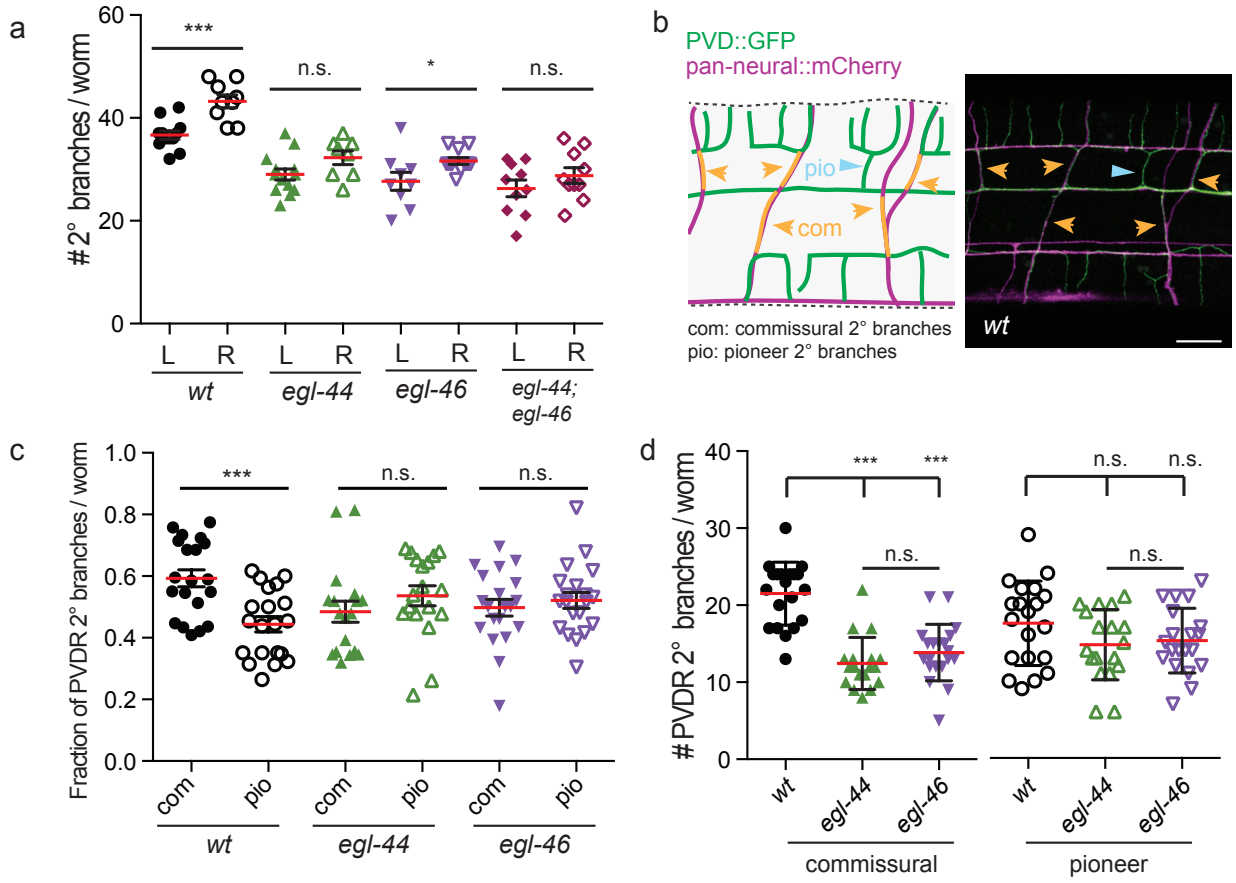

Figure 3.5: EGL-44 and EGL-46 promote commissural branching. (a) Number of 2° branches for PVDR on the right side (R) vs PVDL on the left (L) (data from **Figure 3.1**), n≥8, **(b)** (left panel) schematic of commissural (com) and pioneer (pio) 2° branches, (right panel) confocal image of *PVD*::GFP (green) with *pan-neural*::mCherry (magenta) showing PVDR commissural 2° branches that fasciculate with motor neuron commissures (orange arrow-heads) and pioneer 2° branches that do not fasciculate with motor neuron commissures (blue arrow-heads), **(c)** fraction of commissural (com) and pioneer (pio) 2° branches for PVDR in different genetic backgrounds, **(d)** number of commissural and pioneer 2° branches for PVDR in different genetic backgrounds. Left is anterior, up is dorsal, scale bar = 10 µm, * $p<0.05$, *** $p<0.001$, n.s. = not significant, unpaired t-test (**a** and **c**), one-way ANOVA with Tukey's test for multiple comparisons (**d**), error bars represent SEM, n≥18.

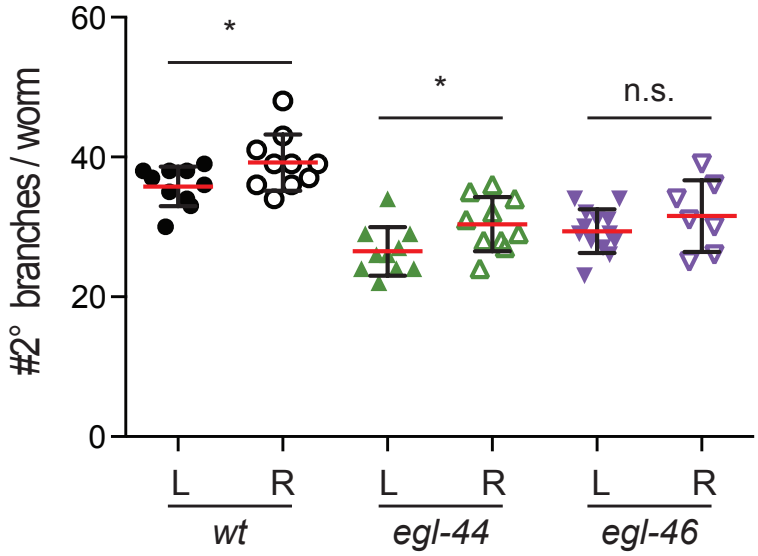

Figure 3.6: PVDR contains more 2° branches than PVDL. Number of 2° branches for PVDR on the right side (R) vs PVDL on the left (L) (data from **Figure 3.2**). * indicates $p<0.05$, n.s. = not significant, unpaired t-test, error bars represent SEM, $n\geq7$.

with the observation that the majority of motor neuron commissures are located on the right side[22] of the worm (**Figure 3.7a-b**), that PVDR contains more 2° branches than PVDL, and that this right-left bias is abrogated by a genetic mutation that selectively eliminates motor neuron commissural outgrowth[29]. We therefore hypothesized that the diminution of right-left bias in *egl-44* and *egl-46* mutants was due to the preferential loss of commissural branches. We tested this hypothesis by identifying the fraction of 2° branches that fasciculate with motor neuron commissures (commissural branches) vs 2° branches that do not fasciculate with motor neuron commissures (pioneer branches) in PVDR (**Figure 3.5b**). In the wild type, PVDR showed a higher fraction (~60%) of commissural than pioneer branches (~40%) ($p<0.001$). This bias was not apparent, however, in mutants of *egl-44* ($p>0.05$) or *egl-46* ($p>0.05$) (**Figure 3.5c**) and cannot be attributed to reduced numbers of motor neuron commissural processes, because these are normal in *egl-44* and *egl-46* mutants ($p>0.05$ across all conditions) (**Figure 3.7**). Next, we quantified the total number of PVDR commissural and pioneer branches and determined that commissural 2° branches are reduced in mutants of *egl-44* and *egl-46* compared to *wt* ($p<0.0001$). However, we did not detect significant differences for the number of PVDR pioneer branches across genotypes ($p>0.05$) (**Figure 3.5d**). These results suggest that the EGL-44/EGL-46 pathway specifically regulates downstream components involved in 2° branches that fasciculate with motor neuron commissures but is not required for pioneer branch outgrowth.

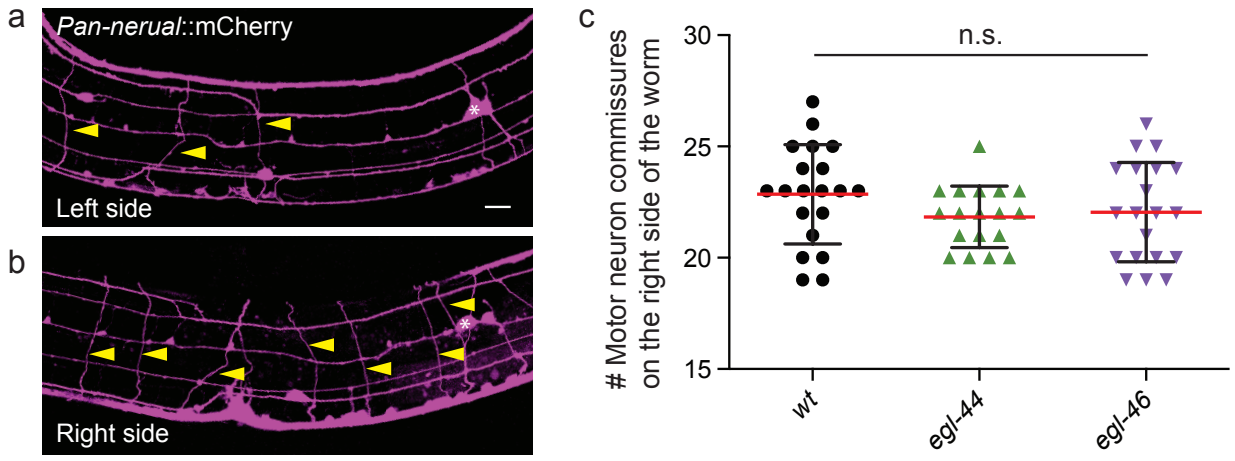

Figure 3.7: EGL-44/EGL-46 are not required for motor neuron commissure asymmetry. **(a-b)** Images of motor neuron commissures (yellow arrowheads) on the left **(a)** and right **(b)** sides of wild-type worms, as visualized with the pan-neural marker *Prab-3::*mCherry, **(c)** number of motor neuron commissures on the right side for *wt*, *egl-44*, and *egl-46*. Left is anterior, up is dorsal, scale bar = 10 μm, * in the images indicates the PVD cell body; yellow arrowheads point to commissures. n.s. = not significant, one-way ANOVA with Tukey's test for multiple comparisons, error bars represent SEM, n≥18.

EGL-44 and HPO-30/Claudin act in parallel pathways to mediate 2° branch number

We previously reported that MEC-3 activates transcription of the claudin-like membrane protein HPO-30 in PVDR neurons to mediate pioneer branch outgrowth; *hpo-30* mutants have a reduction in pioneer vs commissural PVDR 2° branches[51]. Because *egl-44* and *egl-46* mutants display the opposite effect of *hpo-30* mutants (i.e., loss of commissural vs pioneer branches), we hypothesized that *egl-44/egl-46* and *hpo-30* function in complementary pathways to regulate 2° branch outgrowth. To test this hypothesis, we generated double mutants of *egl-44* and *hpo-30* (**Figure 3.8a-c**, **Figure 3.9**) and determined that *egl-44;hpo-30* mutants displayed significantly fewer 2° branches in PVDR than either single mutant alone ($p>0.05$ for *hpo-30* vs. *egl-44*, $p<0.05$ for *hpo-30* vs. *egl-44;hpo-30*, $p<0.01$ for *egl-44* vs. *egl-44;hpo-30*) (**Figure 3.8e**). This result is consistent with a model that places *egl-44* and *hpo-30* in separate pathways to control 2° branching in PVD.

If EGL-44 selectively promotes commissural branch outgrowth while HPO-30 acts on pioneer branches, then double mutants of *egl-44;hpo-30* should also show fewer commissural branches than *hpo-30* but not *egl-44*. We quantified commissural branches for these three mutant backgrounds and found this hypothesis is correct ($p>0.05$ for *egl-44* vs. *egl-44;hpo-30*, $p<0.05$ for *hpo-30* vs. *egl-44;hpo-30*, $p<0.01$ for *hpo-30* vs. *egl-44*) (**Figure 3.8f**). We performed a similar analysis and confirmed an additional expectation that double mutants of *egl-44;hpo-30* should show fewer pioneer branches than *egl-44* but not *hpo-30* ($p>0.05$ for *hpo-30* vs. *egl-44;hpo-30*, $p<0.001$ for *hpo-30* vs. *egl-44*, $p<0.0001$ for *egl-44* vs. *egl-44;hpo-30*) (**Figure 3.8g**).

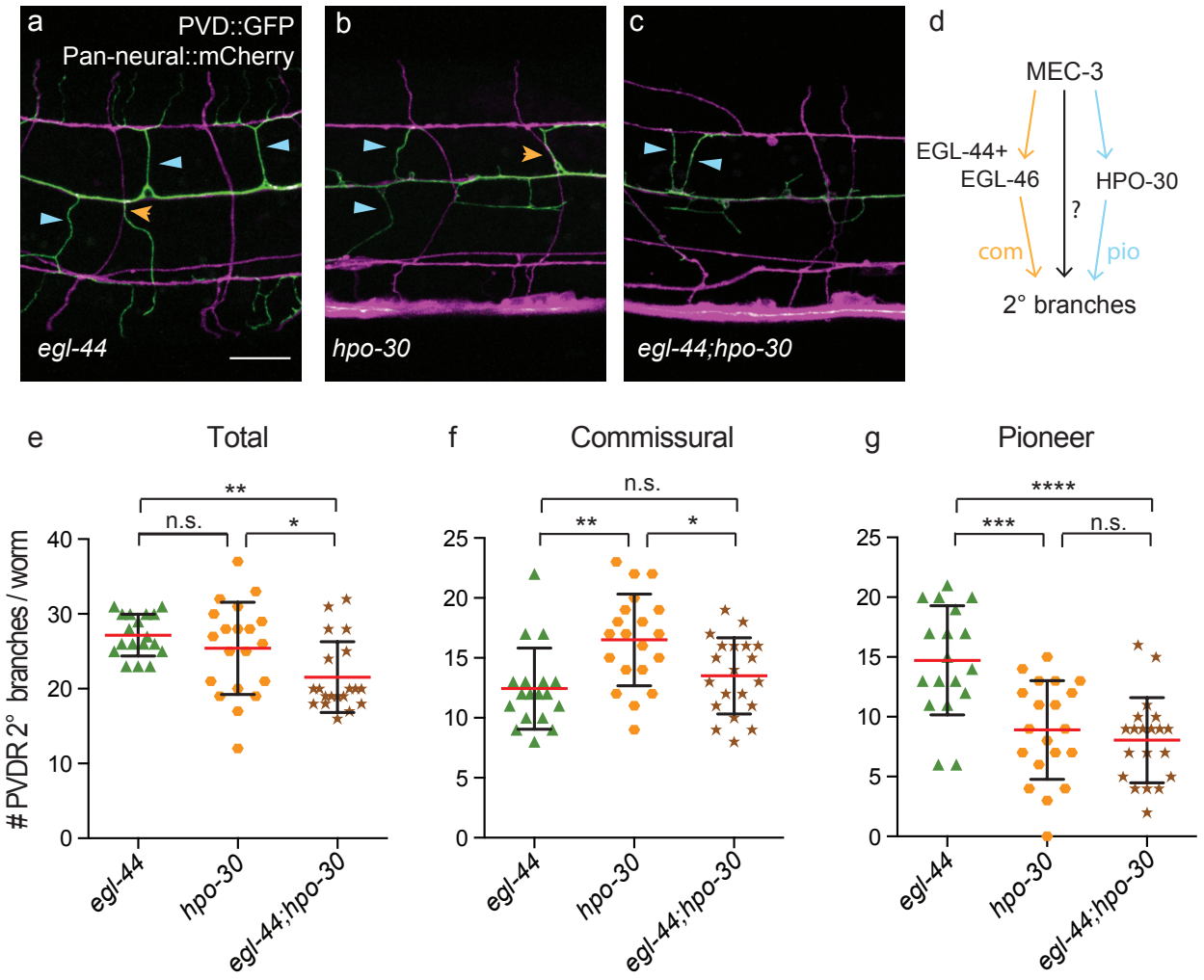

Figure 3.8: EGL-44 and HPO-30 act in parallel pathways to mediate 2° branch outgrowth. **(a-c)** Confocal images of *egl-44* **(a)**, *hpo-30* **(b)**, and *egl-44;hpo-30* **(c)** mutants, PVDR labeled with *ser2prom3::*GFP (green) and motor neuron commissures marked with *Prab-3::*mCherry (magenta), commissural (orange arrowheads) vs pioneer (blue arrow heads) 2° branches, **(d)** proposed genetic pathways for MEC-3-dependent outgrowth of commissural (com) and pioneer (pio) 2° branches, **(e-g)** quantification of total **(e)**, commissural **(f)**, and pioneer **(g)** 2° branches in PVDR for *egl-44* and *hpo-30* single mutants and for *egl-44;hpo-30* double mutant animals. Left is anterior, up is dorsal, scale bar = 10 µm, * indicates $p<0.05$, ** indicates $p<0.01$, *** indicates $p<0.001$, **** indicates $p<0.0001$, n.s. = not significant, one-way ANOVA with Tukey's test for multiple comparisons, error bars represent SEM, $n\geq18$. Data for *egl-44* single mutants are the same as in **Figure 3.5**.

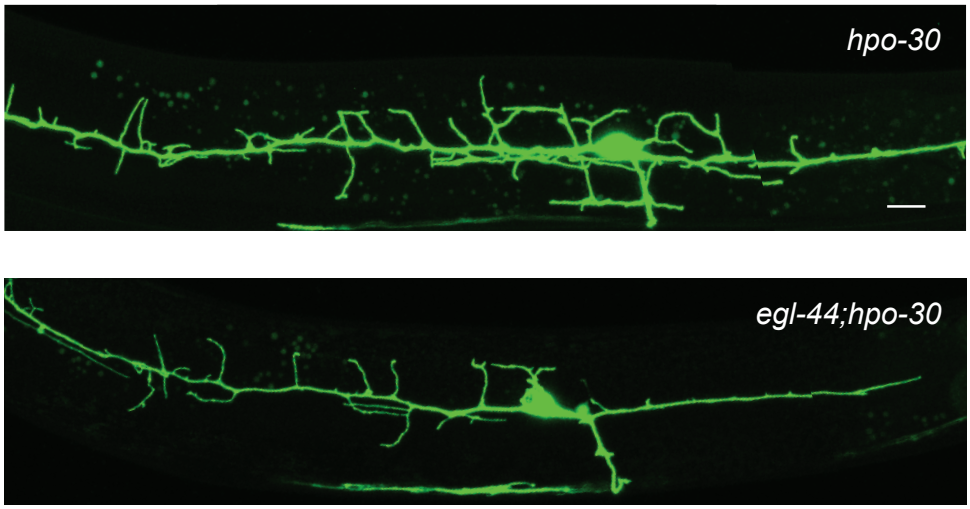

Figure 3.9: Mutant phenotypes of *hpo-30* and *egl-44;hpo-30*. Confocal images of *hpo-30* (top) and *egl-44;hpo-30* (bottom) mutants as visualized with *F49H12.4::*GFP. Left is anterior, up is dorsal, scale bar = 10 μm.

These results suggest that commissural and pioneer PVD 2° branches are defined by separate genetic pathways. However, the significant number of residual 2° branches (roughly 50% of wild-type) in double mutants of *egl-44;hpo-30* and the absence of all 2° branches in a *mec-3* mutant suggests that MEC-3 likely regulates at least one additional pathway that promotes 2° branch outgrowth (**Figure 3.8d**). Thus, the EGL-44/EGL-46 pathway selectively promotes commissural branches; the HPO-30 pathway selectively promotes pioneer branches; and at least one more MEC-3-regulated pathway is involved.

MEC-3 determines 1° branch length and axon length

Because the *mec-3* phenotype (i.e., the absence of all higher order branches) highlights a critical role for MEC-3 in PVD lateral branching, we also considered that MEC-3 may also affect other features of PVD architecture. In the wild type, the anterior 1° branch extends from the PVD soma to the base of the pharynx while the posterior 1° branch projects from the cell soma to the anus. We measured the lengths of anterior and posterior 1° branches (**Figure 3.10a**) and found that both the anterior and posterior branches were shorter in comparison to body length in mutants of *mec-3* ($p<0.0001$ vs *wt*) but not in mutants of *egl-44*, *egl-46*, or *egl-44;egl-46* ($p>0.05$, each compared to *wt*) (**Figure 3.10b-e**). This difference was particularly noticeable in a fraction of *mec-3* mutants where the posterior 1° branch was completely absent ($p<0.001$, *mec-3* vs. *wt*) (**Figure 3.10f-g**). In contrast, mutants of *egl-44*, *egl-46*, and *egl-44;egl-46* never showed this specific defect (data not shown).

We also observed that the axon length in *mec-3* mutants appeared to be longer than in the wild type. Normally, the PVD axon adopts an L-shaped trajectory, whereby it projects ventrally

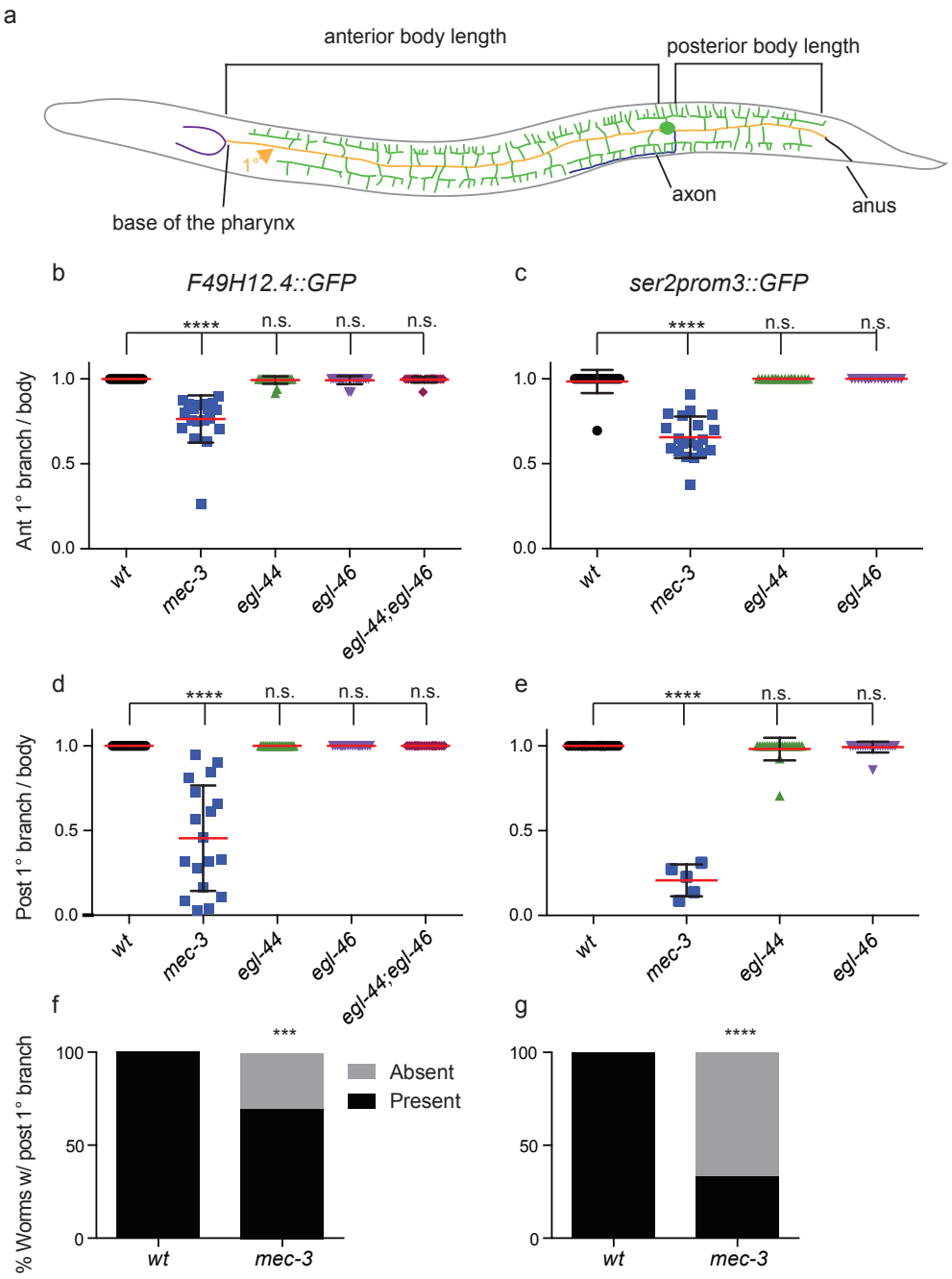

Figure 3.10: MEC-3 regulates 1° branch length. (a) Schematic showing anterior and posterior 1° branches (gold) and body regions relative to the location of the PVD cell body, **(b-c)** ratio of anterior 1° branch length to anterior body, visualized with *F49H12.4::GFP* **(b)** and *ser2prom3::GFP* **(c)**, **(d-e)** ratio of posterior 1° branch length to posterior body, visualized with *F49H12.4::GFP* **(d)** and *ser2prom3::GFP* **(e)**, **(f-g)** percentage of worms with (black) or without (gray) the posterior 1° process when visualized with *F49H12.4::*GFP **(f)** and *ser2prom3::*GFP **(g)**. Left is anterior; up is dorsal, **** indicates $p<0.0001$, n.s. = not significant, one-way ANOVA with Tukey's test for multiple comparisons (**b-e**), Fisher's exact test (**f-g**), error bars represent SEM, $n\geq18$.

from the cell soma and then turns anteriorly upon entering the ventral nerve cord[22]. This overall morphology is preserved in *mec-3* mutants, which do not show visible PVD axon guidance defects (data not shown) but do display a significantly longer axonal projection into the ventral nerve cord. PVD axonal length was not perturbed in *egl-46* mutants ($p<0.0001$ for *wt* vs. *mec-3* and for *egl-46* vs. *mec-3*, $p>0.05$ for *wt* vs. *egl-46*) (**Figure 3.11a**). Finally, to ask if MEC-3 regulates synaptic components, we tagged the presynaptic vesicle-associated protein, RAB-3, with mCherry. We found that mCherry::RAB-3 was localized throughout the length of the *mec-3* mutant axon, similar to the wild type. This result suggests that *mec-3* is not required for the trafficking or localization of the presynaptic apparatus (**Figure 3.11b**).

MEC-3 and EGL-44/EGL-46 share redundant roles in regulating PVD-specific genes

Our results are consistent with a model whereby MEC-3 regulates *egl-46* expression to control a group of downstream effector genes that promote commissural branch outgrowth. Additional results suggest, however, that a subset of PVD genes may be co-regulated by MEC-3 and by EGL-44/EGL-46. The reporter genes *ser2prom3::*GFP and *F49H12.4::*GFP are highly expressed in PVD in wild type, and this PVD expression is maintained in single mutants of either *mec-3*, *egl-44*, or *egl-46*, and in double mutants of *egl-44;egl-46*. The PVD expression of *ser2prom3*::GFP and *F49H12.4*::GFP is not detectable, however, in double mutants of either *egl-44;mec-3* or *egl-46;mec-3* but is visible in the adjacent PDE neuron (**Figure 3.12**, **Figure 3.13**). To confirm that the loss of GFP expression in PVD was not due to loss of the PVD neuron in *egl-44;mec-3* and *egl-46;mec-3* double mutants, we used the pan-neural marker *Prab-3::mCherry*, which labels all neurons in the worm. In these animals, a single mCherry-labeled

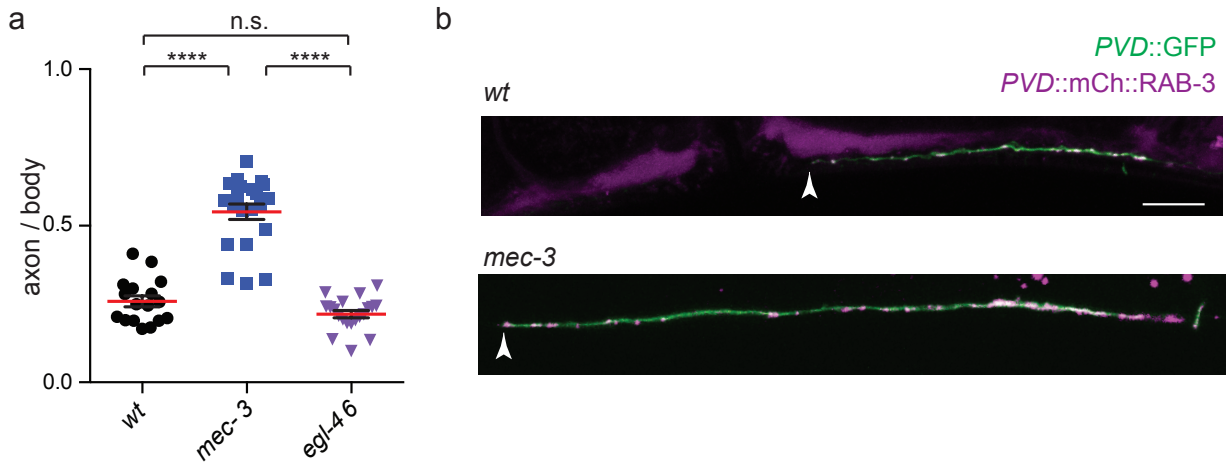

Figure 3.11: MEC-3 regulates PVD axon length. (a) Ratio of axon length to anterior body, as indicated in **Figure 3.10a**, **(b)** confocal images of the PVD axon (green) with mCherry-tagged RAB-3 (magenta), white arrowheads denote RAB-3 puncta localized to the tip of the axon. Left is anterior; up is dorsal, **** indicates $p<0.0001$, n.s. = not significant, one-way ANOVA with Tukey's test for multiple comparisons, error bars represent SEM, $n\geq17$.

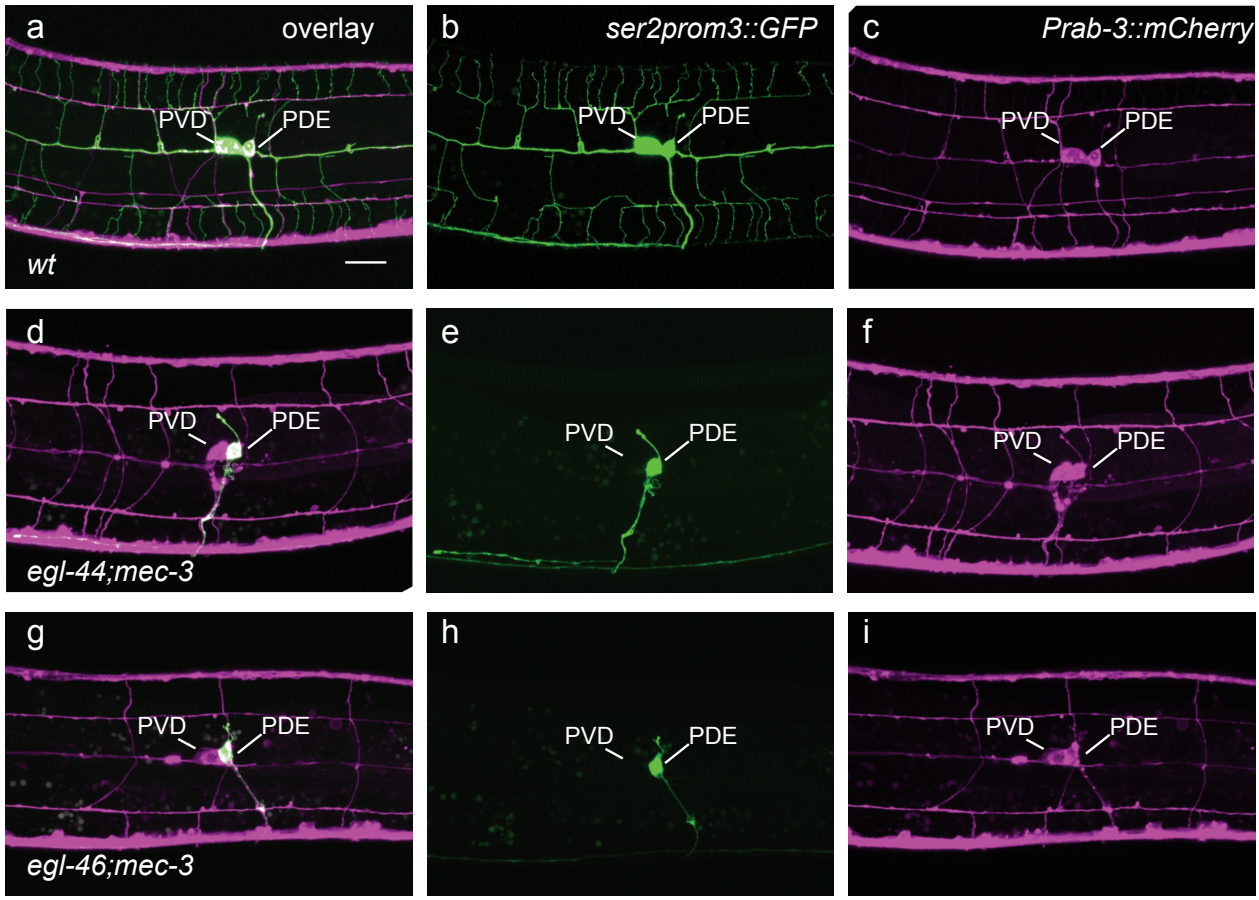

Figure 3.12: *mec-3* and *egl-46* share redundant roles in regulating the *ser2prom3* promoter. Confocal images of PVD marked with *ser2prom3::*GFP **(b, e, h)**, or the pan-neural promoter *Prab-3::*mCherry **(c, f, i)**, or both **(a, d, g)** in wild type **(a-c)** and double mutants of *egl-44;mec-3* **(d-f)** and *egl-46;mec-3* **(g-i)**. Images are maximum-projections. Left is anterior, up is dorsal. Scale bar = 10 μm.

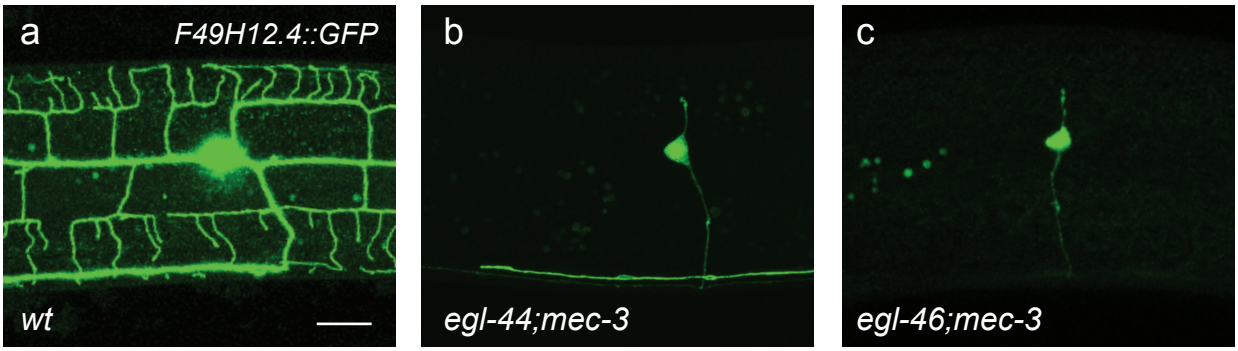

Figure 3.13: *mec-3* and *egl-46* share redundant roles in regulating the *F49H12.4* promoter. Confocal images of wild type **(a)** and double mutants of *egl-44;mec-3* **(b)** and *egl-46;mec-3* **(c)** labeled with *F49H212.4::*GFP. Images are maximum-projections. Left is anterior, up is dorsal. Scale bar = 10 μm.

cell body is clearly visible directly anterior to PDE in the location usually occupied by PVD (**Figure 3.12**). These results suggest that *mec-3* and *egl-44*/*egl-46* may independently regulate a cohort of "PVD-specific" genes.

Since double mutants of *mec-3* and *egl-46* show no GFP in the PVD neuron, this suggests that EGL-46 may be regulated by another transcription factor such that in the absence of MEC-3 EGL-46 can still activate the *F49H12.4* and *ser2prom3* promoters to drive GFP. To test this hypothesis, we used single molecule fluorescent in situ hybridization (smFISH) to visualize the relative expression levels of EGL-46 in *wt* vs. *mec-3* mutant animals. We hypothesized that if MEC-3 is the sole regulator of EGL-46, then there should be no EGL-46 expression in PVD in *mec-3* mutants. However, EGL-46 mRNA puncta were still clearly visible in mutants of *mec-3* (**Figure 3.14a-b**), though to a lesser extent than in the wild type ($p<0.001$) (**Figure 3.14c**). Taken together, the results presented in **Figure 3.12**, **Figure 3.13**, and **Figure 3.14a-c** suggest that EGL-46 is regulated by MEC-3 but may also act independently of MEC-3 to regulate genes in PVD (**Figure 3.14d**).

Fluorescence intensity measurements

Having established that (1) MEC-3, EGL-44, and EGL-46 are required for 2° branch number, that (2) MEC-3 regulates multiple transcriptional pathways for different aspects of dendritic branch outgrowth, and that (3) EGL-44/EGL-46 share redundant roles with MEC-3 to regulate PVD-specific genes, we wanted to investigate the relationship between these three transcription factors and how they may regulate each other. The finding that mutants of *egl-46* show less 2° branches but not to the extent of that of *mec-3* mutants suggests that MEC-3

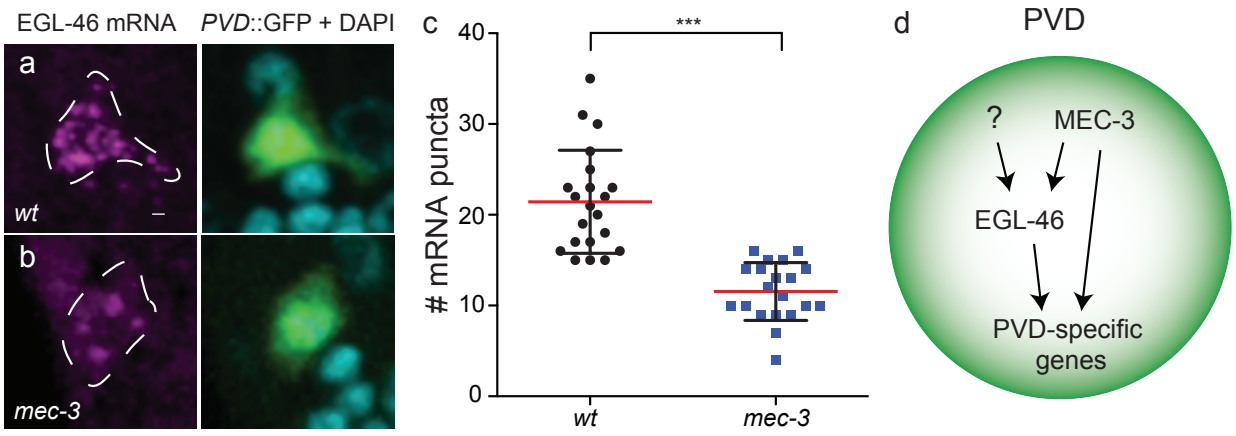

Figure 3.14: Multiple regulators of EGL-46 expression. (a-b) Confocal images of EGL-46 smFISH expression (magenta) in PVD, visualized by cytosolic GFP marker with DAPI nuclear marker in *wt* **(a)** and mec-3 mutants **(b)**, **(c)** quantification of number of discrete smFISH puncta observed in *wt* and *mec-3* mutant animals, **(d)** schematic showing relationship between MEC-3 and EGL-46 in PVD. Images are partial z-stacks to demonstrate representative signal. Left is anterior, up is dorsal, scale bar = 1 μm, *** indicates $p<0.001$, Mann-Whitney test, error bars represent SD, $n>20$.

regulates *egl-46*. Additionally, A previous microarray analysis to determine the levels of RNA expression in PVD in wild type and *mec-3* mutant worms suggested that MEC-3 regulates the expression of EGL-46 but not EGL-44[51]. Therefore, we hypothesized that MEC-3 regulates *egl-46* but not *egl-44* to mediate an EGL-46-dependent pathway. Furthermore, we demonstrated that MEC-3 regulates *egl-46* with smFISH, but because there was still signal of EGL-46 expression in *mec-3* mutants, another regulator of EGL-46 probably exists in PVD. EGL-44 has previously been shown to regulate *egl-46* in the nociceptor neurons in the head (FLP-L and FLP-R) that show similar morphology to PVD[55]. Therefore, we hypothesized that EGL-44 regulates *egl-46* but that EGL-46 does not regulate *egl-44*. To test these hypotheses, we used promoter-GFP constructs for the respective genes and measured the fluorescence intensity of the GFP signal in the PVD cell body.

Our first hypothesis was that *mec-3* was not regulated by EGL-44 or EGL-46. Fluorescence intensity of *Pmec-3::GFP*[55] (**Figure 3.15a-c**) was not significantly different in mutants of *egl-44* or *egl-46* when compared to *wildtype* ($p>0.05$) (**Figure 3.15d**). This is consistent with our hypothesis that MEC-3 is upstream of EGL-46 and suggests that neither EGL-46 nor EGL-44 regulate *mec-3*.

Our second hypothesis was that neither MEC-3 nor EGL-46 regulate *egl-44*. However, intriguingly, we were unable to detect GFP in the PVD cell body under the *egl-44* promoter[56] (**Figure 3.16**). Therefore, we tried to visualize GFP-tagged EGL-44 driven by the *egl-44* promoter[55], but we were also unable to detect GFP in the PVD cell body using this reporter construct (**Figure 3.17a**). To ensure that the construct was actually present in the worms, we crossed this reporter gene into *egl-44* mutant worms with a PVD cytosolic marker and scored the number of 2° branches. Our results from this analysis indicated partial rescue of the *egl-44*

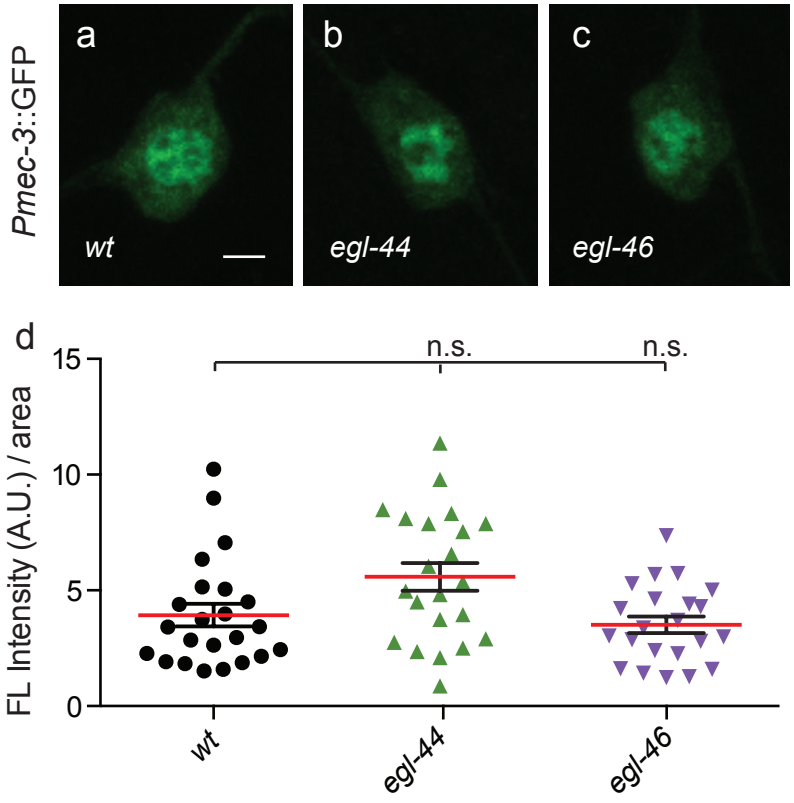

Figure 3.15: *egl-44* and *egl-46* are not required for regulation of the *mec-3* promoter. Confocal images of *Pmec-3::*GFP in the PVD cell body of *wt* **(a)** and mutants of *egl-44* **(b)** and *egl-46* **(c)**, **(d)** quantification of mean fluorescent intensity across conditions. Left is anterior; up is dorsal, scale bar = 2 μm, * indicates $p<0.05$, n.s. = not significant, one-way ANOVA with Dunn's test for multiple comparisons, error bars represent SEM, $n \geq 22$.

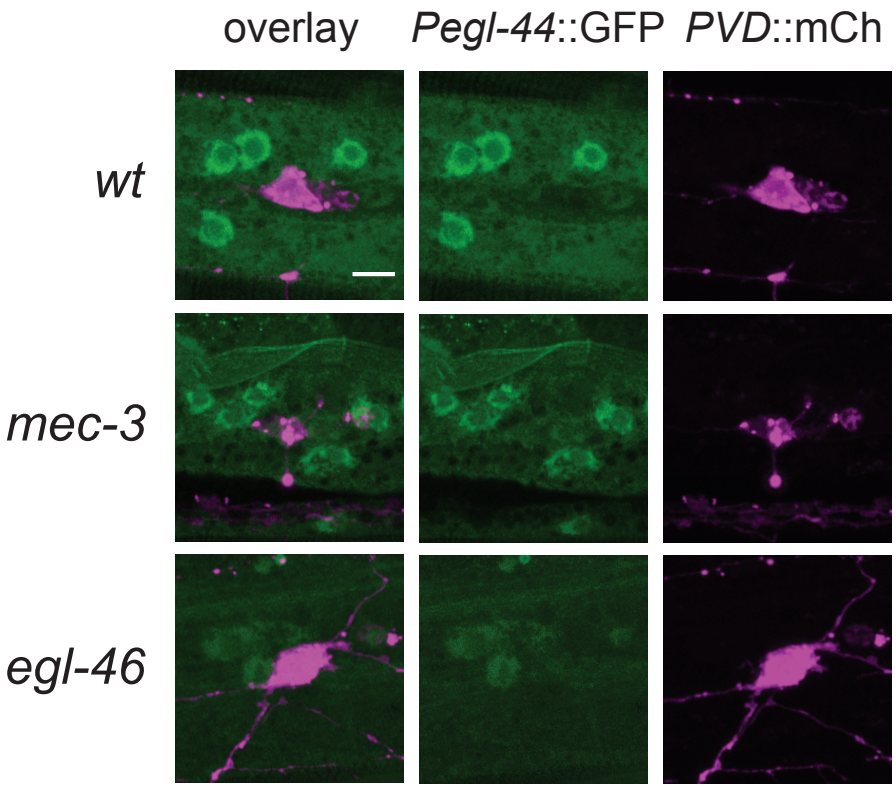

Figure 3.16: *Pegl-44*::GFP is not detected in PVD. Confocal images of *Pegl-44*::GFP (middle column), *F49H12.4*::mCherry (right column), and both (left column) for *wt* (top row), and mutants of *mec-3* (middle row) and *egl-46* (bottom row). Images are maximum-projections. Left is anterior; up is dorsal, scale bar = 2 μm.

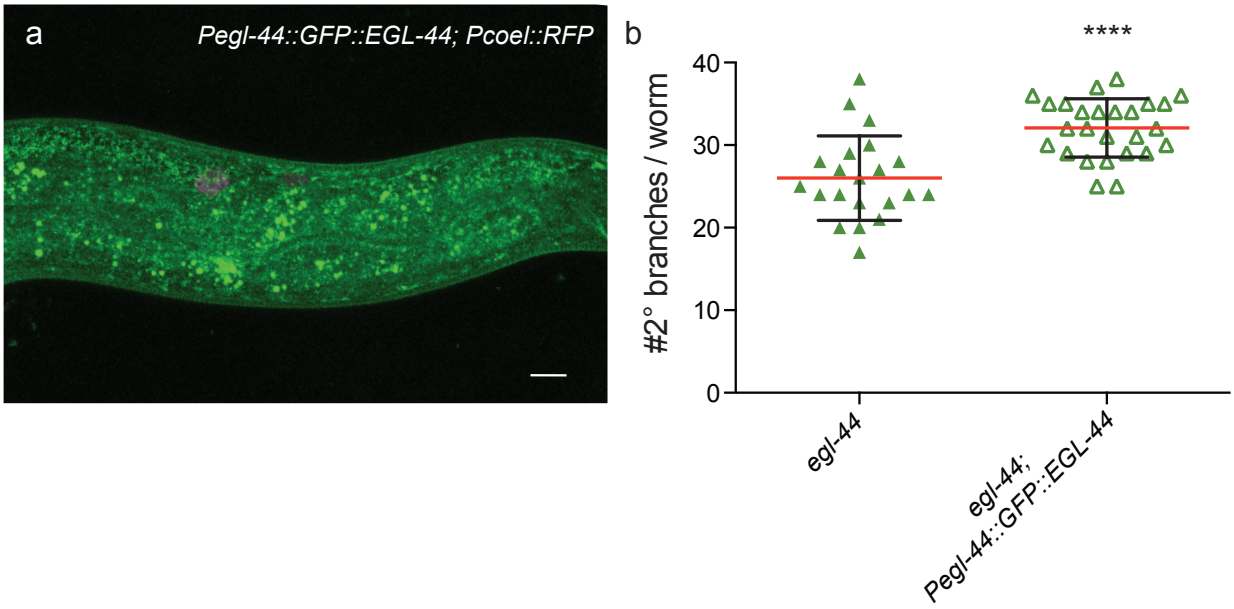

Figure 3.17: *Pegl-44::*GFP::EGL-44 is not detected in PVD. (a) Confocal image of *Pegl-44::*GFP::EGL-44 (green) and co-injection marker *Pcoel*::RFP (magenta) in a wild-type worm, **(b)** quantification of 2° branches in mutants of *egl-44* with or without the *Pegl-44::*GFP::EGL-44 construct. Left is anterior, up is dorsal, scale bar = 10 μm, **** indicates $p<0.0001$, unpaired t-test, error bars represent SEM, $n \geq 21$.

mutant phenotype. Mutants of *egl-44* that carried the plasmid *Pegl-44::*GFP::EGL-44 showed an increased number of 2° branches compared to *egl-44* mutants without the plasmid ($p<0.0001$) (**Figure 3.17b**). Thus, we concluded that the GFP::EGL-44 construct was not detectable in PVD, and so we were unable to measure if it was regulated by MEC-3 or EGL-46 in this context.

Our final hypothesis was that *egl-46* is regulated by both MEC-3 and EGL-44. We were able to detect GFP expression in the PVD cell body under the *egl-46* promoter[56] (**Figure 3.18a**). Surprisingly, we did not see a decrease of *Pegl-46*::GFP expression in *mec-3* mutants ($p>0.05$), but there was an increase of GFP expression in mutants of *egl-44* ($p<0.001$) (**Figure 3.18b**). Furthermore, we noticed that GFP expression was barely detectable at the L3 larval stage for both *wt* and mutants of *mec-3*, but not for mutants of *egl-44*. Thus, we separated the data from **Figure 3.18b** into distinct larval stages. When comparing the L2 and L3 larval stages within a genotype, we saw a decrease in expression for both *wt* ($p<0.001$) and for *mec-3* mutants ($p<0.05$), but not for mutants of *egl-44* ($p>0.05$) (**Figure 3.18c**).

Due to the surprising results described above, we obtained an additional promoter-fusion construct for *egl-46*, *Pegl-46*::dsRed (**Figure 3.19a**). However, though the relative expression of *Pegl-46*::dsRed in mutants of *mec-3* was less than that of wild-type worms, this difference was not significant ($p>0.05$) (**Figure 3.19b**).

These results fail to support our hypothesis that *egl-46* is regulated by MEC-3 and conflicts our previous microarray results[51], the smFISH results presented earlier in this chapter, and RNA-Seq results that will be presented in **Chapter 4**. This discrepancy is further examined in the **Discussion** section below.

We also wanted to confirm regulation of *hpo-30* by MEC-3 but not EGL-44, as our model predicts that EGL-44 does not regulate *hpo-30* because they are in separate genetic

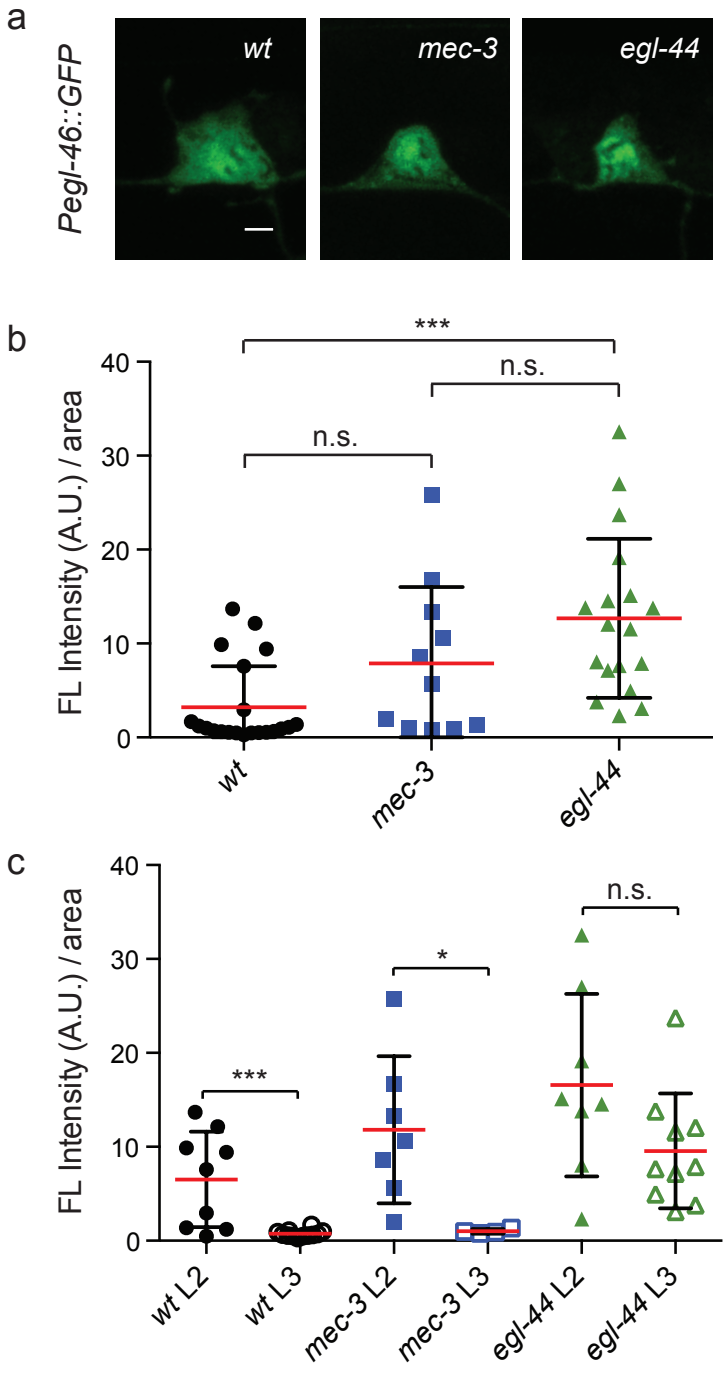

Figure 3.18: Expression of *Pegl-46*::GFP. (a) Confocal images of the PVD cell body expressing *Pegl-46::*GFP, **(b)** quantification of mean fluorescent intensity across conditions for L2 and L3 stages, combined, **(c)** data from **b**, separated by stage. Left is anterior; up is dorsal, scale bar = 2 µm, * indicates $p<0.05$, *** indicates $p<0.001$, n.s. = not significant, one-way ANOVA with Tukey's test for multiple comparisons, error bars represent SEM, $n\geq11$.

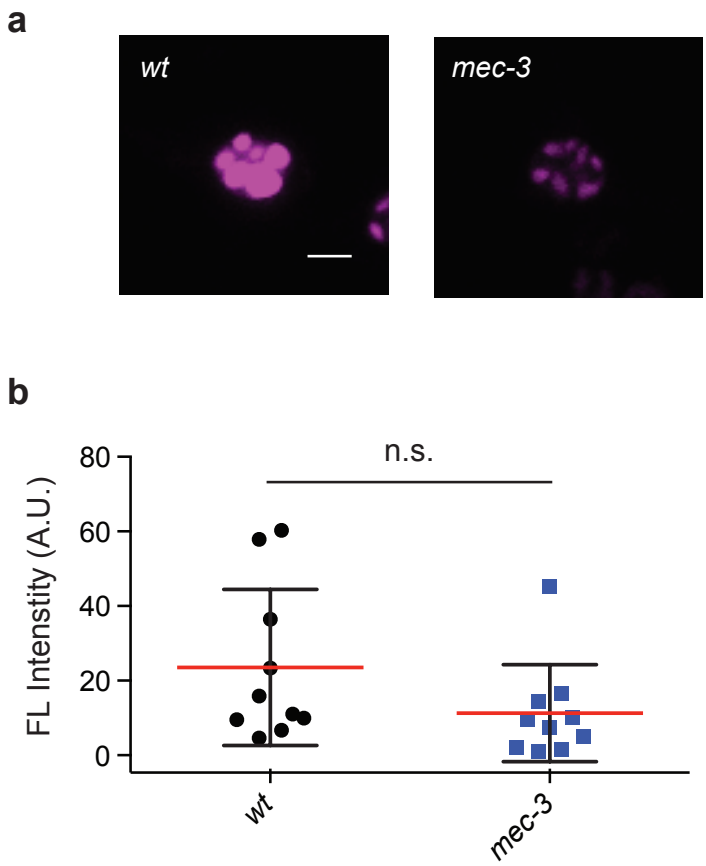

Figure 3.19: Expression of *Pegl-46*::dsRed. (a) Confocal images of the PVD cell body expressing *Pegl-46::*dsRed in *wt* (left) and *mec-3* mutants (right), **(b)** quantification of mean fluorescence intensity across conditions for L2 and L3 stages, combined. Left is anterior; up is dorsal, scale bar = 2 μm, n.s. = not significant, unpaired t-test, error bars represent SEM, n≥11.

pathways. However, we found that *Phpo-30*::GFP expression was increased in mutants of *egl-44* when compared to *wt* ($p<0.01$) and decreased in mutants of *egl-44* when compared to mutants of *mec-3* ($p<0.0001$) (**Figure 3.20a**). More confusing was that *Phpo-30*::GFP expression increased in mutants of *mec-3* when compared to *wt* ($p<0.0001$), conflicting previously published results[51]. It is worth noting that the *wt* measurements are low. This discrepancy could be because those samples do not accurately represent the population as a whole; however, due to the high number of samples quantified (n=26) and the data being collected on multiple days, this is not likely. These results suggest that both MEC-3 and EGL-44 normally suppress *hpo-30* during the L2-L3 larval stages, conflicting with our microarray results[51] and RNA-Seq data (**Chapter 4**).

Discussion

The unique architectural features that define separate classes of neurons depend on the execution of specific genetic programs that drive morphogenesis. The importance of this developmental axis is underscored by the striking neuron-specific defects that are commonly observed for mutations that disable individual transcription factors[51,58,65,139,140]. Thus, the goal of elucidating the molecular pathways that govern neuron morphology requires the discovery of the downstream effectors of transcriptional activity. In our strategy to achieve this objective, we used an experimental approach in *C. elegans* that exploits the ready accessibility of the PVD nociceptive neuron for molecular genetic analysis and its stereotypical morphology for live cell imaging[29,51,52].

The characteristic dendritic morphology of PVD is radically simplified by mutations that inactivate the MEC-3 LIM homeodomain transcription factor. In *mec-3* mutants, lateral

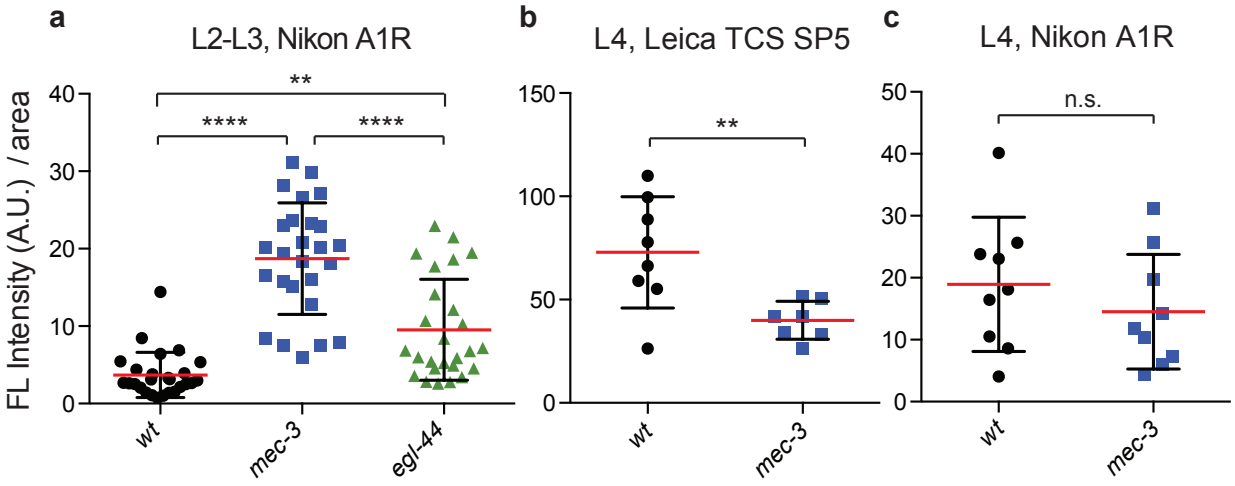

Figure 3.20: Expression of *Phpo-30*::GFP. (a) Quantification of mean fluorescence intensity across conditions for L2-L3 stages, combined, **(b-c)** quantification of mean fluorescence intensity across conditions for the L4 stage as measured on a Leica TCS SP5 confocal microscope **(b)** or a Nikon A1R confocal microscope **(c)**. ** indicates $p<0.01$, **** indicates $p<0.0001$, n.s. = not significant, one-way ANOVA with Tukey's test for multiple comparisons (**a**), unpaired t-test (**b** and **c**), error bars represent SEM, $n\geq7$.

branching fails and dendritic menorahs are largely absent[50]. A previous study[51] demonstrated the biased effect of *hpo-30* mutants on pioneer 2° branches and suggested a different MEC-3-regulated gene must be required for commissural 2° dendrites. We surmised that this component could be the MEC-3 target and TFIIA-like zinc finger transcription factor EGL-46, since lateral branches are also reduced in number but not completely eliminated in *egl-46* mutants[29,51,52]. Here, we have confirmed this hypothesis by determining that commissural branches are preferentially dependent on EGL-46 and its transcription factor binding partner EGL-44 (**Figure 3.5d**). Thus, parallel acting pathways involving either *hpo-30* or *egl-44*/*egl-46* are needed for the full complement of PVD menorahs (**Figure 3.8d**).

Although *hpo-30* preferentially affects pioneer branches, higher order branching for all menorahs is also disrupted. In contrast, menorahs containing pioneer 2° branches are apparently intact in *egl-44* and *egl-46* mutants. Thus, our results suggest that EGL-44/EGL-46 regulate downstream effectors that act selectively in commissural dendrites. Potential targets of EGL-46 in PVD, based on a dataset presented in **Chapter 4**, are discussed in **Chapter 5**.

Our observation that the *mec-3* PVD branching defect is more severe than that of double mutants in which both *hpo-30* and *egl-44* are inactivated suggests that dendrite morphogenesis also depends on other MEC-3-regulated components (**Figure 3.8d**). In addition, MEC-3 controls the length of the PVD 1° dendrites and the axon (**Figure 3.10** and **Figure 3.11**). Our ongoing studies of *mec-3*-regulated targets are designed to detect these genes (see **Chapter 4**). Finally, our results have also identified PVD-expressed markers that are redundantly regulated by both MEC-3 and the EGL-44/EGL-46 complex (**Figure 3.12** and **Figure 3.13**). These observations point to a potentially complex transcriptional regulatory mechanism in which MEC-3 directs assembly of key architectural components of the PVD neuron by activating expression of *egl-46*

and *hpo-30* and also functions in concert with EGL-44/EGL-46 to control a subset of PVD-specific traits (**Figure 3.14d**). The strong conservation of MEC-3-related LIM homeodomain proteins and of EGL-44 and EGL-46 in vertebrate genomes argues that similar transcriptional networks may regulate neuronal morphogenesis in the brain[53,56,137,141–143].

Discrepancies among the fluorescence intensity measurements

Promoter sequences are based on a region upstream of the gene of interest. It is possible that for *egl-44* and *egl-46*, the entire promoter region may not have been included in these constructs. Additionally, reporter constructs that are injected as plasmids are not expressed at the natural or normal levels endogenous to the animal. The amount of expression cannot be controlled with these plasmids and may vary with the amount of construct originally injected. Furthermore, expression of fluorescent markers, especially when there are multiple markers in combination, may cause biological reactions that impact expression. For example, sometimes too many markers make the worms "unhappy" or sick, and they will "kick out" a marker. The worms described above expressed multiple GFP and mCherry markers, and the presence of all of these markers may have influenced the relative expression patterns. Another reason why these data may not be indicative of the true biology is because they directly contradict existing evidence that EGL-44 promotes *egl-46*[55]. In our results, we observed that in mutants of *egl-44*, *Pegl-46*::GFP expression increased, suggesting that EGL-44 suppresses *egl-46*. While reporter constructs are useful tools for visualizing relative expression, they are not necessarily directly correlated with the correct expression levels of the gene.

Additionally, the relative fluorescence intensity measurements between *wt* and *mec-3* mutants in **Figure 3.20a** not only conflict our hypothesis but also conflict previously published work from our lab[51] using the same strains that showed decreased fluorescence of *Phpo-30*::GFP in *mec-3* mutants compared to wild type. Two variables may account for the discrepancy between the current results and previously reported results. First, the published data were collected from L4 animals, whereas the current data were collected at L2/L3. Secondly, the published data were collected on a Leica TCS SP5 confocal microscope, whereas the current data were collected on a Nikon A1R confocal microscope. To deeply interrogate this point, I first replicated the published results by measuring the fluorescence intensity of *Phpo-30*::GFP in *wt* versus *mec-3* mutants at the L4 larval stage on the Leica TCS SP5 confocal microscope ($p<0.01$) (**Figure 3.20b**). However, when I measured fluorescence intensity of *Phpo-30*::GFP in *wt* versus *mec-3* mutants at the L4 larval stage on the Nikon A1R confocal microscope, I did not see a difference between *wt* and *mec-3* mutants ($p>0.05$) (**Figure 3.20c**). Perhaps if I collected data at L2/L3 on the Leica TCS SP5, I would get results that support my hypothesis; conversely, perhaps the Nikon A1R measurements are the "true" results. But due to similar discrepancies discussed above and the robustness of the microarray and RNA-Seq datasets, I did not pursue this further. However, that two separate results were obtained, depending on the microscope used, is concerning and should be taken into consideration for future experiments that rely solely on fluorescence intensity measurements.

Acknowledgements

We thank C. J. Smith (University of Notre Dame) for generating the *PVD*::mCherry::RAB-3 plasmid, T. D. O'Brien (University of Texas) for generating the *Phpo-30*::GFP strains, K. Shen (Stanford University) for *wyIs378* and O. Hobert (Columbia University) for *otIs181*. Additional strains were provided by the *Caenorhabditis* Genetics Center (CGC), which is funded by NIH Office of Research Infrastructure Programs (P40 OD010440). This work was supported by NIH grant R01NS079611 to DMM, NSF grant DGE:1445197 to SDP, a Vanderbilt Undergraduate Summer Research Program grant to MN, and a National Top Talent Undergraduate Program (NTTUTP) Fudan University grant to XYS.

Author contributions

David M. Miller, III, and Barbara M. J. O'Brien designed the study; Sierra D. Palumbos performed the smFISH experiment; Michaela Novakovic generated double mutants of *egl-46*/*egl-44* with *mec-3* for marker gene analysis and quantified 1° branch presence/absence; Xueying Shang quantified 1° branch outgrowth defects in *mec-3* mutants; Lakshmi Sundararajan generated the *PVD*::mCherry::RAB-3 transgenic line; all other genetics, data collection, and analyses were performed by Barbara M. J. O'Brien; David M. Miller, III, and Barbara M. J. O'Brien wrote the manuscript. A portion of this work was published in *Developmental Biology* in 2017.

CHAPTER 4 : CELL-SPECIFIC RNA-SEQ PROFILING OF PVD NEURONS IDENTIFIES MEC-3-REGULATED GENES THAT DRIVE DENDRITIC BRANCHING

Introduction

While PVD is a useful model for studies of dendrite morphogenesis because of its stereotypical and well-characterized dendritic architecture, the molecular mechanisms that regulate key features of PVD architecture are unknown. One way to identify these components is to detect genes that are highly expressed in PVD but not in other *C. elegans* cells. This strategy was used in a previous study[29] that identified genes that are differentially expressed in PVD. However, many of these genes may not be specifically involved in branching because this approach identified genes involved in all biological aspects in wild-type animals. Mutants of the LIM-Homeobox domain transcription factor (TF) MEC-3 display a striking phenotype in which PVD menorahs fail to emerge from the 1° branch. This result suggests that MEC-3 regulates genes that promote lateral branching **(Figure 4.1)**[50]. Thus, the identification of transcripts that are misregulated in mutants of *mec-3* should reveal genes involved in dendritic branching. A previous study in the Miller Lab[51] identified transcriptional targets of MEC-3 using an mRNA tagging strategy. In this approach, mRNA was immunoprecipitated from a transgenic worm expressing epitope (FLAG) tagged polyA binding protein (3XFLAG-PAB-1) in PVD neurons. Differentially expressed genes (DEGs) identified from microarray analysis of *mec-3* vs. *wt* were targeted in an RNAi screen to identify MEC-3-regulated genes required for dendritic branching. Although, this approach did identify a claudin-like protein, HPO-30, that helps stabilize PVD lateral branches[51], the RNAi screen did not detect hits that block lateral branching as expected

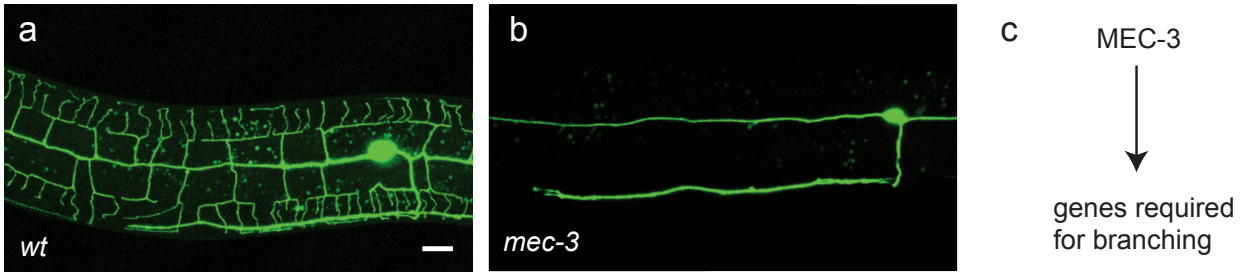

Figure 4.1: MEC-3 regulates genes required for branching. (a-b) Confocal images of PVD visualized with *F49H12.4*::GFP for *wt* **(a)** and *mec-3* **(b)**, **(c)** schematic of pathway for MEC-3 and genes required for branching. Images in **a** and **b** are the same as those in **Figure 3.1**. Left is anterior, up is dorsal, scale bar = 10 μm.

from the highly penetrant *mec-3* phenotype. One explanation for this outcome is that the *mec-3* regulated dataset derived from the mRNA tagging strategy likely included transcripts from other neurons including OLL and PDE, which also express the *ser2prom3* promoter used for the 3XFLAG-tagged PAB-1 transgene. This study was also limited by the likely failure to detect transcripts due to the reduced sensitivity of microarray versus RNA-Seq[144]. Thus, I developed an alternative strategy to identify MEC-3-regulated transcripts that exploits a new method, RNA-Seq Analysis of *C. elegans* Cells (SeqCel) recently developed in the Miller Lab[145]. In this approach, the target cell is isolated by fluorescence-activated cell sorting (FACS) for RNA-Seq analysis. My approach exploited the multicolor sensitivity of FACS in an intersectional strategy that uniquely labeled PVD with a combination of fluorescent reporter genes. This scheme has now yielded a highly specific RNA-Seq profile of the wild type PVD neuron and identified candidate MEC-3 regulated transcripts.

Materials and Methods

Genetic strains

Strains were maintained at 20°C as previously described[21]. Stains containing specific fluorescent reporters were generated by crossing previously known and established strains, as indicated in each subsection of Part I of the **Results** section. A complete list of strains used for sorting and the strains used to for making the fluorescent combinations is outlined in **Table 4.1**.

Table 4.1. Genetic strains used in this study

Strain	Genotype
CB1338	*mec-3 (e1338) IV*
MT372	*lin-22 (n372) IV*
NC1404	*wdIs52 (F49H12.4::GFP + Punc-119::UNC-119) II*
NC1686	*wdIs51 (F49H12.4::GFP + Punc-119::UNC-119) X*
NC1738	*mec-3(e1338); wdIs52 (F49H12.4::GFP + Punc-119::UNC-119) II*
NC1845	*wdIs60 (F49H12.4::mCherry + Punc-119::UNC-119)*
NC3043	*mec-3(e1338) IV; wyId585 (ser2prom3::myr-mCherry::unc-54 3'UTR, podr1::GFP) IV*
NC3105	*wdIs95 (F49H12.4::mCherry + Punc-119::UNC-119)*
OH12525	*otIs521 (eat-4prom8::tagRFP; ttx-3::GFP)*
OH1422	*otIs138 (ser2prom3::GFP + rol-6(su1006)) X*
OH7193	*otIs181 (dat-1::mCherry + ttx-3::mCherry) III; him-8(e1489) IV*
otIs396	*otIs396 : otIs396 (ace-1prom2::NLS::tagRFP)*
TV15918	*wyIs585 (ser2prom3::myr-mCherry::unc-54 3'UTR, podr1::GFP) IV*
NC3017	*wyIs585 (ser2prom3::myr-mCherry::unc-54 3'UTR, podr1::GFP) IV; wdIs52 (F49H12.4::GFP + punc-119) II*
NC3042	*mec-3(e1338) IV; wyIs585 (ser2prom3::myr-mCherry::unc-54 3'UTR, podr1::GFP) IV; wdIs52 (F49H12.4::GFP + punc-119) II*
NC3040	*wyIs585 (ser2prom3::myr-mCherry::unc-54 3'UTR, podr1::GFP) IV; wdIs51 (F49H12.4::GFP + punc-119) X*
NC3157	*otIs138 (ser2prom3::GFP + rol-6(su1006)) X; wdIs60 (F49H12.4::mCherry)*
NC3078	*otIs138 (ser2prom3::GFP + rol-6(su1006)) X; lin-22 (n372) IV*
NC3079	*mec-3 (e1338) IV; lin-22 (n372) IV; otIs138 (ser2prom3::GFP + rol-6(su1006)) X*
NC3076	*lin-22 (n372) IV; wdIs52 (F49H12.4::GFP + unc-119) II*
NC3077	*mec-3 (e1338) IV; lin-22 (n372) IV; wdIs52 (F49H12.4::GFP + unc-119) II*
NC3093	*lin-22 (n372) IV; otIs138 (ser2prom3::GFP + rol-6(su1006)) X; otIs521 (eat-4prom8::tagRFP; ttx-3::GFP)*
NC3094	*mec-3 (e1338) IV; lin-22 (n372) IV; otIs138 (ser2prom3::GFP + rol-6(su1006)) X; otIs521 (eat-4prom8::tagRFP; ttx-3::GFP)*
NC3097	*otIs138 (ser2prom3::GFP + rol-6(su1006)) X; otIs396 (ace-1prm2::NLS::tagRFP)*
NC3182	*otIs181 (dat-1::mCherry + ttx-3::mCherry) III; otIs138 (ser2prom3::GFP + rol-6(su1006)) X; otIs396 (ace-1prm2::NLS::tagRFP)*
NC3183	*mec-3 (e1338); otIs181 (dat-1::mCherry + ttx-3::mCherry) III; otIs138 (ser2prom3::GFP + rol-6(su1006)) X; otIs396 (ace-1prm2::NLS::tagRFP)*

Generation of the integrant *wdIs95*

The wdEx624 plasmid containing *F49H12.4*::mCherry + *Punc-119*::UNC-119 was injected into *unc-119* worms. UNC-119 was used as the co-injection marker, whereby worms expressing the wdEx624 plasmid showed wild-type behavior, rescued by *Punc-119*::UNC-119. 150 transgenic animals at stage L4 or younger were picked onto a 60 mm plate and irradiated for thirty minutes. Following irradiation, animals were placed onto 100 mm plates, five animals per plate, and were left at room temperature for 7-8 days. A small (~1cm^3) chunk was extracted from each plate using a flame-sterilized spatula and placed onto a fresh 60 mm plate. The following day, when the animals recovered, twenty transgenic worms were picked from each 60 mm plate and placed onto fresh 60 mm plates, with one worm per plate. After allowing the worms to self-fertilize and their progeny to grow, plates were screened. Plates containing 100% worms expressing mCherry in PVD were considered to be integrated lines. One line expressed bright mCherry in PVD and was given the name *wdIs95* and chosen for this study. All plates used contained nematode growth medium (NGM) seeded with OP50 *E. coli*.

RNA-Seq

Wild-type and *mec-3* mutant *otIs138;otIs396;otIs181* animals, along with N2 and *otIs138* controls, were pelleted for 2.5k RPM for 2.5 minutes at room temperature, thoroughly washed with M9 Buffer to remove bacterial contamination, and grown on 150 mm 8P plates seeded with NA22 *E. coli* for approximately 40 hr at 20°C until they reached the late L2/early L3 larval stage.

The SeqCel method[145] was used to generate RNA-Seq profiles of late L2/early L3 larval PVD neurons. Specifically, upon reaching the late L2/early L3 stage, worms were washed with M9 buffer to remove bacterial contamination and incubated for 4 minutes in freshly thawed SDS-DTT solution (0.25% SDS, 200 mM DTT, 20 mM HEPES, 3% sucrose pH = 7.5–8.0) to soften the cuticle. Next, worms were neutralized and washed five times with 1X Egg Buffer. Incubation in Pronase (15 mg/mL) with the addition of pipetting ~40X with a medium-sized pipette tip was used to break open the worms so the cells could be sorted. The sample then was filtered to remove debris using a 5 μm filter. Immediately prior to sorting, DAPI was added to identify damaged or dead cells. GFP+ cells were sorted into an Eppendorf tube containing Trizol-LS (Invitrogen) using a BD FACSAria at the Flow Cytometry Core at Vanderbilt University. The N2 and *otIs138* strains were used as non-fluorescent and GFP+ controls, respectively.

Prior to the SDS-DTT incubation, an aliquot of worms was flash-frozen in liquid nitrogen to be used as the whole-worm internal reference sample for subsequent transcriptome analyses. These samples were ground using a mortar and pestle and dissolved in Trizol-LS (Invitrogen). After the sorted cells (and whole worm references) were placed into Trizol-LS, RNA was extracted, and DNA contamination removed using the Zymo DNA-free RNA Kit (Zymo Research, Irving, CA) according to manufacturer's instructions. RNA quality was determined by an Agilent Bioanalyzer at the VANTAGE Core at Vanderbilt University. RNA with RNA Integrity Numbers (RIN) scores of seven and above were sequenced at VANTAGE (Vanderbilt University). 5-10 ng of total RNA from the Zymo kit was converted to cDNA using polydT primers to capture mRNA and amplified prior to library preparation using Takara-Clontech SMARTer technology. Libraries were then constructed using an Illumina kit and sequenced on

an Illumina HiSeq 3000 system to generate 75 base paired-end reads. RNA sequencing resulted in 30-60 million reads per sample.

All experimental procedures were performed in triplicate.

Analysis of RNA-Seq data

Differentially expressed genes (DEGs) in PVD between *wt* and *mec-3* mutants were identified using an EDGE test with CLC Genomics Workbench software (Qiagen). We defined significant DEGs as being downregulated in *mec-3* mutants compared to *wt* worms with a $\log_2$(fold change) ≤ -2 and FDR corrected p-value < 0.05. Additionally, the whole-worm internal reference controls for both *wt* and *mec-3* worms were compared to further specify the DEGs. DEGs identified in the whole-worm internal reference that overlapped with DEGs identified in PVD were removed from the dataset to generate a PVD-specific MEC-3-regulated list of targets.

Results

The goal of this study was to use fluorescence-activated cell sorting (FACS) to isolate PVD neurons and extract RNA from the cells. This RNA could then be compared to identify expressed genes (EG) of PVD cells in both wild-type and *mec-3* mutant worms. More specifically, we wanted to identify genes regulated by MEC-3 that are specific to the development of the elaborate dendritic architecture found in PVD.

This results section is divided into two major parts. The first part describes the logic and process of finding a strain optimal for FACS. Strains and combinations of fluorescent markers

fail to produce good FACS profiles for various reasons; thus, the first part of this project consisted of finding a strain from which we could confidently isolate PVD neurons. The second part of the results section describes MEC-3 targets identified from RNA of sorted PVD cells.

Part 1: Identifying an optimal strain for sorting

Strategy 1: PVD is the only GFP/mCherry double-labeled cell

Our rationale was to use a combination of two different promoters to drive separate fluorescent proteins, with the intention of differentiating double-labeled PVD cells from single-labeled cells in the worm. Specifically, the *wyIs585* strain (*ser2prom3*::mCherry; *Podr-1*::GFP), which labels PVD, OLL, and PDE with mCherry and AWC with GFP[99] was crossed with the *wdIs52* strain (*F49H12.4*::GFP; *Punc-119*::UNC-119), which labels PVD, PDE, AQR, and an unidentified tail neuron with GFP[29,146] (**Figure 4.2a-b**). The *wyIs585* strain was also crossed with the *wdIs51* strain (also *F49H12.4*::GFP; *Punc-119*::UNC-119), but this strain was not sorted. This fluorescent labeled promoter combination resulted with PVD (and sometimes PDE) as the only double-labeled cell (**Figure 4.2c-e**). However, when the cells from these worms were sorted, no distinction could be made between the sorting strain and *wyIs585* (compare **Figure 4.2h** with **Figure 4.2g**). It was, therefore, determined that this line could not be used for further experiments.

Strategy 2: PVD is the only GFP/mCherry double-labeled cell, using alternate promoters

Next, we used a different set of promoters to isolate PVD as the only GFP+/mCherry+ double-labeled cell. For this combination, the *otIs138* strain (*ser2prom3*::GFP; *rol-6*), which

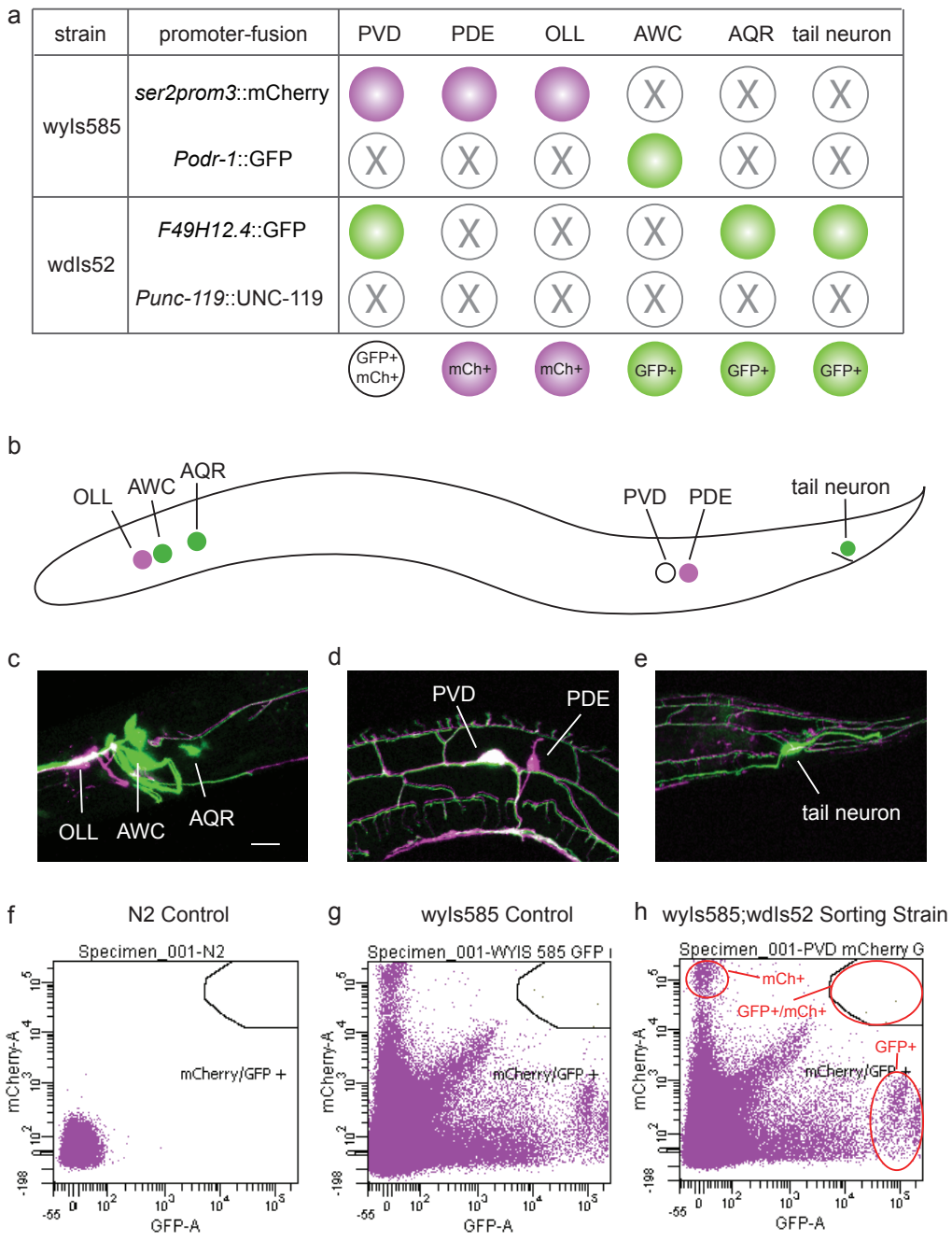

Figure 4.2: Strategy 1, PVD is the only GFP/mCherry double-labeled cell. (a) Rationale table for the combination of promoter-fusion constructs that would result in PVD being the only double-labeled cell with *ser2prom3*::mCherry and *F49H12.4*::GFP, **(b)** schematic of fluorescently labeled cells in the worm, **(c-e)** confocal images of the resulting strain with cell types indicated, **(f-h)** example graphs of fluorescence intensity of cells as detected by flow-cytometry for mCherry versus GFP for wild-type controls without **(f)** and with **(g)** fluorescently labeled cells and the resulting strain shown in **c-e (h)**. Note: to prevent bleed through of mCherry and GFP, two separate images were taken and could not be completely aligned, which accounts for why they do not align properly in **c-e**. Left is anterior, up is dorsal, scale bar = 10 µm.

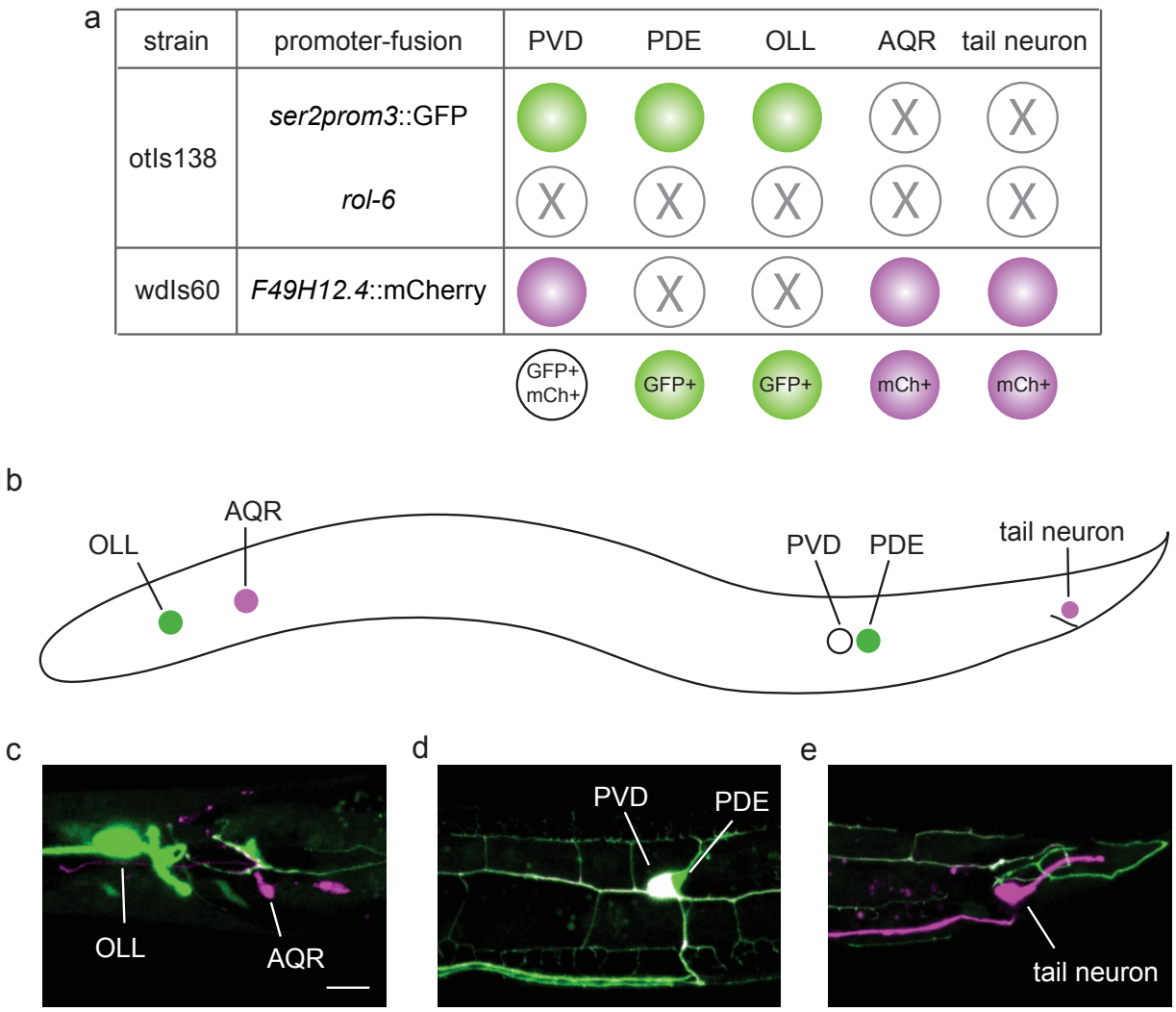

Figure 4.3: Strategy 2, PVD is the only GFP/mCherry double-labeled cell, using alternate promoters. (a) Rationale table for the combination of promoter-fusion constructs that would result in PVD being the only double-labeled cell with *ser2prom3*::GFP and *F49H12.4*::mCherry, **(b)** schematic of fluorescently labeled cells in the worm, **(c-e)** confocal images of the resulting strain with cell types indicated. Left is anterior, up is dorsal, scale bar = 10 µm.

labels PVD, OLL, and PDE with GFP[50], was crossed with the *wdIs60* strain (*F49H12.4*::mCherry; *Punc-119*::UNC-119), which labels PVD, sometimes PDE, AQR, and an unidentified tail neuron with mCherry (**Figure 4.3a-b**). This combination resulted with PVD (and sometimes PDE) as the only double-labeled cell (**Figure 4.3c-e**). However, when the markers were combined through a genetic cross, we observed that the brightness of GFP and mCherry was not equal (note in **Figure 4.3d** that the dendrites are green, compared to **Figure 4.2d**, where mCherry is seen throughout the dendrites at a comparable level to GFP). Thus, a newly integrated strain, *wdIs95* (*F49H12.4*::mCherry; *Punc-119*::UNC-119) (see **Materials and Methods**) was crossed with the *otIs138* strain. The brightness of *PVD*::mCherry for the *wdIs95* strain, though outcrossed 3X after integration, was not consistent (data not shown). Therefore, we decided to use a different approach for PVD sorting.

Strategy 3: Increase the number of PVD cells

Our next approach increased the number of PVD cells relative to the other GFP+ cells in the worm. The *lin-22* mutation induces a lineage defect that causes the V1-V4 cells, which normally give rise to seam cells and hypodermal cells, to adopt the V5 lineage, which gives rise to the posterid and PVD[147]. This results in 10 total PVD cells, 5 on each side. Mutants of *lin-22* were crossed with the *otIs138* strain (*ser2prom3*::GFP; *rol-6*), resulting in 10 GFP-labeled PVD cells and 2 GFP-labeled OLL cells, and perhaps PDE cells as well **(Figure 4.4a-c**). Similarly, mutants of *lin-22* were crossed with the *wdIs52* strain (*F49H12.4*::GFP; *Punc-119*::UNC-119), resulting in GFP labeling 10 PVD cells (and sometimes PDE), 1 AQR, and 1 unidentified tail neuron (data not shown). Although this strategy increased the number of GFP+ cells and resulted

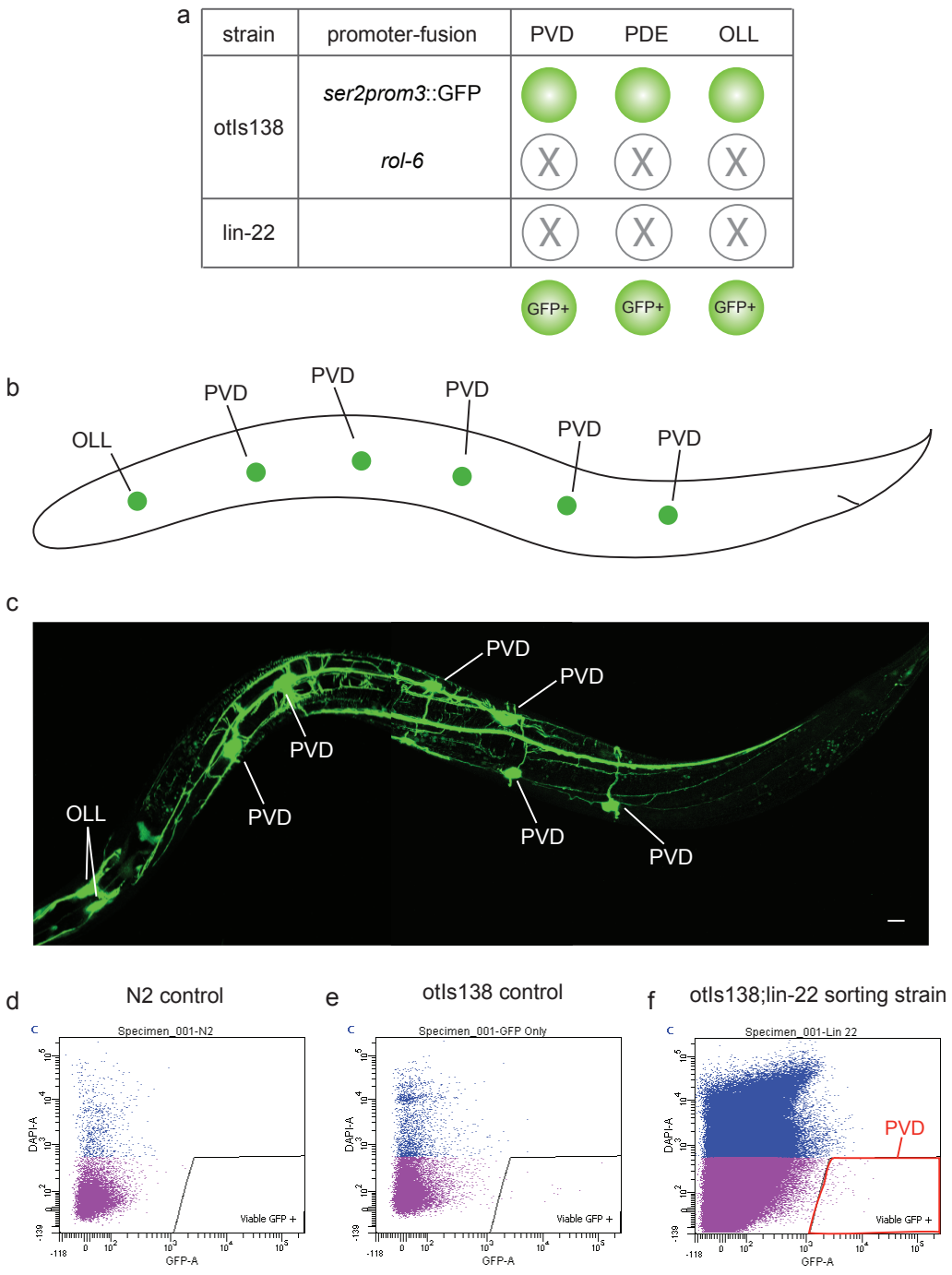

Figure 4.4: Strategy 3, Increase the number of PVD cells. (a) Rationale table for the combination of promoter-fusion constructs and *lin-22* mutation that would result in PVD being labeled with *ser2prom3*::GFP, **(b)** schematic of fluorescently labeled cells in the worm, **(c)** confocal image of the resulting strain with cell types indicated, **(d-f)** example graphs of fluorescence intensity of cells as detected by flow-cytometry for DAPI versus GFP for wild-type controls without **(d)** and with **(e)** fluorescently labeled cells and the resulting strain shown in **c (f)**. Note: PDE is not labeled on the schematic in **b** or on the image in **c** to prevent clutter, but PDE may express GFP. Left is anterior, up is dorsal, scale bar = 10 μm.

in a ratio of roughly 5:1 PVD:OLL, we were not able to pull out as many GFP-labeled cells as expected (**Figure 4.4d-f**).

Strategy 4: PVD as the only GFP+ cell

We hypothesized that we could isolate PVD through double-labeling OLL and sorting PVD as the only GFP+ cell. We obtained the *otIs521* strain (*eat4prom8*::TagRFP) from the Hobert Lab, which labels OLL, OLQ, and RIA with RFP, and crossed it with the *otIs138* strain. This resulted in OLL as being double-labeled with GFP and TagRFP and PVD (and sometimes PDE) being the only GFP+ cells. Additionally, we included the *lin-22* mutation with this strain to increase the number of PVD cells that could be identified. Unfortunately, the co-injection marker used for making the *otIs521* strain was *Pttx-3*::GFP, which labels AIY with GFP. Thus, PVD was not the only GFP+ cell in this line, so this was not used for sorting. **Figure 4.5** illustrates the logic for this strategy (**Figure 4.5a-b**) and an example image (**Figure 4.5c**).

Strategy 5: PVD as the only GFP+ cell, using alternate promoters

We continued our approach to generate an appropriate strain and obtained a different strain that marked OLL with mCherry, *otIs396*[148], that did not contain any GFP. The *otIs396* strain (*ace-1prom2*::tagRFP) labels OLL and CEP with RFP. Crossing this strain with *otIs138* resulted in PVD, and sometimes PDE, being the only cells that were GFP+. **Figure 4.6** summarizes the *otIs138;otIs396* strain. The *otIs138;otIs396* strain double-labeled OLL, but PDE was clearly visible in many of the worms. Thus, using the same logic of maintaining PVD as the only GFP+ cell, we sought to double-label PDE.

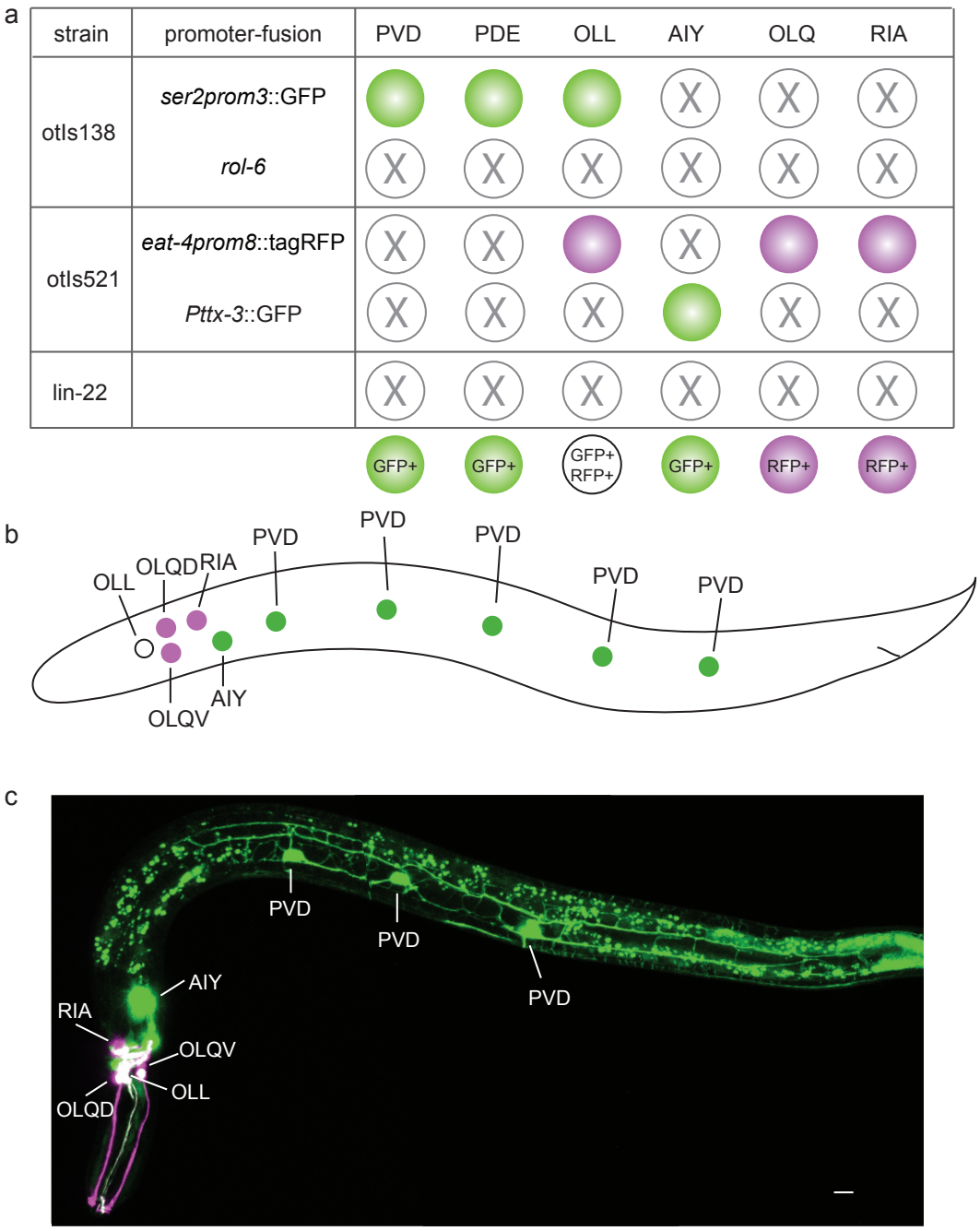

Figure 4.5: Strategy 4, PVD as the only GFP+ cell. (a) Rationale table for the combination of promoter-fusion constructs and *lin-22* mutation that would result in PVD being labeled with *ser2prom3*::GFP and OLL being double-labeled with *ser2prom3*::GFP and *eat4prom8*::tagRFP, **(b)** schematic of fluorescently labeled cells in the worm, **(c)** confocal image of the resulting strain with cell types indicated. Note: PDE is not labeled on the schematic in **b** or on the image in **c** to prevent clutter, but PDE may express GFP. Left is anterior, up is dorsal, scale bar = 10 µm.

a

strain	promoter-fusion	PVD	PDE	OLL	CEP
otIs138	*ser2prom3*::GFP	●	●	●	X
	rol-6	X	X	X	X
otIs396	*ace-1prom2*::NLS::tagRFP	X	X	●	●
		GFP+	GFP+	GFP+ RFP+	RFP+

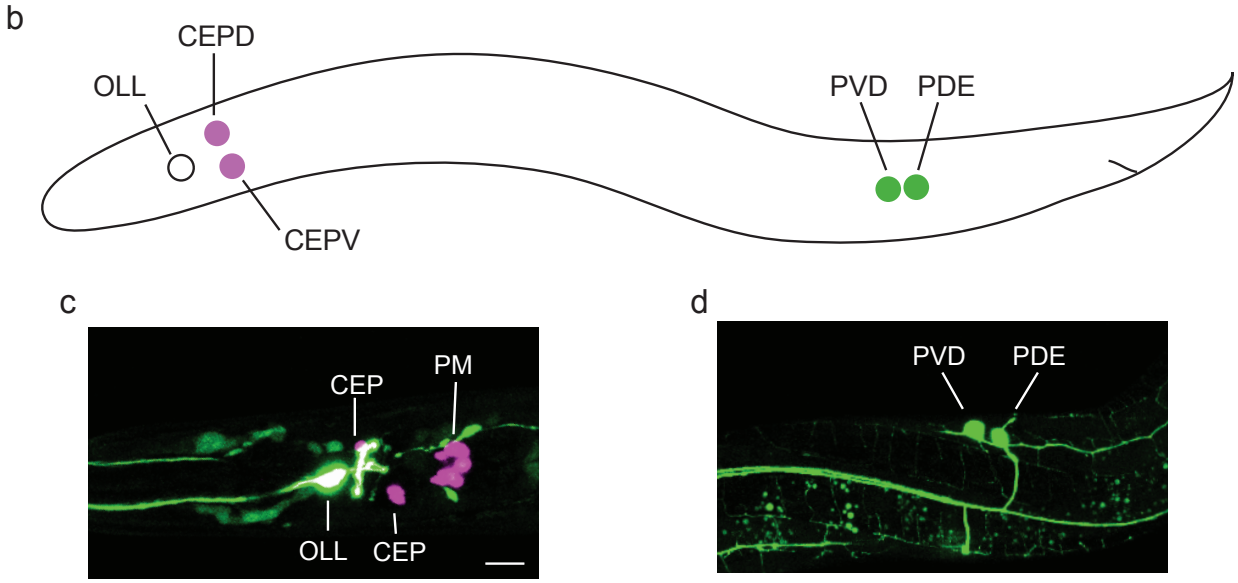

Figure 4.6: Strategy 5, PVD as the only GFP+ cell, using alternate promoters. (a) Rationale table for the combination of promoter-fusion constructs that would result in PVD and PDE being the only single-labeled GFP+ cells with *ser2prom3*::GFP, **(b)** schematic of fluorescently labeled cells in the worm, **(c-d)** confocal images of the resulting strain with cell types indicated. Note: pharyngeal muscles (PM) may also show expression, which has been seen for the *ace-1* promoter[149] but has not been previously noted for the *ace-1prom2* promoter. Left is anterior, up is dorsal, scale bar = 10 µm.

Strategy 6: Final strain has PVD as the only GFP+ cell

We obtained the *otIs181* strain (*Pdat-1*::mCherry; *Pttx-3*::mCherry), which labels PDE, CEP, ADE, and AIY with mCherry[150], and crossed it into the *otIs138;otIs396* line. This final strain allowed PVD to be the only single-labeled cell with GFP. This strain is summarized in **Figure 4.7**.

Part II: The PVD FACS profile and determination of MEC-3 target genes

A small cluster of GFP+ cells could be clearly separated using FACS with the *otIs138;otIs396;otIs181* strain (**Figure 4.8a**). Using this strain, we sorted PVD cells from both wild-type and *mec-3* mutant worms. RNA was then extracted from the sorted cells, and RNA expression levels of wild-type and *mec-3* mutant animals were compared (for details, see **Materials and Methods**). The resultant set of DEGs are plotted in **Figure 4.8b**.

Confirmation of the approach with known genes in PVD vs. whole-worm reference

We first wanted to confirm that this method effectively isolated PVD by looking for known PVD genes in the dataset and confirming that they were upregulated relative to the whole-worm reference. **Table 4.2** summarizes these findings.

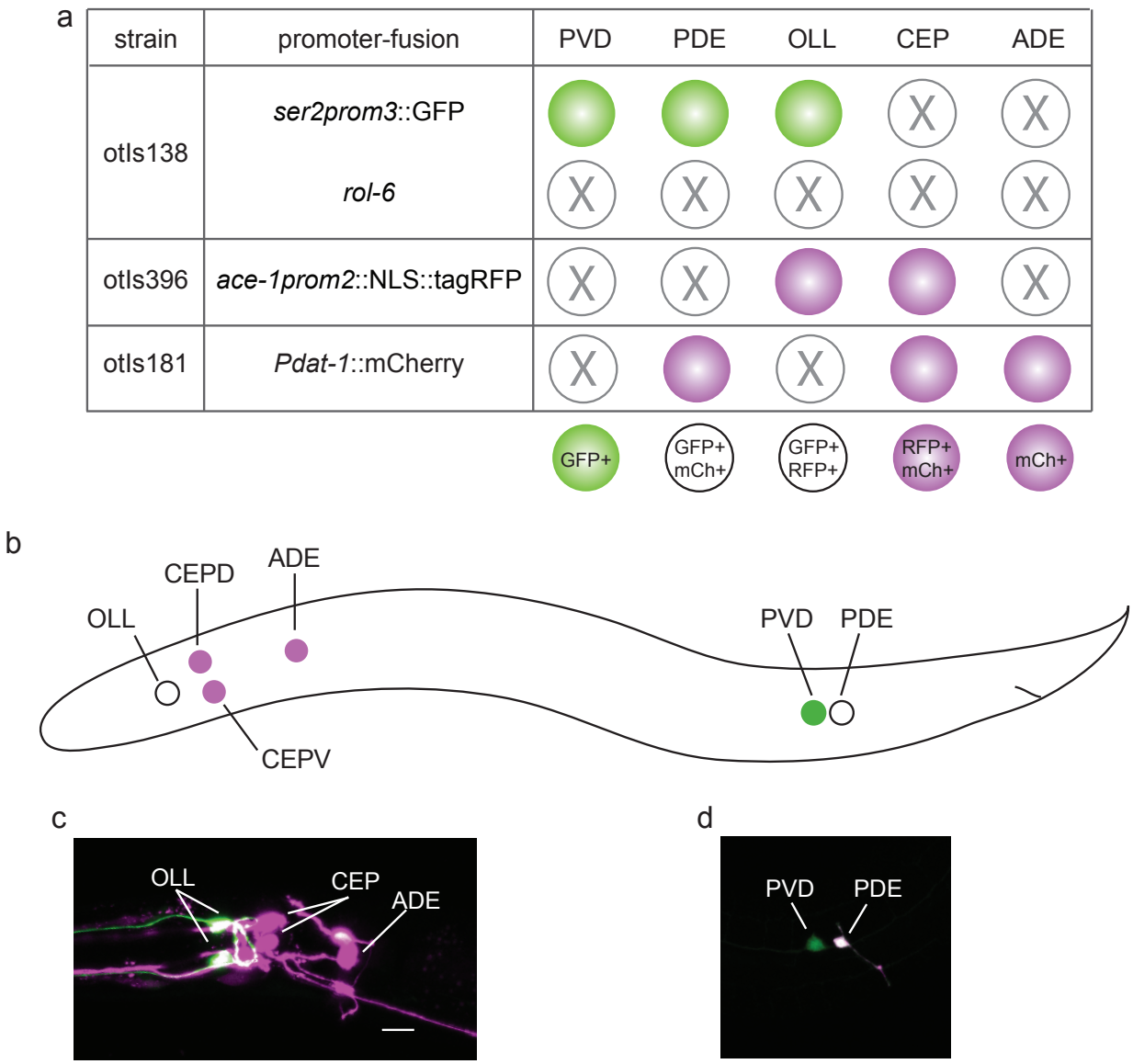

Figure 4.7: Strategy 6, Final strain has PVD as the only GFP+ cell. (a) Rationale table for the combination of promoter-fusion constructs that would result in PVD being the only single-labeled GFP+ cell with *ser2prom3*::GFP, **(b)** schematic of fluorescently labeled cells in the worm, **(c-d)** confocal images of the resulting strain with cell types indicated. Left is anterior, up is dorsal, scale bar = 10 µm.

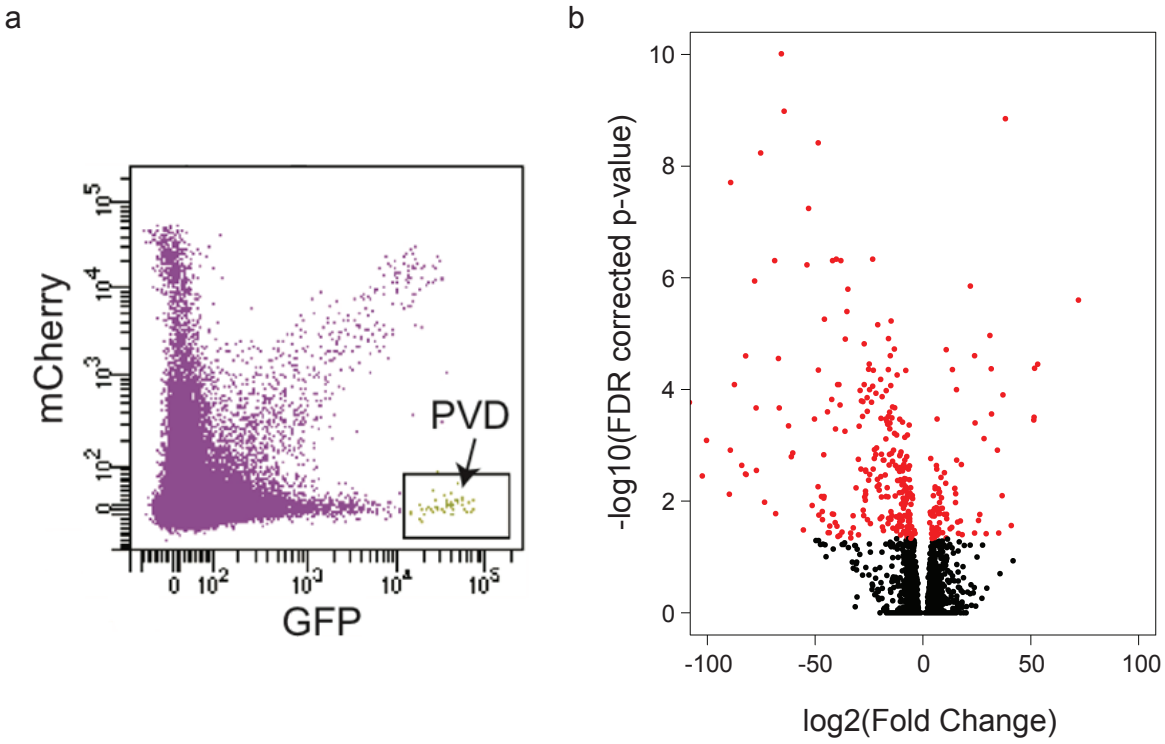

Figure 4.8: Differentially expressed genes in *mec-3* versus *wildtype*. (a) Example graph of fluorescence intensity of cells as detected by flow-cytometry for mCherry versus GFP for strain shown in **Figure 4.7**, **(b)** volcano plot showing the spread of transcripts detected. Red indicates FDR corrected p-value < 0.05 and $\log_2$(fold change) ≥ 2 and ≤ -2. Note: outliers have been excluded for this plot.

Table 4.2. Confirmation genes of sorted PVD cells

Gene	Classification	Average RPKM PVD	Average RPKM Internal Reference
alr-1	AristaLess (Drosophila homeodomain) Related	9.3263	2.4446
asic-1	Acid-sensing/Amiloride-Sensitive Ion Channel family	16.5071	3.3453
ced-10	CEll Death abnormality	4.5683	3.0187
deg-3	DEGeneration of certain neurons	446.9947	149.8392
del-1	DEgenerin Like	268.7958	55.5368
des-2	DEgeneration Suppressor	463.5755	99.3157
dma-1	Dendrite Morphology Abnormal	1155.3938	226.3110
egl-46	EGg Laying defective	228.7839	24.5125
F49H12.4	not known	62.0025	17.1675
hpo-30	Hypersensitive to POre-forming toxin	39.3774	8.3305
kpc-1	Kex-2 Proprotein Convertase family	92.2214	15.7088
lgc-12	Ligand-Gated ion Channel	421.0531	78.3969
mec-2	MEChanosensory abnormality	170.9556	26.7651
mec-3	MEChanosensory abnormality	1211.4922	144.0828
mec-10	MEChanosensory abnormality	138.7891	48.3725
mec-12	MEChanosensory abnormality	5107.5637	659.9739
mig-10	abnormal cell MIGration	67.0405	20.2158
rab-10	RAB family	38.4599	24.5395
sax-7	Sensory AXon guidance	72.4758	41.6599
unc-5	UNCoordinated	8.0466	4.7120
unc-8	UNCoordinated	3.8783	1.5461
unc-34	UNCoordinated	8.4362	2.7975
unc-40	UNCoordinated	8.9868	6.8279
unc-86	UNCoordinated	247.7448	47.9799

266 genes are differentially expressed in mec-3 *mutants*

Our initial analysis identified 304 genes that were downregulated ($\log_2$(fold change) ≤ -2 and FDR corrected p-value < 0.05) in *mec-3* mutants compared to *wt* in PVD. Additionally, 72 genes were downregulated in the *mec-3* whole-worm internal reference compared to the *wt* whole-worm internal reference. Of those 72 genes, 38 overlapped with the 304 genes that were found in the PVD dataset (**Figure 4.9**[151], **Table 4.3**). Since our goal was to identify PVD-specific genes, we removed those 38 genes from our PVD dataset, resulting in the final set of 266 genes that are in PVD and differentially expressed in *mec-3* mutants. We list the top 20 genes in **Table 4.4** and **Table 4.5** according to greatest $\log_2$(fold change) and lowest FDR corrected p-value, respectively.

In addition to highlighting the top 20 genes according to fold change and p-value, we also looked at the set of genes we used to confirm our method listed in **Table 4.2**. From that set of genes, 17 were downregulated in *mec-3* compared to *wt* (**Table 4.6**), while 7 were not shown to be regulated by *mec-3* in our dataset (**Table 4.7**).

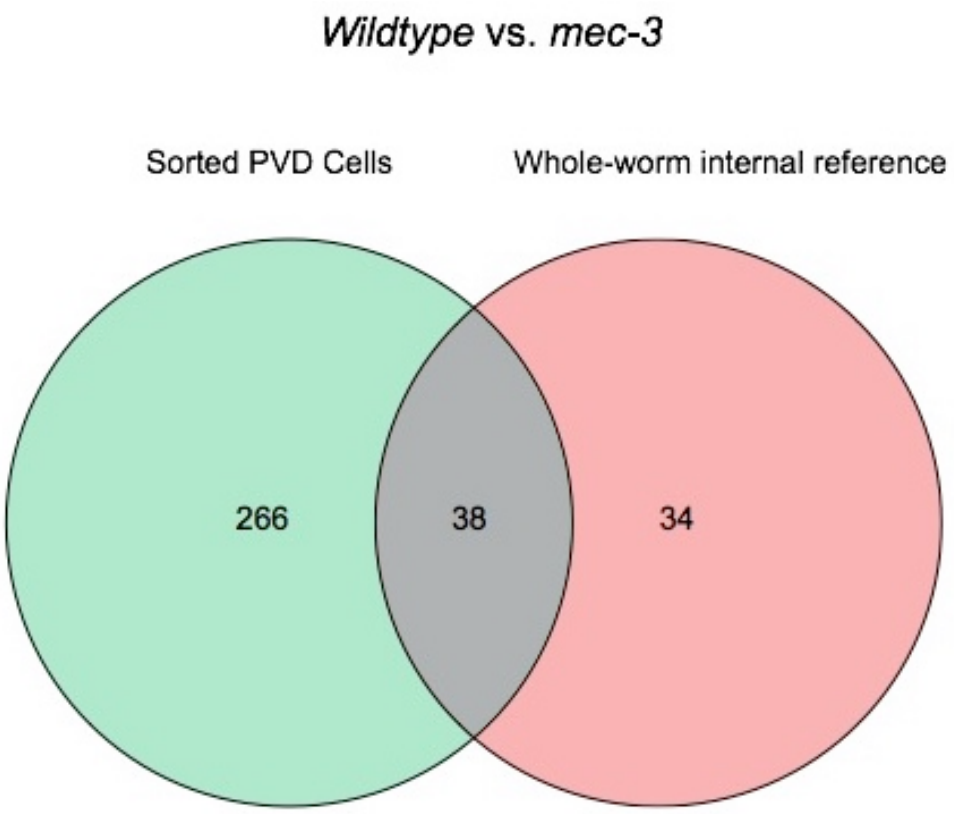

Figure 4.9: Shared genes downregulated in sorted PVD cells and whole-worm internal references. Genes downregulated in *mec-3* mutants in sorted PVD cells were compared to genes downregulated in *mec-3* mutants in the whole-worm internal reference samples. Venn diagram shows the number of genes downregulated in *mec-3* mutants compared to *wt* in sorted PVD cells (left, 266), the whole-worm internal reference samples (right, 34), and the overlap of shared genes in common (middle, 38). See **Table 4.3** for the list of shared genes. Venn diagram was made using the online Venny tool[151] and modified in Adobe Illustrator for clarity.

Table 4.3. Shared genes downregulated in *mec-3* mutants

		Sorted PVD Cells		Whole-worm internal reference	
Gene	**Classification**	**log_2(fold change)**	**FDR corrected p-value**	**log_2(fold change)**	**FDR corrected p-value**
C14E2.12	not known	-215.7852	0.0003	-149.2398	2.20693E-13
C30E1.9	not known	-33.4476	0.0457	-67.5262	1.87121E-07
C36A4.14	not known	-43.2089	0.0280	-32.3386	0.0043
C36C9.10	not known	-38.1142	4.93868E-07	-70.7864	1.66894E-35
F07H5.3	not known	-1253.7222	9.96288E-17	-344.9514	2.24921E-31
F31C3.13	not known	-249.9142	1.50368E-08	-1017.5348	3.3354E-12
F31C3.14	not known	-89.3866	0.0012	-203.6039	8.79059E-05
F31C3.15	not known	-2587.8568	4.83249E-13	-2567.2784	2.75307E-23
F46A8.13	not known	-286.6033	2.00689E-07	-72.2817	6.63525E-06
K07C5.13	not known	-23.3282	8.75585E-05	-23.7875	6.53823E-05
mec-3	MEChanosensory abnormality	-100.4134	0.0008	-10.4554	3.43693E-06
mec-7	MEChanosensory abnormality	-144.5969	2.24507E-10	-12.4277	2.52964E-31
mec-10	MEChanosensory abnormality	-338.9180	1.72721E-12	-12.9518	0.0029
MTCE.22	not known	-29.6058	0.0005	-13.7416	0.0004
MTCE.24	not known	-19.4842	0.0003	-10.0577	0.0018
nhr-73	Nuclear Hormone Receptor family	-5.6112	0.046199635	-13.7834	2.71989E-15
rrn-1.1	Ribosomal RNA	-7743.9851	7.59407E-19	-6832.8828	2.85503E-48
rrn-1.2	Ribosomal RNA	-7744.2436	7.59407E-19	-6799.7979	1.36267E-48
rrn-2.1	Ribosomal RNA	-298.8487	2.90814E-10	-311.0476	5.6743E-20
rrn-3.1	Ribosomal RNA	-210.1699	6.89306E-05	-604.7288	1.83746E-11
rrn-3.56	Ribosomal RNA	-122.8762	0.0004	-369.3208	1.0236E-05
skr-2	SKp1 Related (ubiquitin ligase complex component)	-14.7845	5.92566E-06	-11.1453	2.46413E-35
T05E11.9	not known	-7095.2639	1.40355E-19	-1088.4917	5.48163E-41
T23G11.12	not known	-37.5678	0.0358	-38.1188	0.0009
T23G5.11	not known	-82.2917	0.0033	-87.0997	1.24598E-08

tts-1	Transcribed Telomerase-like Sequence	-481.7026	6.71174E-15	-1336.9128	9.82643E-24
tts-2	Transcribed Telomerase-like Sequence	-128.9312	7.78714E-06	-53.6703	4.22785E-06
W03A5.8	not known	-18.8279	0.0290	-27.6793	4.9363E-06
Y105C5A.14	not known	-40.7010	0.0243	-27.0332	0.0194
Y106G6D.5	not known	-48.6936	0.0055	-64.2345	2.31071E-07
Y17D7B.7	not known	-407.9960	5.46067E-08	-101.2981	5.5018E-10
Y17D7C.3	not known	-148.5011	6.59808E-06	-49.6661	1.08928E-05
Y41C4A.29	not known	-61.0709	0.0016	-32.7535	0.0024
Y48G10A.6	not known	-2676.2868	4.52633E-16	-33.4624	1.73787E-23
Y82E9BL.9	not known	-42.0171	0.0170	-46.0740	3.91481E-05
ZC513.7	not known	-169.3728	1.18339E-08	-185.4251	3.19104E-20
ZK131.12	not known	-46.6828	0.0153	-72.8935	1.77233E-08
ZK131.13	not known	-46.6293	0.0216	-74.6144	5.00908E-07

Table 4.4. Genes downregulated in *mec-3* mutants, greatest fold-change

Gene	Classification	$\log_2$(fold change)	FDR corrected p-value
B0507.8	not known	-752.1003	6.17752E-12
lgc-12	Ligand-Gated ion Channel	-589.2131	2.44518E-13
F56A12.2	not known	-579.0466	3.28407E-10
Y57G11C.39	not known	-497.2480	4.004E-10
K07C10.3	not known	-388.1612	3.81284E-09
srh-74	Serpentine Receptor, class H	-363.0293	3.34329E-07
srh-276	Serpentine Receptor, class H	-299.0821	8.59748E-06
grl-18	GRound-Like (grd related)	-184.6978	4.09961E-05
cpna-4	CoPiNe domain protein, Atypical	-180.6468	1.14825E-09
Y17D7C.4	not known	-167.4169	0.001473134
deg-3	DEGeneration of certain neurons	-164.5529	9.49559E-11
linc-25	Long Intervening Non-Coding RNA	-143.1449	2.5003E-05
R05G9.5	not known	-141.1530	1.01721E-07
npr-2	NeuroPeptide Receptor family	-123.1241	4.93369E-08
R166.6	not known	-122.4959	7.69329E-05
linc-14	Long Intervening Non-Coding RNA	-115.2567	0.000378341

F40G12.2	not known	-108.3558	0.000170322
R07B1.6	not known	-102.3838	0.003553876
K11G9.7	not known	-89.8230	0.007509929
kcnl-4	KCNN (potassium K ChaNNel, calcium activated)-Like	-89.1714	1.96164E-08

Table 4.5. Genes downregulated *mec-3* mutants, lowest p-value

Gene	Classification	log_2(fold change)	FDR corrected p-value
lgc-12	Ligand-Gated ion Channel	-589.2131	2.44518E-13
B0507.8	not known	-752.1003	6.17752E-12
deg-3	DEGeneration of certain neurons	-164.5529	9.49559E-11
F54G2.1	not known	-65.6723	9.72303E-11
F56A12.2	not known	-579.0466	3.28407E-10
Y57G11C.39	not known	-497.2480	4.004E-10
F15G9.1	not known	-64.4238	1.03388E-09
cpna-4	CoPiNe domain protein, Atypical	-180.6468	1.14825E-09
K07C10.3	not known	-388.1612	3.81284E-09
T03F6.4	not known	-48.6095	3.81284E-09
des-2	DEgeneration Suppressor	-75.3167	5.80979E-09
kcnl-4	KCNN (potassium K ChaNNel, calcium activated)-Like	-89.1714	1.96164E-08
npr-2	NeuroPeptide Receptor family	-123.1241	4.93369E-08
dma-1	Dendrite Morphology Abnormal	-53.0788	5.71635E-08
R05G9.5	not known	-141.1530	1.01721E-07
srh-74	Serpentine Receptor, class H	-363.0293	3.34329E-07
pes-7	Patterned Expression Site	-23.3366	4.62352E-07
kcnl-1	KCNN (potassium K ChaNNel, calcium activated)-Like	-40.1620	4.6248E-07
glb-9	GLoBin related	-68.7993	4.91998E-07
F41G3.1	not known	-41.9029	4.91998E-07

Table 4.6. Confirmation genes downregulated in *mec-3* mutants

Gene	Classification	log_2(fold change)	FDR corrected p-value
asic-1	Acid-sensing/Amiloride-Sensitive Ion Channel family	-9.9996	0.0201
deg-3	DEGeneration of certain neurons	-164.5529	9.49559E-11
del-1	DEgenerin Like	-27.2568	8.17622E-05
des-2	DEgeneration Suppressor	-75.3167	5.80979E-09
dma-1	Dendrite Morphology Abnormal	-53.0788	5.71635E-08
egl-46	EGg Laying defective	-40.5495	0.0005
F49H12.4	not known	-12.2292	0.0342
hpo-30	Hypersensitive to POre-forming toxin	-26.5303	0.0029
kpc-1	Kex-2 Proprotein Convertase family	-12.2315	0.0007
lgc-12	Ligand-Gated ion Channel	-589.2131	2.44518E-13
mec-2	MEChanosensory abnormality	-14.0933	0.0019
*mec-3**	MEChanosensory abnormality	-100.4134	0.0008
*mec-10**	MEChanosensory abnormality	-338.9180	1.72721E-12
mec-12	MEChanosensory abnormality	-23.0411	4.5407E-05
mig-10	abnormal cell MIGration	-7.5012	0.0016
sax-7	Sensory AXon guidance	-7.2340	0.0007
unc-86	UNCoordinated	-10.8291	0.0178

*Removed from dataset due to overlap, see **Table 4.3**.

Table 4.7: Confirmation genes not downregulated in *mec-3* mutants

Gene	Classification	log_2(fold change)	FDR corrected p-value
alr-1	AristaLess (Drosophila homeodomain) Related	-2.2880	1
ced-10	CEll Death abnormality	-1.2485	1
rab-10	RAB family	-2.0279	1
unc-5	UNCoordinated	-1.2311	1
unc-8	UNCoordinated	-1.4175	1
unc-34	UNCoordinated	-2.1193	1
unc-40	UNCoordinated	-1.6042	1

Discussion

We generated a worm strain using multiple promoter-fusion constructs to specifically label PVD. We used this strain to isolate PVD in late L2/early L3 worms using FACS. From these sorted PVD cells and from an internal whole-worm reference, we extracted RNA from *wt* and *mec-3* mutant worms and compared the RNA expression levels. Through this process, we identified 266 targets of MEC-3 in PVD. Several of the targets we identified have previously been studied in PVD (**Table 4.6**). However, some of the targets we identified, shown in **Table 4.4** and **Table 4.5**, have not been previously investigated in PVD.

CPNA-4/copine (BLAST[122] e-value = 5e-41 for *H. sapiens* copine-1 isoform c) is a member of the copine domain protein, atypical family. While CPNA-4 has not been studied, a similar protein, CPNA-1, has been shown to be located at integrin adhesion sites and is required for myosin localization in muscles[152]. CPNA-1, however, is not expressed in PVD. Perhaps CPNA-4 has a similar role in PVD for dendrite outgrowth and stabilization. As illustrated in Zihni et al.,[153] interactions between integrins within focal adhesions interact with claudins. Since HPO-30 is a claudin, there is a possibility that CPNA-4 may interact with HPO-30 or in the HPO-30 pathway[51] (see **Chapter 3**) to affect dendrite stabilization.

F54G2.1 is similar to isoform 2 of BAI1-associated protein 3 (BAP3) (BLAST[122] e-value = 6e-125), which may function as an adhesion-G-Protein Coupled Receptor (adhesion-GPCR)[154]. Adhesion-GPCR's play major roles in dendrite development and axon guidance[1,155]. For example, two GPCR-like proteins, *CELSR2* and *CELSR3*, both affect dendritic patterning: knockdown of *CELSR3* showed decreased dendritic branching, while *CELSR2* knockdown showed the opposite effect with more complex dendritic arborization[156]. The BAI proteins BAI1

and BAI3 have also been shown to be required for proper dendrite development and plasticity[157,158], and similarity of genetic structure among the BAI proteins suggests BAP3 (the homolog of F54G2.1) may also share a role in dendrite morphogenesis. Additional targets from this dataset are discussed in future directions proposed in the final chapter of this dissertation (**Chapter 5**) as they relate to the projects presented in **Chapter 2** and **Chapter 3**.

Our dataset was created from worms at the late L2/early L3 stage when 2° and 3° branches are developing. EGL-46[29,51,52] (**Chapter 3**), HPO-30[51] (**Chapter 3**), and DMA-1[92] have been previously studied for their roles in 2° branch development, and that they show up in our dataset as being downregulated in *mec-3* mutants (see **Table 4.6**) supports our hypothesis that MEC-3 regulates genes required for higher order branch development. While this dataset adds additional candidates involved in higher order branching, there are several reasons why this list may not be exhaustive. First, since we isolated PVD from animals at the L2/L3 stage, it is possible that we did not capture genes required at earlier stages for 1° branch development or at later stages for 3° and 4° branches. Or, it may be that MEC-3 does not regulate genes required for those stages of development. Second, at least three genes required for 2° branch number were not in the dataset: *unc-5*, *un-40*, and *unc-34*, though upregulated in PVD compared to the whole-worm internal reference (**Table 4.2**), were not downregulated in *mec-3* mutants (**Table 4.7**). These proteins have been shown to be necessary for 2° branch number[32] and 3° branch self-avoidance[32,52] (Sundararajan et al., personal communication; **Chapter 2**). That they were not targets of MEC-3 in this dataset suggests MEC-3 does not regulate these genes. Another possibility is that these genes are not activated by MEC-3 during the late L2/early L3 larval stage, when we isolated the PVD cells. Third, our dataset excludes genes that did not reach the cutoff point of being significantly downregulated, as defined by $p<0.05$. Finally, this list may not

be complete because genes involved in dendrite morphogenesis of both PVD and other cells that are not PVD-specific were removed (**Table 4.3**). Nonetheless, this dataset identifies genes potentially involved in higher order dendrite development that merit further research.

Acknowledgements

We thank the *Caenorhabditis* Genetics Center (CGC), which is funded by NIH Office of Research Infrastructure Programs (P40 OD010440) for *mec-3* and *lin-22* mutants, the Kang Shen Lab (Stanford University) for the *wyIs585* strain, and the Oliver Hobert Lab (Columbia University) for the *otIs138*, *otIs521*, *otIs396*, and *otIs181* strains.

Author contributions

David M. Miller, III, devised and supervised the study; Michaela Novakovic made *wyIs585;mec-3*, *wyIs585;wdIs52;mec-3*, and *wdIs52;lin-22*; Rebecca McWhirter sorted the final strain and analyzed the RNA-seq data to identify DEGs; Barbara M. J. O'Brien made all other strains and performed the experiments.

CHAPTER 5 : DISCUSSION AND FUTURE DIRECTIONS

Neuron development is a complex process that requires multiple genetic and transcriptional pathways acting at different developmental stages. The two nociceptor neurons in the body of *C. elegans*, PVD-L and PVD-R, are ideal models for studying these pathways due to their complex dendritic arborization, the ability to visualize development of the neurons because they are post-embryonically derived, and the manipulability of the *C. elegans* genome. The work described in this dissertation explored several aspects of PVD development using a combination of genetics, RNA-sequencing, and fluorescent microscopy. **Chapter 2** explored the role of *T24F1.4/c-tomoregulin* in 3° branch development and its potential involvement in the UNC-6 pathway, which led to the discovery that a shrinker-causing mutation causes 3° branch overlap. **Chapter 2** also demonstrated how components of the UNC-6 pathway are involved in 1°, 2°, and 3° branch development. **Chapter 3** showed that the EGL-46/EGL-44 pathway is required for commissural 2° branching and described the influence of MEC-3 on 1° branch length and axon length. Finally, **Chapter 4** highlighted additional targets of MEC-3 that were discovered using the SeqCel method to generate RNA-Seq data using isolated RNA from sorted PVD cells. These results, along with some future directions, are discussed below.

T24F1.4/c-tomoregulin is not required for 3° branch self-avoidance

T24F1.4/c-tomoregulin was originally identified as a target of MEC-3 from a microarray profile and RNAi screen[51]. In pursuit of characterizing the gene, it's role in the UNC-6-dependent pathway for 3° branch self-avoidance, protein topology, and specific domain functions, it was discovered that a background mutation was present, separate from the

T24F1.4(tm5213) allele. This background mutation was responsible for the defect originally described. When it was discovered that T24F1.4/c-tomoregulin was not required for dendritic development, and because no phenotype could be characterized for *T24F1.4* mutants using the tests and measurements described in these chapters, subsequent study of this gene was terminated. However, investigators interested in EGF-like proteins and signaling pathways, YXXΦ signal sequences, or homologs of h-tomoregulin may find that studying T24F1.4/c-tomoregulin in PVD is a useful model system for their endeavors.

In the RNA-Seq dataset described in **Chapter 4**, it was found that *T24F1.4* was expressed at higher levels in PVD vs. the whole-worm internal reference (average PVD RPKM = 13.15 vs. average internal reference RPKM = 2.56), suggesting *T24F1.4/c-tomoregulin* functions in PVD. However, when comparing *mec-3* vs. *wt* sorted PVD cells, there was no statistical difference in expression levels of *T24F1.4* (average PVD *wt* RPKM = 13.15 vs. average PVD *mec-3* RPKM = 3.76, FDR corrected p-value = 0.39), indicating *T24F1.4* is not regulated by MEC-3.

A shrinker-causing mutation causes 3° branch self-avoidance defects in PVD

The shrinker-causing mutation that resulted in self-avoidance defects, discussed in the **Discussion** section of **Chapter 2**, was not identified. However, the shrinker behavioral phenotype suggests that the mutation is related to GABA signaling in motor neurons[116]. Furthermore, 3° branch overlap was observed in a known shrinker mutant, *unc-25* (**Figure 2.16**). That a mutation in GABA signaling would affect PVD 3° branch overlap is intriguing for two reasons. First, the GABA motor circuit is separate from the nociceptor circuit, implying that any

influence of the GABA signaling pathway on PVD development would have to be indirect, perhaps through a muscle-derived cue during the late L3 larval stage (see **Chapter 2 Discussion**). Second, 1° and 2° branch characteristics were not disrupted, implying that the role of this developmental pathway for PVD is specific to 3° (and perhaps 4°) branches.

In the **Discussion** section of **Chapter 2**, a model was proposed whereby a muscle-derived cue is required for 3° branch self-avoidance. The secretion of this cue is dependent on GABA signaling, either directly or because it is dependent on relative levels of excitation and inhibition. Follow-up studies to identify the specific relationship between the shrinker-causing mutation and 3° branch overlap would initially need to identify the mutated gene. One potential method is whole-genome sequencing (WGS) of *"shrinker"* mutants versus wild type to identify candidate genes. This approach, however, is only useful if the mutation is obvious, such as a large insertion or deletion, and not a single nucleotide variant (SNV), since SNVs are so prevalent in genomes[159,160]. An alternate candidate approach of known shrinker-associated genes could test effects on 3° branch self-avoidance. Ten genes have been identified (wormbase.org) as causing the shrinker phenotype when mutated and are summarized in **Table 5.1**.

Table 5.1. Known shrinker-causing genes

Gene	Description
gas-2	unknown
snt-1	ortholog of synaptotagmin
twk-18	two-P domain potassium channel subunit
unc-25	ortholog of glutamic acid decarboxylase (GAD)
unc-30	ortholog of Pitx family homeodomain transcription factors
unc-43	type II calcium/calmodulin-dependent protein kinase (CaMKII)
unc-46	type 1 transmembrane protein similar to lysosomal associated membrane glycoprotein (LAMP) domain
unc-47	transmembrane vesicular GABA transporter
unc-49	GABA receptor
unc-68	ryanodine receptor ortholog

SNT-1/synaptotagmin[161] and UNC-43/CAMKII[162] are involved in neurotransmission. However, they are not specific to GABA motor neurons, as UNC-25 is, and so are not likely candidates. Although UNC-43/CAMKII has been shown to regulate neuromuscular junction morphology[163], gross neurite outgrowth and guidance was not noted to be defective.

Twk-18 is expressed in the body wall muscle[164] and has been related to secretion of DBL-1, a member of the transforming growth factor beta (TGFβ) superfamily[165]. DBL-1/TGFβ and UNC-129/TGFβ are both highly expressed in body wall muscles, where 3° branch development occurs. Furthermore, TGFβ enhances the repulsion of UNC-6 via the UNC-5/UNC-40 heterodimer through its interaction with UNC-5[166]. Thus, one possibility is that in *unc-25* mutants, secretion of TGFβ is decreased, resulting in 3° branch overlap. However, mutants of both *dbl-1*[94] and *unc-129*[52,94] show no 3° branch overlapping defects, indicating that TGFβ is not required for 3° branch self-avoidance.

UNC-68, a ryanodine receptor (RyR) ortholog, is required for UNC-6 localization in muscles, and accumulation of Venus::UNC-6 specifically in body-wall muscles of *unc-68* mutants suggests a role for UNC-68 in UNC-6 secretion[167]. This is an intriguing finding because UNC-6 secretion at this location fits well with the model of UNC-6's involvement in 3° branch self-avoidance[52]. If UNC-6 is secreted by body-wall muscles and is then used as a short-range cue, as the proposed model[52] suggests, then disruption of UNC-6 secretion in this location could lead to 3° branch overlap. While accumulation of Venus::UNC-6 was not seen in body-wall muscles of *unc-25* mutants[167], over excitation of muscles by a lack of GABA in *unc-25* mutants may result in excess secretion of UNC-6. Though studies of UNC-6-bound-UNC-40 rescued self-avoidance defects in *unc-6* mutants[32], and constitutively active UNC-5 causes hyper-

retraction of 3° branches (Sundararajan et al., personal communication), the effect of UNC-6 overexpression has not been tested to confirm that excess UNC-6 would not result in defects.

While little is known about GAS-2, the remaining shrinker-associated genes in **Table 5.1** are directly related to GABA signaling[116,168]: UNC-49 is a GABA receptor expressed in body-wall muscles[169]; UNC-46 is a transmembrane protein required, along with the vesicular GABA transporter (VGAT) UNC-47, to load GABA into synaptic vesicles[170,171]; and both UNC-47/VGAT and UNC-25/glutamic acid decarboxylase (GAD)[135], which converts glutamate to GABA, are regulated by the homeodomain transcription factor UNC-30[115]. If the 3° branch overlapping defect seen in *unc-25* mutants in **Chapter 2** (**Figure 2.16**) is a result of defective GABA signaling, mutants of *unc-30*, *unc-46*, *unc-47*, and *unc-49* should show a similar defect. Furthermore, if GABA influence on muscles inhibits secretion of guidance cues such as TGFβ and UNC-6, and disruption of this inhibition causes the 3° branch overlapping defect, then overexpression of TGFβ and UNC-6 in these mutants should rescue the defect.

The above model and experimental suggestions are based on the result that *unc-25* mutants display overlapping 3° branches in PVD, and the most direct link between GABA signaling and PVD 3° branches is the shared location of PVD 3° branches and muscles. However, the possibility remains for a more complex pathway, and all known functions and developmental influences of UNC-25 should be considered.

Downstream targets of EGL-46/EGL-44

The transcription factors EGL-46 and EGL-44 work together to selectively promote 2° branches that fasciculate with pre-existing motor neuron commissures (**Chapter 3**). One way to

identify downstream effectors of these TFs would be to sort PVD cells in *egl-46* mutants. However, the genes regulated by EGL-46 are likely in the list of targets of MEC-3 found in **Chapter 4** because EGL-46 is also a target of MEC-3. Below, I highlight several candidates from the dataset presented in **Chapter 4** that may act downstream of EGL-46.

Adhesion molecules allow neurites to fasciculate with neighboring cells. PLX-2/PLEXIN, SAX-7/L1CAM, and FRM-5.1/FERM are good candidates to consider due to their similarity to, or association with, adhesion molecules. UNC-69/SCOCO and UNC-76/FEZ are also good candidates because they are required for fasciculation. These MEC-3 targets are summarized in **Table 5.2**.

Table 5.2. Known adhesion-associated genes

Gene	Description	log_2(fold change)	FDR corrected p-value
frm-5.1	FERM domain (protein 4.1-exrin-radixin-moesin) family	-11.7524	0.0043
plx-2	plexin/semaphorin receptor	-9.025	0.0134
sax-7	L1CAM/cell adhesion receptor molecules	-7.234	0.0007
unc-69	SCOC (small coil-coil) protein	-5.17	0.0468
unc-76	FEZ (fasciculation and elongation; zygin/zeta-1) family	-6.4719	0.0282

PLX-2/PLEXIN is a semaphorin receptor that has been implicated in axon development through interactions with the Semaphorin-2A ortholog MAB-20/Sema2, a weak interaction that is enhanced with the cell adhesion molecule LAD-2/L1CAM[172]. However, MAB-20 activation of PLX-2 has been shown to result in growth cone collapse and is thus considered to be a repulsive cue[172,173]. Still, this candidate could be explored for a role in 2° branch outgrowth, as it may not act as a repulsive cue in this context. Conversely, it may act in either the HPO-30/claudin-

mediated pathway for pioneer 2° branch development or an additional MEC-3-regulated pathway for 2° branch development described in the next section.

SAX-7/L1CAM has been extensively studied in PVD dendrite development[93,94,99–103], but these studies focused on expression of SAX-7 in hypodermal cells for dendrite outgrowth through interaction with the leucine-rich repeat (LRR) transmembrane protein DMA-1/LRR located on the PVD membrane. These studies have also specifically focused on 3° and 4° branches. Expression of SAX-7 in PVD does not rescue the menorah-like structure that includes 2°, 3°, and 4° branches[99,100]. However, a cell-autonomous role for SAX-7 in 2° branch outgrowth and stabilization, regardless of 3° or 4° branch phenotype, has not been reported. Thus, it could potentially act downstream of EGL-46/EGL-44 for commissural 2° branch outgrowth. Studies to identify this specific role would have to account for the gross morphological defects in PVD in *sax-7* mutants[99,100]. These challenges could be overcome, for example, through cell-specific RNAi knockdown of SAX-7 in PVD, which would maintain the wild-type expression levels of SAX-7 expressed in the hypodermal cells that are required for 3° and 4° branches.

While FRM-5.1/FERM has not been directly studied in *C. elegans*, ERM- and FERM-domain proteins have been implicated in dendrite development[174] and axon fasciculation[175]. As a FERM-domain-containing protein, FRM-5.1 may have a similar function in PVD. UNC-69/SCOCO physically interacts with UNC-76/FEZ during axon outgrowth and guidance and is required for fasciculation of axon bundles in *C. elegans*[176]. The fasciculation mechanism of these proteins may act in 2° branch outgrowth. Although these gene candidates are best known for their roles in axon development, they may act downstream of EGL-46/EGL-44 for 2° branch development in PVD. Alternatively, they may actually be involved PVD axon development,

which has also been shown to be regulated by MEC-3 (**Chapter 3**) and is discussed in a later section.

An additional MEC-3-regulated pathway is required for 2° branch development

In **Chapter 3**, it was shown that EGL-46/EGL-44 are required for a subset of commissural 2° branches and that HPO-30 is required for a subset of pioneer 2° branches, identifying two parallel pathways for two categories of 2° branches in PVD. However, mutants of *egl-46* and *egl-44* still possess some commissural 2° branches, and mutants of *hpo-30* still possess some pioneer branches[51], indicating these two pathways are not solely required for commissural and pioneer branch development, respectively. The existence of a third pathway for 2° branch development was confirmed with the observation that 2° branches persist in double mutants of *egl-44* and *hpo-30*, in contrast to *mec-3* mutants, which show no 2° branches.

MEC-3 targets identified in **Chapter 4** that show decreased 2° branches when mutated should be categorized into an EGL-46-dependent, HPO-30-dependent, or unknown-dependent pathway. If the newly identified MEC-3 target is found to enhance the phenotype of both *egl-44* and *hpo-30* single mutants, triple mutants could determine if there is more than one additional pathway for 2° branch number. If triple mutants phenocopy the *mec-3* mutant phenotype, i.e. having no 2° branches, then the third and final pathway will have been identified. However, if the triple mutant has significantly less 2° branches than *elg-44;hpo-30* double mutants, but still has 2° branches, then it can be concluded that a third pathway has been identified and at least one more pathway exists. Discovery of the additional pathway(s) will shed light on why EGL-46 and

HPO-30 are required for only a subset of commissural and pioneer branches, respectively, and the necessity of additional pathways in this process.

MEC-3 is required for 1° branch development

MEC-3 (**Chapter 3**) and components of the UNC-6 pathway (**Chapter 2**) are required for proper 1° branch development in terms of length, guidance, and number. HPO-30 may also play a role in posterior 1° branch length since the posterior 1° branch in *hpo-30* mutants frequently does not extend all the way to end of the tail (personal observation). One intriguing discovery was that only *unc-34* mutants occasionally lacked the posterior 1° branch, though this was not found to be significant compared to the wild type (**Chapter 2**). No other mutants tested (*unc-6*, *unc-5*, *unc-40*, *mig-10*, *egl-44*, *egl-46*, *hpo-30*), aside from *mec-3* (**Chapter 3**), lacked the posterior 1° branch, indicating that only *mec-3* and *unc-34* could act in the same genetic pathway for posterior 1° branch outgrowth. However, *unc-34* was not found to be significantly downregulated in *mec-3* mutants compared to *wt* ($\log_2$(fold change) = -2.1193, FDR corrected p-value = 1) (**Chapter 4**).

The studies outlined in this dissertation focused on 2° and 3° branch development, but the observations for 1° branch defects, scored at the L4 larval stage, are worth investigating in future studies. It is not likely that the dataset presented in **Chapter 4** will help in identifying components required for 1° dendrite development because the 1° branches were fully developed by the time the cells were sorted[29]. But future studies to identify MEC-3 targets required specifically for 1° branch development may use the SeqCel[145] method at the L1 and early L2 larval stages.

UNC-34/Ena/VASP and MIG-10/Lpd in PVD dendrite development

Previous studies have shown that MIG-10 and UNC-34 function together in UNC-6-dependent pathways regulating axonal growth cone guidance[89,90]. However, work in the Miller Lab showed that while both UNC-34 and MIG-10 are required for PVD self-avoidance, these components function in independent pathways, with UNC-34 acting downstream of UNC-6[32]. Data presented in **Chapter 2** showed that both UNC-34 and MIG-10 are required for 2° branch number, but the dataset presented in **Chapter 4** showed that only MIG-10, not UNC-34, was significantly downregulated in *mec-3* mutants ($\log_2$(fold change) = -7.5012, FDR corrected p-value = 0.0016). Mutants of *unc-5* and *unc-40* also showed decreased 2° branches (**Chapter 2**) but were also not downregulated in *mec-3* mutants (**Chapter 4)**. This is consistent with a model whereby components of the UNC-6 pathway are required for 2° branch development but are not regulated by MEC-3. If this model is correct, and UNC-34 – but not MIG-10 – is part of the UNC-6 pathway, then this would place *unc-34* and *mig-10* in separate genetic pathways for dendrite development. Together, these findings point to a complex relationship between MEC-3, UNC-34, MIG-10, and UNC-6 and their roles in PVD dendrite development.

MEC-3 is required for axon development

It was shown in **Chapter 3** that MEC-3 is implicated in regulating axon length. Axon development has been studied extensively, but this process has not been investigated in PVD neurons. Downstream targets of MEC-3 in PVD required for axon development were not likely identified by the dataset in **Chapter 4** because axon development is complete by the L2 stage[29].

However, components of axon maintenance and excitability may be included. For example, KCNL-1 (BLAST e-value = 7e-112 for *H. sapiens* Isoform 1 of small conductance calcium-activated potassium channel protein 3) and KCNL-4 (BLAST e-value = 7e-60 for *H. sapiens* Isoform 1 of small conductance calcium-activated potassium channel protein 1) share conserved domains with mammalian small conductance potassium (SK) channels[177] (**Table 4.4**). SK channels are voltage-independent and are activated by the increased intracellular calcium following hyperpolarization[178]. They are thought to generate the afterhypolarization (AHP) phase and regulate the frequency of axonal firing. These are properties of axonal function and not development. Studies focused on MEC-3-dependent PVD axon development could use the SeqCel method[145] in L1 animals to identify components required for this process.

Conclusion

The work presented in this doctoral dissertation describes a diverse set of transcriptional and genetic pathways for 1°, 2°, and 3° branch development of the PVD nociceptor neurons in *C. elegans*. Specific criteria for scoring 1° branch defects (**Chapter 2**), along with the finding that MEC-3 is required for 1° branch length (**Chapter 3**), will help guide future studies examining specific components of 1° branch development. Identification of the commissural pathway, regulated by the transcription factors EGL-46 and EGL-44 (**Chapter 3**) will help guide studies to elucidate complementary pathways for the development of subsets of sister dendrites. Finally, the RNA-Seq dataset presented in **Chapter 4** identified additional targets of MEC-3 that may be involved in dendritic development. These findings have simultaneously answered questions of transcriptional and genetic pathways required in higher order dendritic branching, while

presenting new and exciting questions that remain to be answered. Illuminating the cellular mechanisms of how dendrites develop will allow researchers to better understand the underlying causes of diseases where dendrites are affected, such as intellectual disabilities (ID)[5], autism spectrum disorders (ASD)[6,7], schizophrenia[6,8,9], major depressive disorder (MDD)[10–14], and bipolar disorder[9]. Research in the specific genetic pathways and mutations that disrupt dendrite outgrowth and stabilization may also lead to advances in personalized medicine and identify therapeutic targets for neurodevelopmental disorders.

REFERENCES

1. Valnegri, P., Puram, S. V. & Bonni, A. Regulation of dendrite morphogenesis by extrinsic cues. *Trends in Neurosciences* **38,** 439–447 (2015).

2. Dubin, A. E. & Patapoutian, A. Nociceptors: The sensors of the pain pathway. *Journal of Clinical Investigation* **120,** 3760–3772 (2010).

3. Woolf, C. J. & Ma, Q. Nociceptors-Noxious Stimulus Detectors. *Neuron* **55,** 353–364 (2007).

4. Cameron, S. & Rao, Y. Molecular mechanisms of tiling and self-avoidance in neural development. *Mol. Brain* **3,** 28 (2010).

5. Kaufmann, W. E. & Moser, H. W. Dendritic anomalies in disorders associated with mental retardation. *Cereb. cortex* **10,** 981–991 (2000).

6. Penzes, P., Cahill, M. E., Jones, K. A., VanLeeuwen, J.-E. & Woolfrey, K. M. Dendritic spine pathology in neuropsychiatric disorders. *Nat. Neurosci.* **14,** 285–293 (2011).

7. Martínez-Cerdeño, V. Dendrite and spine modifications in autism and related neurodevelopmental disorders in patients and animal models. *Developmental Neurobiology* **77,** 393–404 (2017).

8. Glausier, J. R. & Lewis, D. A. Dendritic spine pathology in schizophrenia. *Neuroscience* **251,** 90–107 (2013).

9. Konopaske, G. T., Lange, N., Coyle, J. T. & Benes, F. M. Prefrontal Cortical Dendritic Spine Pathology in Schizophrenia and Bipolar Disorder. *JAMA Psychiatry* **71,** 1323 (2014).

10. Kang, H. J. *et al.* Decreased expression of synapse-related genes and loss of synapses in major depressive disorder. *Nat. Med.* **18,** 1413–1417 (2012).

11. Drevets, W. C. *et al.* Subgenual prefrontal cortex abnormalities in mood disorders. *Nature* **386,** 824–827 (1997).

12. Drevets, W. C. Functional anatomical abnormalities in limbic and prefrontal cortical structures in major depression. in *Progress in Brain Research* **126,** 413–431 (2000).

13. Cotter, D. Reduced Neuronal Size and Glial Cell Density in Area 9 of the Dorsolateral Prefrontal Cortex in Subjects with Major Depressive Disorder. *Cereb. Cortex* **12,** 386–394 (2002).

14. Cotter, D., Mackay, D., Landau, S., Kerwin, R. & Everall, I. Reduced glial cell density and neuronal size in the anterior cingulate cortex in major depressive disorder. *Arch. Gen.*

Psychiatry **58,** 545–553 (2001).

15. McKee, A. C., Kowall, N. W. & Kosik, K. S. Microtubular reorganization and dendritic growth response in alzheimer's disease. *Ann. Neurol.* **26,** 652–659 (1989).

16. Flood, D. G., Guarnaccia, M. & Coleman, P. D. Dendritic extent in human CA2-3 hippocampal pyramidal neurons in normal aging and senile dementia. *Brain Res.* **409,** 88–96 (1987).

17. Flood, D. G., Buell, S. J., Horwitz, G. J. & Coleman, P. D. Dendritic extent in human dentate gyrus granule cells in normal aging and senile dementia. *Brain Res.* **402,** 205–216 (1987).

18. Anderton, B. H. *et al.* Dendritic changes in Alzheimer's disease and factors that may underlie these changes. *Progress in Neurobiology* **55,** 595–609 (1998).

19. Falke, E. *et al.* Subicular Dendritic Arborization in Alzheimer's Disease Correlates with Neurofibrillary Tangle Density. *Am. J. Pathol.* **163,** 1615–1621 (2003).

20. Terry, R. D. *et al.* Physical basis of cognitive alterations in alzheimer's disease: Synapse loss is the major correlate of cognitive impairment. *Ann. Neurol.* **30,** 572–580 (1991).

21. Brenner, S. The genetics of Caenorhabditis elegans. *Genetics* **77,** 71–94 (1974).

22. White, J. G., Southgate, E., Thomson, J. N. & Brenner, S. The Mind of a Worm. *Philos. Trans. R. Soc. Lond. B. Biol. Sci.* **314,** 1–340 (1986).

23. Altun, Z. F. & Hall, D. H. Worm Atlas. *Wormatlas* (2009). doi:10.3908/wormatlas.1.14. Edited for the web by Laura A. Herndon. Last revision: April 30, 2012

24. Sulston, J. E. & Horvitz, H. R. Post-embryonic cell lineages of the nematode, Caenorhabditis elegans. *Dev. Biol.* **56,** 110–156 (1977).

25. Sulston, J. E., Schierenberg, E., White, J. G. & Thomson, J. N. The embryonic cell lineage of the nematode Caenorhabditis elegans. *Developmental Biology* **100,** 64–119 (1983).

26. The C. elegans Sequencing Consortium. Genome Sequence of the Nematode C. elegans: A Platform for Investigating Biology. *Science* **282,** 2012–2018 (1998).

27. Ishii, N., Wadsworth, W. G., Stern, B. D., Culotti, J. G. & Hedgecock, E. M. A laminin-related matrix protein, UNC-6, guides pioneer axon migrations in C. elegans. *Neuron* **9,** 873–881 (1992).

28. Sun, K. L. W., Correia, J. P. & Kennedy, T. E. Netrins: versatile extracellular cues with diverse functions. *Development* **138,** 2153–2169 (2011).

29. Smith, C. J. *et al.* Time-lapse imaging and cell-specific expression profiling reveal dynamic branching and molecular determinants of a multi-dendritic nociceptor in C. elegans. *Dev. Biol.* **345,** 18–33 (2010).

30. Albeg, A. *et al.* C. elegans multi-dendritic sensory neurons: Morphology and function. *Mol. Cell. Neurosci.* **46,** 308–317 (2011).

31. Hall, D. H. & Treinin, M. How does morphology relate to function in sensory arbors? *Trends Neurosci.* **34,** 443–451 (2011).

32. Smith, C. J. Morphological and molecular characterization of somatosensory neurogenesis. (Vanderbilt University, 2012).

33. Chalfie, M. & Thomson, J. N. Organization of neuronal microtubules in the nematode Caenorhabditis elegans. *J. Cell Biol.* **82,** 278–289 (1979).

34. Chalfie, M. & Sulston, J. Developmental genetics of the mechanosensory neurons of Caenorhabditis elegans. *Dev. Biol.* **82,** 358–370 (1981).

35. Chalfie, M. *et al.* The neural circuit for touch sensitivity in Caenorhabditis elegans. *J. Neurosci.* **5,** 956–64 (1985).

36. Way, J. C. & Chalfie, M. The mec-3 gene of Caenorhabditis elegans requires its own product for maintained expression and is expressed in three neuronal cell types. *Genes Dev.* **3,** 1823–1833 (1989).

37. Way, J. C. & Chalfie, M. mec-3, a homeobox-containing gene that specifies differentiation of the touch receptor neurons in C. elegans. *Cell* **54,** 5–16 (1988).

38. Wicks, S. R. & Rankin, C. H. Integration of mechanosensory stimuli in Caenorhabditis elegans. *J. Neurosci.* **15,** 2434–2444 (1995).

39. Chatzigeorgiou, M. *et al.* Specific roles for DEG/ENaC and TRP channels in touch and thermosensation in C. elegans nociceptors. *Nat. Neurosci.* **13,** 861–868 (2010).

40. Treinin, M. & Chalfie, M. A mutated acetylcholine receptor subunit causes neuronal degeneration in C. elegans. *Neuron* **14,** 871–877 (1995).

41. Treinin, M., Gillo, B., Liebman, L. & Chalfie, M. Two functionally dependent acetylcholine subunits are encoded in a single Caenorhabditis elegans operon. *Proc. Natl. Acad. Sci. U. S. A.* **95,** 15492–15495 (1998).

42. Venkatachalam, K. & Montell, C. TRP Channels. *Annu. Rev. Biochem.* **76,** 387–417 (2007).

43. Colbert, H. A. & Bargmann, C. I. Odorant-specific adaptation pathways generate olfactory plasticity in C. elegans. *Neuron* **14,** 803–812 (1995).

44. Colbert, H. A., Smith, T. L. & Bargmann, C. I. OSM-9, a novel protein with structural similarity to channels, is required for olfaction, mechanosensation, and olfactory adaptation in Caenorhabditis elegans. *J. Neurosci.* **17,** 8259–69 (1997).

45. Jansen, G., Weinkove, D. & Plasterk, R. H. A. The G-protein γ subunit gpc-1 of the nematode C.elegans is involved in taste adaptation. *EMBO J.* **21,** 986–994 (2002).

46. Kindt, K. S. *et al.* Caenorhabditis elegans TRPA-1 functions in mechanosensation. *Nat. Neurosci.* **10,** 568–577 (2007).

47. Mano, I. & Driscoll, M. DEG/ENaC channels: A touchy superfamily that watches its salt. *BioEssays* **21,** 568–578 (1999).

48. Huang, M. & Chalfie, M. Gene interactions affecting mechanosensory transduction in Caenorhabditis elegans. *Nature* **367,** 467–470 (1994).

49. O'Hagan, R., Chalfie, M. & Goodman, M. B. The MEC-4 DEG/ENaC channel of Caenorhabditis elegans touch receptor neurons transduces mechanical signals. *Nat. Neurosci.* **8,** 43–50 (2005).

50. Tsalik, E. L. *et al.* LIM homeobox gene-dependent expression of biogenic amine receptors in restricted regions of the C. elegans nervous system. *Dev. Biol.* **263,** 81–102 (2003).

51. Smith, C. J. *et al.* Sensory neuron fates are distinguished by a transcriptional switch that regulates dendrite branch stabilization. *Neuron* **79,** 266–280 (2013).

52. Smith, C. J., Watson, J. D., VanHoven, M. K., Colón-Ramos, D. A. & Miller, D. M. Netrin (UNC-6) mediates dendritic self-avoidance. *Nat. Neurosci.* **15,** 731–737 (2012).

53. Desai, C., Garriga, G., McIntire, S. L. & Horvitz, H. R. A genetic pathway for the development of the Caenorhabditis elegans HSN motor neurons. *Nature* **336,** 638–646 (1988).

54. Yu, H., Pretot, R. F., Burglin, T. R. & Sternberg, P. W. Distinct roles of transcription factors EGL-46 and DAF-19 in specifying the functionality of a polycystin-expressing sensory neuron necessary for C. elegans male vulva location behavior. *Development* **130,** 5217–5227 (2003).

55. Wu, J., Duggan, A. & Chalfie, M. Inhibition of touch cell fate by egl-44 and egl-46 in C. elegans. *Genes Dev.* **15,** 789–802 (2001).

56. Feng, G. *et al.* Developmental stage-dependent transcriptional regulatory pathways control neuroblast lineage progression. *Development* **140,** 3838–47 (2013).

57. Corty, M. M., Matthews, B. J. & Grueber, W. B. Molecules and mechanisms of dendrite development in Drosophila. *Development* **136,** 1049–61 (2009).

58. Jinushi-Nakao, S. *et al.* Knot/Collier and Cut Control Different Aspects of Dendrite Cytoskeleton and Synergize to Define Final Arbor Shape. *Neuron* **56,** 963–978 (2007).

59. Jan, Y.-N. & Jan, L. Y. Branching out: mechanisms of dendritic arborization. *Nat. Rev. Neurosci.* **11,** 316–328 (2010).

60. Li, W., Wang, F., Menut, L. & Gao, F. B. BTB/POZ-zinc finger protein abrupt suppresses dendritic branching in a neuronal subtype-specific and dosage-dependent manner. *Neuron* **43,** 823–834 (2004).

61. Sugimura, K., Satoh, D., Estes, P., Crews, S. & Uemura, T. Development of morphological diversity of dendrites in Drosophila by the BTB-zinc finger protein abrupt. *Neuron* **43,** 809–822 (2004).

62. Crozatier, M. & Vincent, A. Control of multidendritic neuron differentiation in Drosophila: The role of Collier. *Dev. Biol.* **315,** 232–242 (2008).

63. Hattori, Y., Sugimura, K. & Uemura, T. Selective expression of Knot/Collier, a transcriptional regulator of the EBF/Olf-1 family, endows the Drosophila sensory system with neuronal class-specific elaborated dendritic patterns. *Genes to Cells* **12,** 1011–1022 (2007).

64. Hattori, Y. *et al.* Sensory-neuron subtype-specific transcriptional programs controlling dendrite morphogenesis: Genome-wide analysis of abrupt and knot/collier. *Dev. Cell* **27,** 530–544 (2013).

65. Grueber, W. B., Jan, L. Y. & Jan, Y. N. Different levels of the homeodomain protein cut regulate distinct dendrite branching patterns of Drosophila multidendritic neurons. *Cell* **112,** 805–818 (2003).

66. Cubelos, B. *et al.* Cux1 and Cux2 regulate dendritic branching, spine morphology, and synapses of the upper layer neurons of the cortex. *Neuron* **66,** 523–535 (2010).

67. Nagel, J. *et al.* Fascin controls neuronal class-specific dendrite arbor morphology. *Development* **139,** 2999–3009 (2012).

68. Kim, M. D., Lily, Y. J. & Yuh, N. J. The bHLH-PAS protein spineless is necessary for the diversification of dendrite morphology of Drosophila dendritic arborization neurons. *Genes Dev.* **20,** 2806–2819 (2006).

69. Dailey, M. E. & Smith, S. J. The dynamics of dendritic structure in developing hippocampal slices. *J. Neurosci.* **16,** 2983–2994 (1996).

70. Wong, W. T. & Wong, R. O. L. Rapid dendritic movements during synapse formation and rearrangement. *Current Opinion in Neurobiology* **10,** 118–124 (2000).

71. Wu, G. Y., Zou, D. J., Rajan, I. & Cline, H. Dendritic dynamics in vivo change during neuronal maturation. *J. Neurosci.* **19,** 4472–4483 (1999).

72. Holtmaat, A. J. G. D. *et al.* Transient and persistent dendritic spines in the neocortex in vivo. *Neuron* **45,** 279–291 (2005).

73. Trachtenberg, J. T. *et al.* Long-term in vivo imaging of experience-dependent synaptic plasticity in adult cortex. *Nature* **420,** 788–794 (2002).

74. Zuo, Y., Lin, A., Chang, P. & Gan, W. B. Development of long-term dendritic spine stability in diverse regions of cerebral cortex. *Neuron* **46,** 181–189 (2005).

75. Baas, P. W., Deitch, J. S., Black, M. M. & Banker, G. A. Polarity orientation of microtubules in hippocampal neurons: uniformity in the axon and nonuniformity in the dendrite. *Proc. Natl. Acad. Sci.* **85,** 8335–8339 (1988).

76. Burton, P. R. Dendrites of mitral cell neurons contain microtubules of opposite polarity. *Brain Res.* **473,** 107–115 (1988).

77. Kapitein, L. C. *et al.* Mixed Microtubules Steer Dynein-Driven Cargo Transport into Dendrites. *Curr. Biol.* **20,** 290–299 (2010).

78. Koleske, A. J. Molecular mechanisms of dendrite stability. *Nat. Rev. Neurosci.* **14,** 536–550 (2013).

79. Vaillant, A. R. *et al.* Signaling mechanisms underlying reversible activity-dependent dendrite formation. *Neuron* **34,** 985–998 (2002).

80. Szebenyi, G. *et al.* Activity-driven dendritic remodeling requires microtubule-associated protein 1A. *Curr. Biol.* **15,** 1820–1826 (2005).

81. Teng, J. *et al.* Synergistic effects of MAP2 and MAP1B knockout in neuronal migration, dendritic outgrowth, and microtubule organization. *J. Cell Biol.* **155,** 65–76 (2001).

82. Maniar, T. A. *et al.* UNC-33 (CRMP) and ankyrin organize microtubules and localize kinesin to polarize axon-dendrite sorting. *Nat. Neurosci.* **15,** 48–56 (2011).

83. Dong, X., Shen, K. & Bülow, H. E. Intrinsic and Extrinsic Mechanisms of Dendritic Morphogenesis. *Annu. Rev. Physiol.* **77,** 271–300 (2015).

84. Aguirre-Chen, C., Bulow, H. E. & Kaprielian, Z. C. elegans bicd-1, homolog of the Drosophila dynein accessory factor Bicaudal D, regulates the branching of PVD sensory

neuron dendrites. *Development* **138,** 507–518 (2011).

85. Zhang, Y., Yang, Y., Zhu, Z. & Ou, G. WASP-Arp2 / 3-dependent Actin Polymerization Influences Fusogen Localization during Cell-Cell Fusion in C . elegans Embryos. 1324–1328 (2017).

86. Yang, Y. *et al.* Spectraplakin Induces Positive Feedback between Fusogens and the Actin Cytoskeleton to Promote Cell-Cell Fusion. *Dev. Cell* **41,** 107–120.e4 (2017).

87. Oren-Suissa, M., Hall, D. H., Treinin, M., Shemer, G. & Podbilewicz, B. The Fusogen EFF-1 Controls Sculpting of Mechanosensory Dendrites. *Science* **328,** 1285–1288 (2010).

88. Krause, M. *et al.* Lamellipodin, an Ena/VASP ligand, is implicated in the regulation of lamellipodial Dynamics. *Dev. Cell* **7,** 571–583 (2004).

89. Chang, C. *et al.* MIG-10/Lamellipodin and AGE-1/PI3K Promote Axon Guidance and Outgrowth in Response to Slit and Netrin. *Curr. Biol.* **16,** 854–862 (2006).

90. Quinn, C. C. *et al.* UNC-6/Netrin and SLT-1/Slit Guidance Cues Orient Axon Outgrowth Mediated by MIG-10/RIAM/Lamellipodin. *Curr. Biol.* **16,** 845–853 (2006).

91. Dickson, B. J. Molecular Mechanisms of Axon Guidance. *Science* **298,** 1959–1964 (2002).

92. Liu, O. W. & Shen, K. The transmembrane LRR protein DMA-1 promotes dendrite branching and growth in C. elegans. *Nat. Neurosci.* **15,** 57–63 (2011).

93. Dong, X. *et al.* Precise regulation of the guidance receptor DMA-1 by KPC-1/furin instructs dendritic branching decisions. *Elife* **5,** 1–22 (2016).

94. Salzberg, Y., Ramirez-Suarez, N. J. & Bülow, H. E. The Proprotein Convertase KPC-1/Furin Controls Branching and Self-avoidance of Sensory Dendrites in Caenorhabditis elegans. *PLoS Genet.* **10,** (2014).

95. Wei, X. *et al.* The unfolded protein response is required for dendrite morphogenesis. *Elife* **4,** 1–20 (2015).

96. Salzberg, Y. *et al.* Reduced Insulin/Insulin-like Growth Factor Receptor Signaling Mitigates Defective Dendrite Morphogenesis in Mutants of the ER Stress Sensor IRE-1. *PLoS Genet.* **13,** 1–17 (2017).

97. Taylor, C. A., Yan, J., Howell, A. S., Dong, X. & Shen, K. RAB-10 Regulates Dendritic Branching by Balancing Dendritic Transport. *PLoS Genet.* **11,** 1–24 (2015).

98. Zou, W., Yadav, S., DeVault, L., Nung Jan, Y. & Sherwood, D. R. RAB-10-Dependent Membrane Transport Is Required for Dendrite Arborization. *PLoS Genet.* **11,** 1–28

(2015).

99. Dong, X., Liu, O. W., Howell, A. S. & Shen, K. An extracellular adhesion molecule complex patterns dendritic branching and morphogenesis. *Cell* **155,** 296–307 (2013).

100. Salzberg, Y. *et al.* Skin-derived cues control arborization of sensory dendrites in Caenorhabditis elegans. *Cell* **155,** (2013).

101. Zou, W. *et al.* A multi-protein receptor-ligand complex underlies combinatorial dendrite guidance choices in C. elegans. *Elife* **5,** 1–25 (2016).

102. Díaz-Balzac, C. A. *et al.* Muscle- and Skin-Derived Cues Jointly Orchestrate Patterning of Somatosensory Dendrites. *Curr. Biol.* **26,** 2379–87 (2016).

103. Liang, X., Dong, X., Moerman, D. G., Shen, K. & Wang, X. Sarcomeres Pattern Proprioceptive Sensory Dendritic Endings through UNC-52/Perlecan in C.elegans. *Dev. Cell* **33,** 388–400 (2015).

104. Liu, X., Wang, X. & Shen, K. Receptor tyrosine phosphatase CLR-1 acts in skin cells to promote sensory dendrite outgrowth. *Dev. Biol.* **413,** 60–69 (2016).

105. Whitford, K. L. *et al.* Regulation of cortical dendrite development by Slit-Robo interactions. *Neuron* **33,** 47–61 (2002).

106. Furrer, M.-P., Vasenkova, I., Kamiyama, D., Rosado, Y. & Chiba, A. Slit and Robo control the development of dendrites in Drosophila CNS. *Development* **134,** 3795–3804 (2007).

107. Dimitrova, S., Reissaus, A. & Tavosanis, G. Slit and Robo regulate dendrite branching and elongation of space-filling neurons in Drosophila. *Dev. Biol.* **324,** 18–30 (2008).

108. Gibson, D. A. *et al.* Dendrite self-avoidance requires cell-autonomous slit/robo signaling in cerebellar purkinje cells. *Neuron* **81,** 1040–1056 (2014).

109. Lawrence Zipursky, S. & Grueber, W. B. The Molecular Basis of Self-Avoidance. *Annu. Rev. Neurosci.* **36,** 547–568 (2013).

110. Lefebvre, J. L., Kostadinov, D., Chen, W. V., Maniatis, T. & Sanes, J. R. Protocadherins mediate dendritic self-avoidance in the mammalian nervous system. *Nature* **488,** 517–521 (2012).

111. Sun, L. O. *et al.* On and Off Retinal Circuit Assembly by Divergent Molecular Mechanisms. *Science* **342,** 1241974–1241974 (2013).

112. Lefebvre, J. L., Sanes, J. R. & Kay, J. N. Development of Dendritic Form and Function. *Annu. Rev. Cell Dev. Biol.* **31,** 741–777 (2015).

113. Puram, S. V. & Bonni, A. Cell-intrinsic drivers of dendrite morphogenesis. *Development* **140,** 4657–4671 (2013).

114. Kanemoto, N. *et al.* Expression of TMEFF1 mRNA in the mouse central nervous system: Precise examination and comparative studies of TMEFF1 and TMEFF2. *Mol. Brain Res.* **86,** 48–55 (2001).

115. Eastman, C., Horvitz, H. R. & Jin, Y. Coordinated transcriptional regulation of the unc-25 glutamic acid decarboxylase and the unc-47 GABA vesicular transporter by the Caenorhabditis elegans UNC-30 homeodomain protein. *J. Neurosci.* **19,** 6225–6234 (1999).

116. Schuske, K., Beg, A. A. & Jorgensen, E. M. The GABA nervous system in C. elegans. *Trends in Neurosciences* **27,** 407–414 (2004).

117. Petersen, T. N., Brunak, S., von Heijne, G. & Nielsen, H. SignalP 4.0: discriminating signal peptides from transmembrane regions. *Nat. Methods* **8,** 785–786 (2011).

118. Boeckmann, B. *et al.* The SWISS-PROT protein knowledgebase and its supplement TrEMBL in 2003. *Nucleic Acids Res.* **31,** 365–370 (2003).

119. von Heijne, G. Net N-C charge imbalance may be important for signal sequence function in bacteria. *J. Mol. Biol.* **192,** 287–290 (1986).

120. Pandey, K. N. Functional roles of short sequence motifs in the endocytosis of membrane receptors. *Front. Biosci.* **14,** 5339 (2009).

121. Bernsel, A., Viklund, H., Hennerdal, A. & Elofsson, A. TOPCONS: Consensus prediction of membrane protein topology. *Nucleic Acids Res.* **37,** 465–468 (2009).

122. Morgulis, A. *et al.* Database indexing for production MegaBLAST searches. *Bioinformatics* **24,** 1757–1764 (2008).

123. Siegel, D. A., Huang, M. K. & Becker, S. F. Ectopic dendrite initiation: CNS pathogenesis as a model of CNS development. *Int. J. Dev. Neurosci.* **20,** 373–389 (2002).

124. Horie, M. *et al.* Identification and characterization of TMEFF2, a novel survival factor for hippocampal and mesencephalic neurons. *Genomics* **67,** 146–52 (2000).

125. Uchida, T. *et al.* A novel epidermal growth factor-like molecule containing two follistatin modules stimulates tyrosine phosphorylation of erbB-4 in MKN28 gastric cancer cells. *Biochem. Biophys. Res. Commun.* **266,** 593–602 (1999).

126. Liang, G., Robertson, K. D., Talmadge, C., Sumegi, J. & Jones, P. A. The gene for a novel transmembrane protein containing epidermal growth factor and follistatin domains is

frequently hypermethylated in human tumor cells. *Cancer Res.* **60,** 4907–4912 (2000).

127. Spencer, W. C. *et al.* A spatial and temporal map of C. elegans gene expression. *Genome Res.* 325–341 (2011).

128. Lim, Y. S., Mallapur, S., Kao, G., Ren, X. C. & Wadsworth, W. G. Netrin UNC-6 and the regulation of branching and extension of motoneuron axons from the ventral nerve cord of Caenorhabditis elegans. *J. Neurosci.* **19,** 7048–7056 (1999).

129. Merz, D. C., Zheng, H., Killeen, M. T., Krizus, A. & Culotti, J. G. Multiple signaling mechanisms of the UNC-6/netrin receptors UNC-5 and UNC-40/DCC in vivo. *Genetics* **158,** 1071–1080 (2001).

130. Hedgecock, E. M., Culotti, J. G., Hall, D. H. & Stern, B. D. Genetics of cell and axon migrations in Caenorhabditis elegans. *Development* **100,** 365–82 (1987).

131. Hedgecock, E. M., Culotti, J. G. & Hall, D. H. The unc-5, unc-6, and unc-40 genes guide circumferential migrations of pioneer axons and mesodermal cells on the epidermis in C. elegans. *Neuron* **4,** 61–85 (1990).

132. Killeen, M. *et al.* UNC-5 function requires phosphorylation of cytoplasmic tyrosine 482, but its UNC-40-independent functions also require a region between the ZU-5 and death domains. *Dev. Biol.* **251,** 348–366 (2002).

133. Tamai, K. K. & Nishiwaki, K. bHLH Transcription factors regulate organ morphogenesis via activation of an ADAMTS protease in C. elegans. *Dev. Biol.* **308,** 562–571 (2007).

134. Gengyo-Ando, K. & Mitani, S. Characterization of Mutations Induced by Ethyl Methanesulfonate, UV, and Trimethylpsoralen in the Nematode Caenorhabditis elegans. *Biochem. Biophys. Res. Commun.* **269,** 64–69 (2000).

135. Jin, Y., Jorgensen, E., Hartwieg, E. & Horvitz, H. R. The Caenorhabditis elegans gene unc-25 encodes glutamic acid decarboxylase and is required for synaptic transmission but not synaptic development. *J. Neurosci.* **19,** 539–548 (1999).

136. Rui, Y. *et al.* Activity-dependent regulation of dendritic growth and maintenance by glycogen synthase kinase 3β. *Nat. Commun.* **4,** (2013).

137. Romanos, T. R., Petersen, J. G., Riveiro, A. R. & Pocock, R. A novel role for the zinc-finger transcription factor EGL-46 in the differentiation of Gas-sensing neurons in Caenorhabditis elegans. *Genetics* **199,** 157–163 (2015).

138. Raj, A., van den Bogaard, P., Rifkin, S. A., van Oudenaarden, A. & Tyagi, S. Imaging individual mRNA molecules using multiple singly labeled probes. *Nat. Methods* **5,** 877–879 (2008).

139. Moore, A. W. hamlet, a Binary Genetic Switch Between Single- and Multiple- Dendrite Neuron Morphology. *Science* **297,** 1355–1358 (2002).

140. Parrish, J. Z., Kim, M. D., Jan, L. Y. & Jan, Y. N. Genome-wide analyses identify transcription factors required for proper morphogenesis of Drosophila sensory neuron dendrites. *Genes Dev.* **20,** 820–35 (2006).

141. Anbanandam, A. *et al.* Insights into transcription enhancer factor 1 (TEF-1) activity from the solution structure of the TEA domain. *PNAS* **103,** 17225–30 (2006).

142. Hunter, C. S. & Rhodes, S. J. LIM-homeodomain genes in mammalian development and human disease. *Molecular Biology Reports* **32,** 67–77 (2005).

143. Rosenbaum, J. N., Duggan, A. & García-Añoveros, J. Insm1 promotes the transition of olfactory progenitors from apical and proliferative to basal, terminally dividing and neuronogenic. *Neural Dev.* **6,** 6 (2011).

144. Zhao, S., Fung-Leung, W. P., Bittner, A., Ngo, K. & Liu, X. Comparison of RNA-Seq and microarray in transcriptome profiling of activated T cells. *PLoS One* **9,** (2014).

145. Spencer, W. C. *et al.* Isolation of specific neurons from C. Elegans larvae for gene expression profiling. *PLoS One* **9,** 1–11 (2014).

146. Watson, J. D. *et al.* Complementary RNA amplification methods enhance microarray identification of transcripts expressed in the C. elegans nervous system. *BMC Genomics* **9,** 84 (2008).

147. Yip, Z. C. & Heiman, M. G. Duplication of a Single Neuron in C. elegans Reveals a Pathway for Dendrite Tiling by Mutual Repulsion. *Cell Rep.* **15,** 2109–2117 (2016).

148. Serrano-Saiz, E. *et al.* Modular control of glutamatergic neuronal identity in C. elegans by distinct homeodomain proteins. *Cell* **155,** 659–673 (2013).

149. Culetto, E. *et al.* Structure and promoter activity of the 5' flanking region of ace-1, the gene encoding acetylcholinesterase of class A in Caenorhabditis elegans. *J. Mol. Biol.* **290,** 951–66 (1999).

150. Flames, N. & Hobert, O. Gene regulatory logic of dopamine neuron differentiation. *Nature* **458,** 885–889 (2009).

151. Oliveros, J. C. Venny. An interactive tool for comparing lists with Venny's diagrams. 2007--2015. h ttp. *bioinfogp. cnb. csic. es/tools/venny/index. html. Accessed* **1,** (2016).

152. Warner, A. *et al.* CPNA-1, a copine domain protein, is located at integrin adhesion sites and is required for myofilament stability in Caenorhabditis elegans. *Mol. Biol. Cell* **24,** 601–16 (2013).

153. Zihni, C., Mills, C., Matter, K. & Balda, M. S. Tight junctions: from simple barriers to multifunctional molecular gates. *Nat. Rev. Mol. Cell Biol.* **17,** 564–580 (2016).

154. Shiratsuchi, T. *et al.* Cloning and Characterization of BAP3 (BAI-Associated Protein 3), a C2 Domain-Containing Protein That Interacts with BAI1. *Biochem. Biophys. Res. Commun.* **251,** 158–165 (1998).

155. Langenhan, T., Piao, X. & Monk, K. R. Adhesion G protein-coupled receptors in nervous system development and disease. *Nat. Rev. Neurosci.* **17,** 550–561 (2016).

156. Shima, Y. *et al.* Opposing roles in neurite growth control by two seven-pass transmembrane cadherins. *Nat. Neurosci.* **10,** 963–969 (2007).

157. Lanoue, V. *et al.* The adhesion-GPCR BAI3, a gene linked to psychiatric disorders, regulates dendrite morphogenesis in neurons. *Mol. Psychiatry* **18,** 943–950 (2013).

158. Duman, J. G. *et al.* The Adhesion-GPCR BAI1 Regulates Synaptogenesis by Controlling the Recruitment of the Par3/Tiam1 Polarity Complex to Synaptic Sites. *J. Neurosci.* **33,** 6964–6978 (2013).

159. 1000 Genomes Project Consortium *et al.* A global reference for human genetic variation. *Nature* **526,** 68–74 (2015).

160. O'Brien, T. D. Investigating the genetic influences of the germline and somatic genomes in three subtypes of lung cancer. (Vanderbilt University, 2017).

161. Mathews, E. A. *et al.* Differential expression and function of synaptotagmin 1 isoforms in *Caenorhabditis elegans*. *Mol. Cell. Neurosci.* **34,** 642–652 (2007).

162. Liu, Q., Chen, B., Ge, Q. & Wang, Z.-W. Presynaptic Ca2+/Calmodulin-Dependent Protein Kinase II Modulates Neurotransmitter Release by Activating BK Channels at Caenorhabditis elegans Neuromuscular Junction. *J. Neurosci.* **27,** 10404–10413 (2007).

163. Caylor, R. C., Jin, Y. & Ackley, B. D. The Caenorhabditis elegans voltage-gated calcium channel subunits UNC-2 and UNC-36 and the calcium-dependent kinase UNC-43/CaMKII regulate neuromuscular junction morphology. *Neural Dev.* **8,** 10 (2013).

164. Kunkel, M. T., Johnstone, D. B., Thomas, J. H. & Salkoff, L. Mutants of a temperature-sensitive two-P domain potassium channel. *J. Neurosci.* **20,** 7517–7524 (2000).

165. Zhang, X. & Zhang, Y. DBL-1, a TGF-β, is essential for Caenorhabditis elegans aversive olfactory learning. *Proc. Natl. Acad. Sci. U. S. A.* **109,** 17081–6 (2012).

166. MacNeil, L. T., Hardy, W. R., Pawson, T., Wrana, J. L. & Culotti, J. G. UNC-129 regulates the balance between UNC-40 dependent and independent UNC-5 signaling

pathways. *Nat. Neurosci.* **12,** 150–5 (2009).

167. Asakura, T., Waga, N., Ogura, K. I. & Goshima, Y. Genes required for cellular UNC-6/Netrin localization in Caenorhabditis elegans. *Genetics* **185,** 573–585 (2010).

168. McIntire, S. L., Jorgensen, E. & Horvitz, H. R. Genes required for GABA function in Caenorhabditis elegans. *Nature* **364,** 334–7 (1993).

169. Bamber, B. A., Beg, A. A., Twyman, R. E. & Jorgensen, E. M. The Caenorhabditis elegans UNC-49 locus encodes multiple subunits of a heteromultimeric GABA receptor. *J. Neurosci.* **19,** 5348–5359 (1999).

170. Schuske, K., Palfreyman, M. T., Watanabe, S. & Jorgensen, E. M. UNC-46 is required for trafficking of the vesicular GABA transporter. *Nat. Neurosci.* **10,** 846–853 (2007).

171. McIntire, S. L., Reimer, R. J., Schuske, K., Edwards, R. H. & Jorgensen, E. M. Identification and characterization of the vesicular GABA transporter. *Nature* **389,** 870–876 (1997).

172. Wang, X. *et al.* The C. elegans L1CAM homologue LAD-2 functions as a coreceptor in MAB-20/Sema2-mediated axon guidance. *J. Cell Biol.* **180,** 233–246 (2008).

173. Dong, B. *et al.* EFN-4/Ephrin functions in LAD-2/L1CAM-mediated axon guidance in Caenorhabditis elegans. *Development* **143,** 1182–1191 (2016). doi:10.1242/dev.128934

174. Cheng, L. L1-Mediated Branching Is Regulated by Two Ezrin-Radixin-Moesin (ERM)-Binding Sites, the RSLE Region and a Novel Juxtamembrane ERM-Binding Region. *J. Neurosci.* **25,** 395–403 (2005).

175. Huang, X., Cheng, H. J., Tessier-Lavigne, M. & Jin, Y. MAX-1, a novel PH/MyTH4/FERM domain cytoplasmic protein implicated in netrin-mediated axon repulsion. *Neuron* **34,** 563–576 (2002).

176. Su, C.-W. *et al.* The short coiled-coil domain-containing protein UNC-69 cooperates with UNC-76 to regulate axonal outgrowth and normal presynaptic organization in Caenorhabditis elegans. *J. Biol.* **5,** 9 (2006).

177. Chotoo, C. K., Silverman, G. A., Devor, D. C. & Luke, C. J. A Small Conductance Calcium-Activated K+ Channel in C. elegans, KCNL-2, Plays a Role in the Regulation of the Rate of Egg-Laying. *PLoS One* **8,** (2013).

178. Adelman, J. P., Maylie, J. & Sah, P. Small-Conductance Ca2+-Activated K+ Channels: Form and Function. *Annu. Rev. Physiol.* **74,** 245–269 (2012).